UCLA
Department
of
Physics

Hadronization Phenomenology From
Strange Hadron Production Measurements
in e+e- Annihilation at 27.4GeV Center-of-mass Energy

Eric Christopher Berg
November, 1994

LOS ANGELES 90024
CALIFORNIA

UNIVERSITY OF CALIFORNIA

Los Angeles

Hadronization Phenomenology From

Strange Hadron Production Measurements

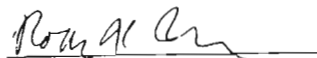in e+e- Annihilation at 27.4GeV Center-of-mass Energy

A dissertation submitted in partial satisfaction of the

requirements for the degree Doctor of Philosophy

in Physics

by

Eric Christopher Berg

1994

The dissertation of Eric Christopher Berg is approved.

Roger K. Ulrich

Eric D'Hoker

Charles D. Buchanan, Committee Chair

University of California, Los Angeles

1994

ii

DEDICATION

This dissertation is dedicated to all sentient beings

with the hope that teaching and true learning will be valued more.

TABLE OF CONTENTS

FIGURES

TABLES

EQUATIONS

ACKNOWLEDGMENTS

VITA

March 14, 1966	Born: Garden Grove, California
1987	Teaching Assistant Department of Physics University of California, San Diego
1987	B.S. Physics Mathematics and Philosophy minors University of California, San Diego
1988	Teaching Assistant Department of Physics University of California, Los Angeles
1989	M.S. Physics University of California, Los Angeles
1989	E771 Experiment on location at FNAL Batavia, Illinois
1990-1992	TPC/2γ Experiment on location at SLAC Stanford, California
1987-1994	Graduate Student Researcher Department of Physics University of California, Los Angeles

PUBLICATIONS

W.A.Barletta, R.C.Berg, A.Boden, C.Buchanan, D.B.Cline, A.Fridman, C.H.Ho, C.Pellagrini, "A Linear Collider Φ Factory and Beam Dynamics Test Machine." Blois CP Violations 1989: 421 (1989).

R.C.Berg, A.F.Boden, C.D.Buchanan, D.B.Cline, T.Foshe, "Methods to Measure (ϵ'/ϵ) to the Level of ~10^{-4} at a Φ Factory." Mod.Phys.Lett.A 6: 1163 (1991).

TPC/Two-Gamma Collaboration (D.Bauer, et al.), "Evidence for Spin One Resonance Production in the Reaction $\gamma\gamma^* \to \pi^+\pi^-\pi^0\pi^0$." Phys.Rev.D 48: 3976 (1993).

TPC/Two-Gamma Collaboration (D. Bauer, et al.), "Study of $\chi(c2)$ Production in $\gamma\gamma$ Collisions." Phys.Lett.B 302: 345 (1993).

TPC/Two-Gamma Collaboration (D. Bauer, et al.), "Measurement of the Kaon Content of Three Prong Tau Decays." Phys.Rev.D 50: 13 (1994).

ABSTRACT OF THE DISSERTATION

Hadronization Phenomenology From

Strange Hadron Production Measurements

in e+e- Annihilation at 27.4GeV Center-of-mass Energy

by

Eric Christopher Berg

Doctor of Philosophy in Physics

University of California, Los Angeles, 1994

Professor Charles D. Buchanan, Chair

This thesis describes the inclusive multiplicity measurements of K^0, Λ^0, Ξ^-, $\Sigma^{*\pm}$, and Ω^- (including antiparticles) as functions of the scaled variables X_P, X_E, and $\ln(1/X_P)$ using data acquired at 27.4GeV E_{cm} with the upgraded TPC/Two-Gamma detector at PEP in 1989-1990. The measured inclusive rates are, respectively: 1.37±.03 (stat.)±.07 (syst.), 0.183±.010±.012, 0.018±.006±.006, 0.018±.009±.006, and 0.0001±.0005±.0002 (with 95% upper limits of 0.070 and 0.013 for $\Sigma^{*\pm}$ and Ω^-). This $\Sigma^{*\pm}$ rate supports the implication from the OPAL Collaboration's measurement that the $\Sigma^{*\pm}$ is overpredicted by string models (e.g.: Lund, UCLA). This Ω^- rate is compatible with string model predictions, is lower than the previous TPC/Two-Gamma results, and is much lower than the rate reported by the Mark II Collaboration at 29GeV. The Λ^0 and $\Sigma^{*\pm}$ X_P spectra support the previous experimental indication that baryon spectra are softer than string model predictions. Mean, median and mode are estimated for the K^0 and Λ^0 $\ln(1/X_P)$ spectra for future comparisons at 10, 58 and 91GeV. To facilitate model builders, world averages for various hadrons are formed from a compilation of similar results at $\sqrt{s} = 10$, 29, and 91GeV. Comparisons with averages at different center-of-mass energies suggest that the actual rates at 29GeV for $\Sigma^{*\pm}$ and Ω^- are slightly higher than those reported here.

I am a creator of experiences; without this I would be all and not I.

I'm curious. Why am I here? What am I like? Where did I come from?

Being I and not all, I must answer MY truth, and not THE truth.

I choose my answers from thoughts of religion, metaphysics, and philosophy.

I'm curious. What have I experienced? What is experience? What can I experience?

Being I and here, I order my memories and hopes in time, and make choices.

I recall, I dream, I decide according to my pleasure and awareness.

I'm curious. What would I experience if I did _____?

I'm here now. Not apart, a part; and therefore causality.

I use trial and error, instinct, an authority, science, and intuition to see it.

We usually see the same thing.

I. INTRODUCTION

A.   PERSPECTIVE ON SCIENCE

Table 1.

SCIENCE: methods and models used to predict events from observations.	
Physics, Chemistry, Engineering	- the physical aspect
Biology, Anthropology, Medicine	- the living aspect
Psychology, Economics, Law	- the thinking aspect
Mathematics, Philosophy	- tools for all aspects
PHYSICS: fundamental perspectives of the physical aspect.	
Classical Mechanics	- macroscopic motions
Thermodynamics	- effects of microscopic motions
Quantum Mechanics	- microscopic transitions
Electromagnetism	- Some neat stuff we've found
Solid State Physics	- Some neat tools we've made
Particle Physics	- What's in there
Astrophysics	- What's out there
PARTICLE PHYSICS: fundamental perspectives of the microscopic.	
Quantum Gravity/ General Relativity	- a fundamental relationship
Quantum Electro-Weak Dynamics	- a fundamental relationship
Quantum Chromo-Dynamics	- a fundamental relationship
Theory of Elementary Particles (TEP)	- theory of all possible transitions
Elementary Particle Physics (EPP)	- experiments at currently 'low energies'
High Energy Physics (HEP)	- experiments at currently 'high energies'

Science is a quick way to predict experiences. By forming a representation of a part of existence, one can summarize all the predictions learned from trial and error. Not only is this representation easier to remember, but applying it to other parts of existence tends to give accurate predictions. This is generally true because existence is a tautology.

Physics is the group of representations of the physical aspect of existence from a fundamentals approach, and Particle Physics is the subgroup that represents the microscopic. Today's "Standard Model" for Particle Physics is a collection of the accepted theories. It is consistent with the other Physics subgroups, with the caveat that Classical Mechanics and Quantum Mechanics may only apply in non-overlapping kinematic regions (see Gell-Mann's theory of decoherence [1] and experimental discussion [2]).

B. PARTICLE PHYSICS TODAY

The Standard Model is expressed within the framework of second quantization as a relativistic field theory of matter. The Lagrangian density completely defines the Standard Model (see Equation 1) [3]. Its variables are described following some general discussion of how the Lagrangian density is used.

$$
\begin{aligned}
L = &\sum_i \overline{\psi}_i \left(i\partial\!\!\!/ - m_i - \frac{e m_i H M_Z}{2 M_W \sqrt{M_Z^2 - M_W^2}} \right) \psi_i - \sum_i e q_i \overline{\psi}_i \gamma^\mu \psi_i A_\mu \\
&- \sum_i \overline{\psi}_i \frac{e M_Z}{\sqrt{8(M_Z^2 - M_W^2)}} \gamma^\mu (1-\gamma^5)(T^+ W_\mu^+ + T^- W_\mu^-) \psi_i \\
&- \sum_i \frac{e M_Z^2}{2 M_W \sqrt{M_Z^2 - M_W^2}} \overline{\psi}_i \gamma^\mu (V^i - A^i \gamma^5) \psi_i Z_\mu - \frac{1}{4} F^{(a)}_{\mu\nu} F^{(a)\mu\nu} \\
&+ \sum_q i \overline{\psi}_q^i \gamma^\mu (D_\mu)_{ij} \psi_q^j - \sum_q m_q \overline{\psi}_q^i \psi_{qi}
\end{aligned}
\tag{1}
$$

The general mathematical methods for deriving various quantities refer back to Hamiltonian and Lagrangian Mechanics. For example, the Hamiltonian can be calculated from the Lagrangian density given a specific reference frame, and can be used with Quantum Mechanics as the generator for transitions from one time value to another (see Equations 2 and 3) [4, 5].

$$
H = \int \left(\frac{\partial L}{\partial \left[\frac{d\eta_\mu}{dt} \right]} \left[\frac{d\eta_\mu}{dt} \right] - L \right) dx^3, \qquad \eta_\mu = \text{each field}
\tag{2}
$$

$$
|...,t\rangle = \left(1 + \sum_{n=1}^\infty \left(\frac{-i}{\hbar} \right)^n \int_{t_0}^t dt_1 \int_{t_0}^{t_1} dt_2 ... \int_{t_0}^{t_{n-1}} dt_n H(t_1) H(t_2)...H(t_n) \right) |...,t_0\rangle
$$

or, for H time independent

$$
|...,t\rangle = e^{-iH(t-t_0)/\hbar} |...,t_0\rangle
\tag{3}
$$

Similarly, the Action can be calculated from the Lagrangian density and can be used with the path-integral formulation of Quantum Mechanics (see Equation 4).

$$
I = \int L \, dx^3 dt
\tag{4}
$$

This formulation states that the square of the integral of $e^{iI/\hbar}$ over all possible paths is the transition rate ($\delta I \to 0$ as $\hbar \to 0$ gives the classical path from Hamilton's Principle) [6]. The resulting dynamical equations are distinguished by the spin of the field represented, and are given in Equation 5 with their source-free solutions [7, 8].

$$
\begin{aligned}
&\text{Spin 0:} \quad (\partial_t^2 - \nabla^2 + m_\phi^2)\phi = 0 \qquad &&\phi(x^\mu) = S_\phi e^{\pm ip_\mu x^\mu} \qquad &&S_\phi \text{ a scalar} \\
&\text{Spin } \tfrac{1}{2}: \quad (i\nabla\!\!\!/ - m_i)\psi_i = 0 \qquad &&\psi_i(x^\mu) = u_i(\vec{p}) e^{\pm ip_\mu x^\mu} \qquad &&u_i \text{ a spinor} \\
&\text{Spin 1:} \quad (\partial_t^2 - \nabla^2)(\partial^\nu A_\mu - \partial^\mu A_\nu) = 0 \qquad &&A_i(x^\mu) = \vec{\varepsilon}_i(p,\lambda) e^{ip_\mu x^\mu} \qquad &&\vec{\varepsilon}_i \text{ a vector}
\end{aligned}
\tag{5}
$$

In review, a $|\text{state}\rangle$ is a set of quantum numbers which completely specifies a subset of everything, and is perceived as independent from the remainder of everything (with the exception of the interactions described by the Lagrangian). A wavefunction is a description of a state in terms of one of its quantum numbers and the accepted (Copenhagen) interpretation is that it's a probability distribution function (Equation 6).

$$
|...,n_i\rangle = \int |...,n_i'\rangle \Psi_{\text{state}}(n_i') \, dn_i'
$$

Probability n_i is between n_i' and $n_i' + dn_i' = |\Psi(n_i')|^2 dn_i'$
$$\tag{6}$$

First quantization forms the basis of Quantum Mechanics. The first step in first quantization is to replace observable variables with quantum number operators in the

Hamiltonian. Classical Mechanics' dynamical equations generally have the meaning structure of "subject-verb-object", and this replacement with operators changes the structure to "subject-verb" only. To form complete sentences, the operators must act on states. The generic "object" is a state with any consistent set of quantum numbers and represents a Hilbert space of all possible states. One can see how linear superposition is preserved in Quantum Mechanics. In a discrete Classical Mechanics theory, conjugate variables, defined in terms of the Lagrangian density, satisfy an equation resembling a commutation relationship (Equation 7) [9].

$$\text{Classically} \quad p_i \equiv \frac{\partial L}{\partial\left[\frac{dq_i}{dt}\right]} \quad \text{and} \quad \frac{\partial q_j \partial p_k}{\partial q_i \partial p_i} - \frac{\partial q_j \partial p_k}{\partial p_i \partial q_i} = \delta_{jk} \tag{7}$$

First quantization of a continuous field theory is completed by writing the Hamiltonian in terms of conjugate operators which satisfy commutation relationships (Equation 8) [10].

$$\text{First quantization} \quad [p_i(\mathbf{x},t),q_j(\mathbf{x}',t)] = -i\delta_{ij}\delta^3(\mathbf{x}-\mathbf{x}') \quad \text{and}$$
$$[q_i(\mathbf{x},t),q_j(\mathbf{x}',t)] = [p_i(\mathbf{x},t),p_j(\mathbf{x}',t)] = 0 \tag{8}$$

Second quantization forms the basis of Relativistic Quantum Field Theory. The general solution for a particular Schrödinger equation (Equation 9) can be written as a Fourier expansion in terms of a canonical variable (for example, momentum of a spin 1/2 field, Equation 10) [11].

$$i\hbar\partial_t\psi = H\psi \tag{9}$$

$$\psi(x^\mu) = \sum_{\pm s} \int \frac{d^3p}{(2\pi)^{3/2}} \sqrt{\frac{m}{E}}\left[b(p,s)u(p,s)e^{-ip_\mu x^\mu} + d^\dagger(p,s)v(p,s)e^{+ip_\mu x^\mu}\right] \tag{10}$$

Second quantization is performed in analogy with first quantization by replacing the coefficients of this expansion with operators. When acting on a state, these operators will create or annihilate a field by altering a sort of "existence quantum number" or number quantum number. Next, these operators are required to satisfy anticommutation or commutation relations (Equation 11) [12], depending on the quantum statistics the field should obey.

$$\text{fermions:} \quad \{b(p,s),b^\dagger(p',s')\} = \delta_{ss'}\delta^3(\vec{p}-\vec{p'})$$
$$\{d(p,s),d^\dagger(p',s')\} = \delta_{ss'}\delta^3(\vec{p}-\vec{p'})$$
$$\{\} = 0 \text{ for other } bb^\dagger dd^\dagger \text{ combinations}$$
$$\text{bosons:} \quad [a(p,\lambda),a^\dagger(p',\lambda')] = \delta_{\lambda\lambda'}\delta^3(\vec{p}-\vec{p'}) \tag{11}$$
$$[] = 0 \text{ for other } aa^\dagger \text{ combinations}$$

Fermi-Dirac statistics apply for half-integer spin fields (anticommutation). The Pauli exclusion principle applies here, so any two fields must occupy distinguishable states. Bose-Einstein statistics apply for integer spin fields (commutation) and any number of fields may have the same exact quantum number set. This is how the Heisenberg uncertainty principle is incorporated in the theory.

Continuing now with a description of the symbols of Equation 1, the specific fields referred to are the fundamental particles listed in Table 2. $\sum_f$ is a sum over all fermions and $\sum_q$ is a sum over the color variations. q_i is the electric charge, m_i is the mass. T^+ and T^- are the weak isospin raising/lowering operators. $A_i = \tau_3(i)$ and $V_i = \tau_3(i) - 2q_i(1-M_w^2/M_Z^2)$ are the axial vector and vector couplings.

Table 2. Fundamental Fields.

Generic	Version	Field Grouping	Variations	Spin	Electric Charge	Anti-particle	Comments
ψ, fermions	quarks (q)	spinor families by flavor: (u:d), (s:c), (t:b)	color charge: (R, B, G)	1/2	(+2/3: -1/3)	yes	only colorless states observed
	leptons (ν & l)	spinor families by individual type: (ν_e, e^-), (ν_μ, μ^-), (ν_τ, τ^-)	none	1/2	(0,-1)	yes	ν_τ not yet observed
χ, bosons	Higgs boson	scalar (H)	none	0	0	no	not yet observed
	Intermediate Vector Bosons	ElectroWeak (A^μ, W^+, W^-, Z^0)	none	1	(0,+1, -1,0)	no	"actions" which act on fermion "objects"
	QCD	Strong (g)	color pairs: $R\bar{B}, R\bar{G}, B\bar{G}$, $B\bar{R}, G\bar{R}, G\bar{B}$, and two mixtures of $(R\bar{R}\ B\bar{B}\ G\bar{G})$	1	0	no	self-coupling dominates low energy processes

The actual quark states (Hamiltonian eigenvalues) are not the flavor eigenvalues in Table 2 with which the $W^\pm$ couples. This is described by a mixing of the second element of the field spinors according to: $d'_i = V_{ij}d_j$, where V is the Kobayashi-Maskawa mixing matrix, given in Equation 12 (where s≡sin, c≡cos and d,s,b≡1,2,3) [13].

$$V_{ij} = \begin{pmatrix} c_{12}c_{13} & s_{12}c_{13} & s_{13}e^{-i\delta} \\ -s_{12}c_{23}-c_{12}s_{23}s_{13}e^{i\delta} & c_{12}c_{23}-s_{12}s_{23}s_{13}e^{i\delta} & s_{23}c_{13} \\ s_{12}s_{23}-c_{12}c_{23}s_{13}e^{i\delta} & -c_{12}s_{23}-s_{12}c_{23}s_{13}e^{i\delta} & c_{23}c_{13} \end{pmatrix} \quad (12)$$

This non-commutation between the Hamiltonian and flavor operators is necessary for the model to include transitions from one spinor to another as in uds→uud,d$\bar{u}$ ($\Lambda \to p^+\pi^-$ decay, for example). C (charge conjugation), P(parity), and T(time reversal) are discrete operators and cause a transition between two values, ±1, or have no effect (0). P violation

is seen and expected by the $P(1+\gamma^5)P^{-1} = (1-\gamma^5)$ part of the Lagrangian. The KM matrix may also have a phase angle, δ, which could be sufficient to describe the observed CP violation (indirect CP violation). These quantum numbers are multiplicative and are given simply by: $C = (-1)^{J=L+S}$, $P = (-1)^{L+1}$, and T = CP. T = CP follows if CPT is a good symmetry, which is true if the action is a) locally gauge invariant $(\phi \Rightarrow \phi e^{i\alpha(x)})$, b) a Lorentz scalar $(ASA^{-1}=S)$, c) a vacuum quantum state exists $(|0\rangle)$ d) (fermions) bosons correspond to (anti-)symmetric eigenstates under exchange of identical particles (i.e.: 'standard' spin statistics).

Calculations of various transition rates are made using Fermi's Golden Rule (Equation 13) [14].

Probability = $Luminosity$ • cross section (= σ)

$$\sigma = \int d\Omega_{cm} |M_{12 \to 34}|^2 \prod_{\text{species k}}^{\text{identicals}} \frac{1}{n_k!} \sqrt{\frac{[s-(m_3+m_4)^2][s-(m_3-m_4)^2]}{[8\pi(m_1+m_2)]^4[s-(m_1+m_2)^2][s-(m_1-m_2)^2]}} \quad (13)$$

Transition amplitudes, M_{fi}, are calculated from the Lagrangian or the Feynman diagram (a shorthand). The simplest way to understand the various terms of the Lagrangian of Equation 1 is with Feynman diagrams. An expression for M_{fi} is constructed directly from a Feynman diagram according to specific rules. An example of an M_{fi} for K^0 decay is given in Equation 14. The terms of Equation 1 are in direct correspondence with the fundamental vertices of Table 3 and Figure 1 [15].

$$M_{fi} = \sum_{i,j}^{u,c,t} \frac{G_F}{2} \int \frac{d^4k}{(2\pi)^4} u_d \gamma_\mu (1-\gamma^5) V_{j1} \frac{k+m_j}{k^2-m_j^2} V_{j2} \gamma^\mu (1-\gamma^5) u_s$$
$$v_d \gamma_\lambda (1-\gamma^5) V_{i1} \frac{k+m_i}{k^2-m_i^2} V_{i2} \gamma^\lambda (1-\gamma^5) v_s \quad (14)$$

Table 3. Fundamental Feynman Diagrams and Their Corresponding Expressions.

Lagrangian Field:	Diagram:	Expression for M_{fi}:
QED A_μ		$i q_i \bar{l} \gamma_\mu l$
QEW W_μ^+		$\dfrac{-i e M_z \bar{\nu} \gamma_\mu (1-\gamma_5) l}{\sqrt{8(M_z^2 - M_w^2)}}$
QEW Z_μ		$\dfrac{-i e M_z^2 \bar{\nu} \gamma_\mu (1-\gamma_5) \nu}{4 M_w \sqrt{M_z^2 - M_w^2}}$
QEW Z_μ		$\dfrac{-ie \bar{l}\gamma_\mu (3M_z^2 - 4M_w^2 + \gamma_5 M_z^2) l}{4 M_w \sqrt{M_z^2 - M_w^2}}$
QED A_μ		$i q_i \bar{q} \gamma_\mu q$
QEW W_μ^+		$\dfrac{-i e M_z \bar{u} \gamma_\mu (1-\gamma_5) d'}{\sqrt{8(M_z^2 - M_w^2)}}$
QEW Z_μ		$\dfrac{-ie \bar{q}\gamma_\mu (\tau_3(1-\gamma_5)M_z^2 - 4q_i(M_z^2 - M_w^2)) q}{4 M_w \sqrt{M_z^2 - M_w^2}}$
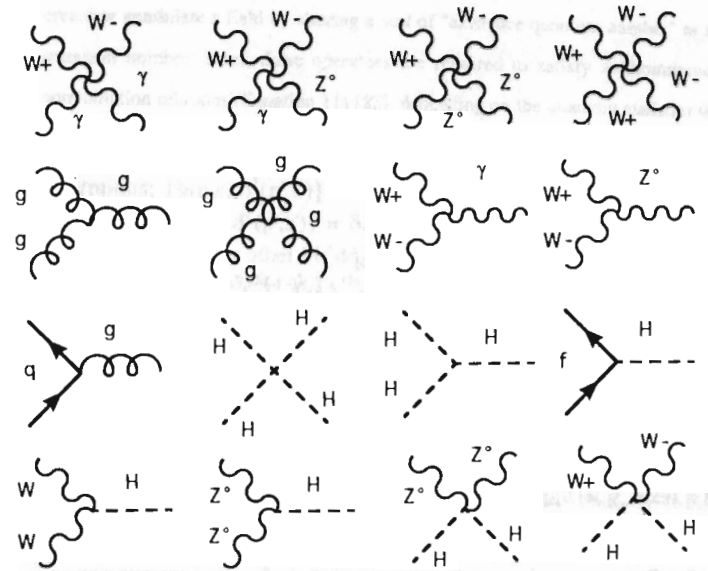
Figure 1. Fundamental Feynman Diagrams in Addition to Table 3.

The Standard Model, as a relativistic field theory, incorporates gravity (the only remaining force) as a perturbation which is usually ignored due to its magnitude (the gravitic to electromagnetic force ratio for two protons in a nucleus is 10^{-36} to 1, for example). The accepted theory of gravity is General Relativity, and has been verified by experiment. Perturbations are calculated by making a local Euclidean approximation and identifying the local residuals as gravity waves or gravitons (spin 2 bosons). Detection of these gravity waves is currently being attempted [16]. General Relativity and Quantum Mechanics have yet to be reconciled as they intrinsically contradict each other (however, see [17] for an alternative approach). An expression of this is that second quantization of General Relativity is non-renormalizable. The popular hope is that a consistent supersymmetric heterotic string theory will be found to explain everything [18].

Many activities of particle physicists for the past two decades have been for the purpose of testing the limits of the standard model. Predictions of the existence of several types of particles have been verified. The precise magnitude and nature of CP violation is being measured. The top quark has tentatively been seen, completing the predicted quark flavor multiplets. In general the standard model has been very successful in describing particle physics. I say 'describing' and not 'explaining' because the model includes several ad-hoc components such as a (Kobayashi-Maskawa) mixing matrix and bare charge renormalization constants. It is hoped that by making further observations, the underlying physics will become apparent.

C. A BRIEF DESCRIPTION OF HADRONIZATION

The production of observables from electron-positron collisions is divided into four stages due to the incompleteness of the standard model as a simple predictive mechanism. This causal segmentation assumes that relativistic quantum field theory and the quark model are accurate. The process is described as the annihilation of e+ and e- forming a virtual boson which then pair produces into $q\bar{q}$. The $q\bar{q}$ evolves and 'hadronizes' into many individual hadrons which then decay according to their nature into stable, observable particles (see Figure 2).
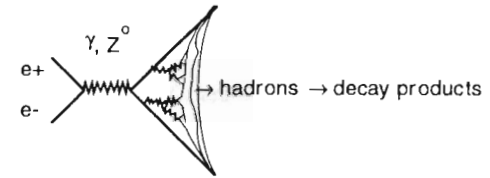
Figure 2. $e^+e^- \rightarrow q\bar{q} \rightarrow$ Stable Particles.

The first stage is the annihilation of e+e- and subsequent pair production of $q\bar{q}$ and is described by quantum electroweak theory. The characteristics and probability of producing a $q\bar{q}$ pair given an e+e- collision is described very well by the theory. The second stage is the $q\bar{q}$ evolution into a collection of partons (i.e.: quarks or gluons). The usual approximation of a perturbative series in terms of the theory's coupling constant diverges because that coupling constant increases as the momentum transfer decreases. What is done is to calculate a portion of the series and rely on the third stage to account for the rest. The third stage, which has been causally separated from the second in order to make quantitative predictions, is the hadronization stage (see [19] for an argument for this

11   12

causal separation). A model describing the transition from partons to hadrons, typically inspired by characteristics of QCD, is used at this point. Various approaches have been, and are still being used for both the $q\bar{q}$ evolution and the parton transition. The fourth stage is the independent decay of these hadrons into stable particles. An empirical table of lifetimes and branching ratios is used to describe this stage, and no predictive elements are present except for several unmeasured branching ratios for heavy hadrons (e.g.: Λ_b) for which 'best guess' approximations are used. The positions and momenta of the stable particles can be compared with experimental observations. Similarly, both sets of 'data' (experimental and predicted) can be processed by a reconstruction algorithm and comparisons of unstable hadrons can be made. The influence of the decay table's particular values on these comparisons is small in most cases (i.e.: for uncharmed hadrons). Uncertainties due to the decay table's values are included in the comparisons made in this thesis. Fragmentation and hadronization are therefore studied by assuming relativistic quantum field theory, the quark model, quantum electroweak theory, and the theoretical predictions of lifetimes and branching ratios are accurate. In this way the second and third stages are directly probed.

D.   SCOPE OF THIS THESIS

The purpose of this study is to add to and summarize the hadron production measurements in e+e- annihilation at 29GeV, and make comparisons with the predictions of several QCD inspired models of the parton-hadron transition. Specifically:

1......... A description of various models of hadron production is given in Chapter II.

2......... Measurements of K°, Λ°, $\Xi-$, $\Sigma*\pm$, and $\Omega-$ production rates and momenta are described in Chapter IV. Chapter III describes the TPC/Two-Gamma detector which produced this final data set using an upgraded vertex chamber. The $\Sigma*\pm$ and $\Omega-$ measurements are of particular interest because the previous measurements, unlike those of K°, Λ° and $\Xi-$, show considerable variation.

3......... A survey of all the published hadron production measurements (omitting charmed hadrons) at 10, 29, and 91GeV is presented in Chapter V. This is especially useful considering this analysis is the last at ~29GeV, the PEP and PETRA energy region.

4......... A detailed statistical comparison between the measurements of K°, Λ°, $\Xi-$, $\Sigma*\pm$, and $\Omega-$ rates, the previous measurements, and several model predictions is expressed in Chapter VI.

E.   REFERENCES

1.   M.Gell-Mann, The Quark and the Jaguar. Freeman Publishers (1994).

2.   B.W.Boreham, "The Classical-Quantum Border: Laser Sharp?"
      Physics Today 47 (7): 13 (July 1994).

3.   Particle Data Group, "Review of Particle Properties." ·
      Phys.Rev.D 45: III.54 and III.59 (1992).

4.   H.Goldstein, Classical Mechanics. 2nd ed. Addison-Wesley: 562 (1980).

5.   J.J.Sakurai, Modern Quantum Mechanics. Benjamin/Cummings: 68-73 (1985).

6.   J.J.Sakurai, ibid., 117-123.

7.   J.Bjorken and S.Drell, Relativistic Quantum Mechanics. McGraw-Hill:
      chapters 1, 3, and 9 (1964).

8.   J.Bjorken and S.Drell, Relativistic Quantum Fields. McGraw-Hill:
      chapter 14 (1965).

9.   H.Goldstein, ibid., 397.

10.   J.Bjorken and S.Drell (1965), ibid., 5-16.

11.   J.Bjorken and S.Drell (1965), ibid., 26-62.

12.   J.Bjorken and S.Drell (1965), ibid., 57-76.

13.   Particle Data Group, ibid., III.65.

14.   C.Quigg, Gauge Theories of the Strong, Weak, and Electromagnetic
      Interactions. Benjamin/Cummings: 308-309 (1983).

15.   C.Quigg, ibid., 113,116,129,131,151,197, and 309-314.

16.   K.Thorne, "LIGO, VIRGO, and the International Network of Laser Interferometer
      Gravitational Wave Detectors." GRP-380, Eight Nishinomiya-Yukawa
      Symposium on Relativistic Cosmology, (1994).

17.   M.Sachs, Quantum Mechanics from General Relativity An Approximation
      for a Theory of Inertia. Reidel Publishing (1986).

18.   L.Dixon, "Whatever Happened to the Theory of Everything?" Beam Line (SLAC),
      volume 24 number 2; 12 (Summer 1994).

19.   L.Rosenberg, "A Study of Hadronization Using Energy Flow from e+e-
      Annihilation into Quarks and Gluons at √s of 29GeV." PhD Thesis, SLAC-289
      (1985).

II. THEORY

A.   e+e- ⇒ $q\bar{q}$

Experiments accelerate many e+ and e- into each other in a near vacuum. Neglecting interactions with anything other than an antiparticle, the number of collisions which occur depends on the number of incident e+ (e-) and the probability for any two to interact, integrated over the spacetime volume for which there is significant probability of interaction. Equation 15 defines the luminosity and cross section as parameters characteristic of the incident number and distribution, and interaction probability respectively.

$$\text{\# collisions/second} = L \, (/\text{cm}^2\text{sec}) \bullet \sigma_{\text{interaction}} \, (\text{cm}^2) \qquad (15)$$

The probability for hadronic interactions, $\sigma_{e+e-\to q\bar{q}}$ can be predicted by the quark-parton model and QEW theory. This cross section is predicted to have an angular dependence $\alpha \, (1+\cos^2\theta)$ where θ is the angle between the outgoing q or $\bar{q}$ and the incoming e+ or e-, assuming quarks are spin 1/2 particles. If polarized e+ e- are collided, or the center-of-mass energy is at a resonance such as the ϕ, B$\bar{B}$, or Z° resonances at 1, 10, or 91 GeV, then the distribution differs. These observations are also in agreement with QEW theory plus the quark-parton model.

The dependence of this total hadronic cross section on E_{cm} ($\equiv\sqrt{s}$) is predicted by QEW theory to be $e_q^2 12\pi\alpha_E^2/3s$, where e_q is the charge of the specific q ($\bar{q}$) produced. In order to calculate the predicted probability of producing any charge (i.e.: flavor) quarks, a simple sum is used because the final states are distinguishable, and no quantum mechanical interference occurs. A relevant comparison to make is with the cross section for e+e-→ $\mu+\mu$-, calculated to be $4\pi\alpha_E^2/3s$. The ratio of these cross sections, R ≡

$\sigma_{e+e-\to hadrons} / \sigma_{e+e-\to \mu+\mu-}$, is predicted to have a step-like character in s as thresholds are passed kinematically allowing more quark flavors. The quark-parton model (with 3 colors) predicts R = 6/3 (1.0<E_{cm}<3.7GeV), 10/3 (3.7<E_{cm}<10.6GeV), 11/3 (10.6<E_{cm}<~350GeV), and 15/3 (~350GeV <E_{cm}), based on naked flavor thresholds. The Z° boson diagrams interfere with the photon diagrams near the Z° mass (91GeV) altering the cross section. Also, virtual QCD loops contribute a factor of *$(1+\alpha_S(s)/\pi+(1.986-0.115N_q)(\alpha_S(s)/\pi)^2)$ to second order [1], where $\alpha_S(s) = g_S^2(s)/4\pi$ and $g_S(s)$ is the energy dependent QCD coupling constant. These predictions are observed within 2% [2] along with many resonances in Figure 3 [3] (see also [4]).

R in e⁺e⁻ Collisions
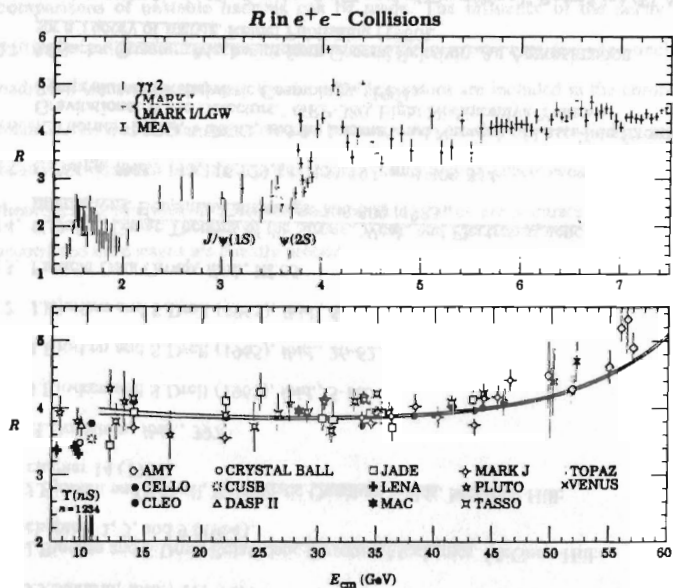
Figure 3. Relative Total Hadronic Cross Section's E_{cm} Distribution.

17

B.   q̄q FRAGMENTATION

The probability of producing a particular set of hadrons with particular momenta given that a q̄q has been produced (and thus <u>some</u> distribution of hadrons must result) is rather difficult to predict. The perturbation technique is the standard approach to a problem like this (e.g.: in QED), the results of which are outlined in Equation 16.

$$\text{Probability}(H_1(p_1^\mu),H_2(p_2^\mu),... | \ q\bar{q}) = \frac{(A+B(\alpha_s)+C(\alpha_s^2)+...)}{(1+\frac{\alpha_s}{\pi}+(1.986-0.115N_q)(\frac{\alpha_s}{\pi})^2+...)} \quad (16)$$

where A, B, and C depend on the particular $H_1(p_1^\mu),H_2(p_2^\mu),...$ distribution

The strong coupling constant, $\alpha_S(s) = 12\pi \ln(s/\Lambda_{QCD}^2)/(33-2n_{fermions})$ where Λ_{QCD} (=100-500MeV) is the renormalization constant for the color charge [1]. Unfortunately, the terms in the perturbative series get larger as the power of α_s increase because α_s is greater than 1 here. However, the initial evolution of the q̄q system can be calculated in this way because there the momentum transferred is large (>Λ_{QCD}) and so α_s is small. This fixed order matrix element calculation has only been done up to second order, and so the initial q̄q evolution can be predicted up to four partons (two possible gluons). There is a substantial gap between this and a specific hadron distribution, and either the hadronization model must take over from here, or the continued parton showering must use approximation methods to estimate the branching fractions in the semi- or non-perturbative region [2]. Currently, models prefer to do the latter, because the increased jet multiplicity at higher E_{cm} requires more hard partons than have been calculated for the fixed order predictions [5].

By studying the divergences in the perturbation series, one can re-sum the terms and, although convergence is still in question, approximate the parton shower evolution.

18

There are two types of divergences, infrared and collinear. The infrared divergences occur when emission of a gluon of energy $E_g \rightarrow 0$ is considered (the probability becomes ∞). The collinear divergences occur when a gluon with direction equal to its parent quark is considered. By resumming the perturbative series (to all orders in α_s) and calculating only the leading order terms for these divergences, the Leading Log Approximation (LLA) prediction can be calculated [6]. The next to leading order terms of the infrared divergent series are proportional to $\sqrt{\alpha_s}$ rather than α_s [7] and inclusion of these is called the Next to Leading Log Approximation (NLLA). The results of the LLA calculation are outlined in Equation 17 for the branching of n partons into n+1 partons [5].

$$d^2\sigma_{n+1} = \sigma_h \frac{\alpha_s(z(1-z)Q^2)}{2\pi Q^2} P(z) \frac{\Delta_s(Q^2_{max})}{\Delta_s(Q^2)} dQ^2 dz \qquad (17)$$

where Q=momentum transfered and $z = \frac{(E+|p_{//}|)_{n+1}}{(E+|p_{//}|)_n}$

Δ_s are the Sudakov form factors, Q_{max} is the cutoff parameter for the parton shower, and P(z) are the Altarelli-Parisi splitting functions which depend on the parton types involved [8]. The value for Q_{max} determines the minimum virtuality of the radiated partons (almost completely gluons). The existence of a Q_{max} has been argued to be reasonable since local parton hadron duality (LPHD) has been approximately observed [9]. $Q_{max} = \Lambda_{QCD}$ corresponds to a specific model, yet $Q_{max} = \Lambda_{QCD} \approx m_{hadron}$ has been seen to give good predictions [9,10]. Instead of assuming exact LPHD, the process is usually turned over to a hadronization model to specify the parton to hadron translation which may include effects like flavor and spin. The Modified Leading Log Approximation (MLLA) additionally includes the angle ordering effect of coherent gluon emission in which gluon production angles are required to be smaller as the momentum transfer decreases, as well

19

as matrix element modifications to the first gluon branching [11]. In general the effects of resumming the divergent terms is to include soft gluon interference in a parton shower, which is seen mainly in the low momentum regions of hadron spectra [12] (with particular predictions for the $\ln(1/x_p)$ shape) and is superior to the fixed order approach which limits jet multiplicity to four.

C.   PARTON HADRONIZATION

When the parton evolution is stopped at a model (or parameter) dependent point, a mechanism for statistically mapping partonic distributions to hadronic distributions takes over. Three general categories of models exist. Independent fragmentation models treat partons as independent objects decaying into hadrons and partons. String fragmentation models are based on the idea that the system's energy is mainly in the field and not the partons. Cluster fragmentation models are based on grouping quarks into clusters which decay into two hadrons or lighter clusters. Many models show good agreement with observed spectra even including non-QCD based models [13]. Each model has its strong and weak points, and much understanding has been generated by combining ideas. Three Monte Carlo implementations of models are discussed further in this thesis: JETSET v6.3 (a Lund string model), UCLA v7.4 (a UCLA string model and offshoot of the Lund model), and HERWIG v4.1 and v5.0 (Webber's cluster model). Other currently successful Monte Carlos are: ARIADNE v3.3 (a color dipole string model), COJETS v6.22 (an independent fragmentation model with LLA shower), NLLJET v2.0 (a NLLA string model), and CALTECH I (Gottschalk's cluster model) [10,11,14].

20

LUND (JETSET 6.3)

The parton evolution uses the MLLA approach discussed above, and the hadronization approach used is based on the Artru-Mennessier string model [1]. A classical color field is predicted to be localized in a narrow tube between quarks, and may have kinks, which can be associated with gluons [10]. The constant energy density for such a string ($\approx$1GeV/fm) is maintained by breaks in the string occurring due to causally independent $q\bar{q}$ pairs tunneling out of the vacuum [15]. The probability for a hadron distribution is $\alpha\, e^{-bA}$, where A is the area in spacetime swept out by the color string in the 1+1 dimensional approximation [10] (see Figure 4).
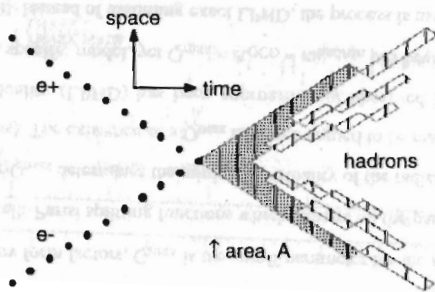
Figure 4. String Fragmentation.

Perpendicular momentum ($p_\perp$) is generated randomly with a Gaussian and is conserved between new $q\bar{q}$ pairs [15]. The "Simple Lund" model produced individual hadrons with energy fraction z determined with the $f(z)=1$ distribution, whereas the "Standard Lund" model used $f(z)=(1+c)(1-z)^c$ and included hard gluon emissions. The "Symmetric Lund" model, implemented currently, uses the Lund Symmetric Fragmentation Function (LSFF), $f_i(z)=(N_i/z)(1-z)^a \exp(-bm_\perp^2/z)$ where $m_\perp^2=m^2+p_\perp^2$, which Lund derives from rapidity

constraints on the ordering of the central hadron (the last one to be generated), also called 'left-right symmetry' [15]. Hadrons are generated from the outside-in randomly choosing which side to do next. Unfortunately, the physical system hadronizes inside-out as argued by Bjorken [15], but the implementation of such a scheme is rather difficult. However, a Lorentz boost can be made such that either outside hadron is created 'first' [15].

Many parameters are used in order to obtain good predictions of the flavor and spin distributions [10]. The s quark suppression of ~1/3 (no $c\bar{c}$, $b\bar{b}$, or $t\bar{t}$ pairs are produced), the vector/pseudoscalar meson suppression of ~1/3, and the suppression of decuplet/octet baryons of ~1/10 are simply imposed with parameters [15]. Similarly, the probability for producing particular diquarks (in order to form baryons) is derived from diquark masses (again for uds flavors) and is imposed with parameters [15]. As a and b increase with a constant ratio, the conservation of charge, flavor, and baryon number becomes more local [15]. Heavy quarks (c,b,t) will follow hyperbolas rather than straight light-cones, thus justifying their tunneling suppression via mass (u$\approx$4MeV, d$\approx$7MeV, s$\approx$130MeV, c$\approx$1.6GeV, b$\approx$5GeV, t$\approx$174GeV). Physicists typically use the JETSET option to fragment heavy quarks with the Peterson function (employing a free parameter) rather than the LSFF; this leads to significantly better agreement with D and B meson spectra [11]. Baryon production via the single "BMB" popcorn mechanism is possible with probability determined by a parameter in order to increase the baryon correlation length to the observed level [16].

The main disagreements this model has with observation have been seen to be the overprediction of η and η' (by 7σ!) [20], the underprediction of the $\Xi^{*o}/\Sigma^{*\pm}$ ratio at 91GeV [2,17], the underprediction of the $\Omega-$ rate at 29 and 91GeV [17,18], the underpredicted increase in baryon rate over meson rate with E$_{cm}$, the prediction of baryon x-spectra harder than observed [10], and the prediction (using the LSFF) of D and B

meson x-spectra harder than observed. Revisions are currently being made as with any model [19]. Table 4 lists the default parameters for JETSET 6.3 as well as those used in this thesis which were determined by W.Gary with tunes to 29GeV flavor-independent characteristics (the version 7.3 decay table is used here).

Table 4. JETSET 6.3 Parameters.

	default [10]	value used here
s/u	0.30	0.30
qq/q	0.10	0.10
$(qq)_{J=1}/(qq)_{J=0}$	0.05	0.05
(us/ud)/(s/d)	0.40	0.40
V/(V+P)$_{ud}$	0.50	0.50
V/(V+P)$_{s}$	0.60	0.60
V/(V+P)$_{c}$	0.75	0.75
a	1.0	0.9
b	0.7	0.5
popcorn	0.5	0.5

UCLA (UCLA 7.31)

This Monte Carlo is integrated with JETSET, and many of its options also are available here. The parton shower used is the MLLA approach [20]. The hadronization scheme used is based on the Lund string model. Instead of assigning probabilities for quarks (diquarks) to tunnel out of the vacuum, probabilities for specific hadrons are determined in a similar outside-in iterative technique. Local flavor (not spin) conservation is enforced by decomposing the prospective hadron into quark (and diquark) constituents at the hadron production vertex (as opposed to earlier in the fragmentation). When a baryon is produced with a constituent diquark, the algorithm for the next hadron remembers this (conserving flavor), yet doesn't require the next hadron to be a baryon. Baryon production via this 'popcorn' mechanism, where any number of mesons may

intercede between correlated baryons (in order of hadron rapidity), is intrinsic to this model, which is based on a 'density of distinguishable final states' approach (see Figure 5). An ad hoc popcorn suppression factor is introduced based on various motivations [20].
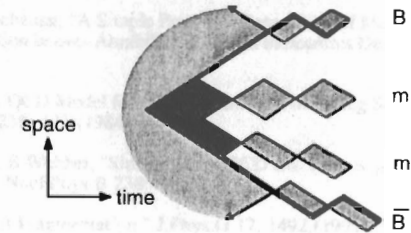
Figure 5. An Example of the Popcorn Mechanism.

The specific prospective hadron and its z-value (α E+p$_{//}$) are chosen based on the probability given by the LSFF, $f(z,m_{hadron})$, where the normalization (N_i) is the same for all hadrons. In other words, the LSFF is used not only to determine hadronic z-values, but also as a probability density function for determining hadronic species. This leads to suppression based on hadron mass rather than quark mass. The LSFF is derived here from the assumption that relative hadron distribution probabilities are proportional to e^{-bA} [20]. As in the Lund model, the a-parameter corresponds to a perimeter law and the b-parameter corresponds to an area law [15]. This area law is predicted by the discrete field theory of Lattice QCD for Wilson loops (2 stationary quarks) [21]. Hadronic phase space is also considered. Transverse momentum is randomly generated with a Gaussian probability density function in a semi-locally conserved way: the mean is set to 1/2 the

total accumulated $p_\perp$ from all the previous hadrons on that side [22]; the width is set at $1/\sqrt{2}$ of the previous width parameter which nicely approximates semi-local $p_\perp$ conservation.

The motivation for using hadron masses instead of quark masses to determine their production distributions is shown clearly by the $\sim e^{-am_h}$ dependence of the average multiplicities of light (uds) hadrons [4]. The agreement with observations is very similar to that of the Lund model, yet there is a drastic decreases in the number of free parameters. The D and B meson spectra are very nicely predicted, as well as the η and η' spectra [20]. In contrast with the Lund model, which basically has a physically well-motivated parameter for each degree of freedom, the UCLA model has very few parameters. The broad range of data predicted accurately, therefore, suggests that this model may indeed be a good description of the physical mechanisms actually occurring. The main disagreements between the UCLA model and observations are: the predicted baryon spectra are too hard (as was also true for the Lund model), the $\Sigma^{*\pm}$ rate is overpredicted by $\sim 6\sigma$ (a factor of 2) at 91GeV, and the $\Omega-$ rate is very underpredicted [20].

WEBBER (HERWIG 4.1 or 5.0)

This model is based on the Field-Wolfram cluster model. The parton shower starts with a real photon jet which effectively boosts the system (unboosting is done after the hadronization is complete) [23]. The direction of this photon is, of course, independent of the fragmentation axis [24]. The shower uses the Altarelli-Parisi splitting functions of the LLA approach, with modified arguments for α_s [23]. The form factors (Δ_s) are calculated by Monte Carlo and implemented using a table [23], and Λ_{QCD} determines the shower characteristics [25]. The model relies on the idea of preconfinement, which is motivated by the existence of jets. Preconfinement is implemented by requiring successive gluon emissions to be at smaller and smaller opening angles (angle-ordering). This is equivalent

to a gluon virtuality threshold [24]. This parton shower proceeds to a parameterized cut off point (at $\frac{\alpha_s}{\pi} \sim 0.5$ [24]) where all gluons are converted to $q\bar{q}$ pairs using a simple form factor [23]. The quarks are then grouped by a simple algorithm. The heavy (c and b) quarks are decayed as free particles to lighter quarks forming two clusters [23]. Large clusters are broken into smaller clusters if their mass exceeds a parameterized threshold. All the clusters are then isotropically decayed into two hadrons in a way similar to resonance decay, which depends on the density of final states available. In this model, isospin symmetry is broken [1,23]. Also, small Lorentz non-invariances are produced, but they have been seen to be negligible [24].

The NLLA approach has been seen to agree with this model's showering scheme [24]; yet needed improvements in the angular-ordering constraint are under development [25]. This Monte Carlo can also make predictions for deep inelastic lepton-lepton, lepton-hadron, and hadron-hadron scattering [26]. The most recent version of the Monte Carlo (5.1) is described in reference [27]. This model is primarily aimed at describing the parton shower physics. It therefore places less importance on flavor predictions (such as those tested in this thesis) than the string models do. With relatively few parameters, it provides qualitatively reasonable flavor production rate predictions, but is not as accurate as string models. In particular, the Webber model severely overpredicts the decuplet and strange baryon rates [10]. Also, the baryon correlation lengths and magnitudes have been seen to be too strong [8].

D.   REFERENCES

1.   TASSO Collaboration, I.R.Tomalin, "Strange Baryon Production in e+e-
     Annihilation." PhD Thesis, RALT-069 (1988).

2.   A.Angelis, "Baryon Production in e+e- Annihilations." J.Phys.G 19: 1233 (1993).

3.   Particle Data Group, "Review of Particle Properties." Phys.Rev.D 50: 1334 (1994).

4.   R.Marshall, "e+e- Annihilation at High Energies." Rep.Prog.Phys. 52: 1329 (1989).

5.   L.Rosenberg, "A Study of Hadronization Using Energy Flow From e+e-
     Annihilation into Quarks and Gluons at $\sqrt{s}$ of 29GeV." PhD Thesis , SLAC-0289
     (1985).

6.   G.Marchesini, B.Webber, "Monte Carlo Simulation of General Hard Processes with
     Coherent QCD Radiation." Nucl.Phys.B 310: 461 (1988).

7.   G.Marchesini, B.Webber, "Simulation of QCD Jets Including Soft Gluon
     Interference." Nucl.Phys.B 238: 1 (1984).

8.   TPC/Two-Gamma Collaboration, James Yen-Tang Oyang, "Inclusive Production
     and Flavor Correlations of Strange Baryons in e+e- Annihilation at $S^{**}(1/2)$ = 29-
     GeV." UMI-92-07711 and UCLA-HEP-91-005, PhD Thesis (1992).

9.   Y.Dokshitzer, V.Khoze, S.Troian, "On the Concept of Local Parton-Hadron
     Duality." J.Phys.G 17: 1585 (1991).

10. W.Hoffman, "Particle Composition in Hadronic Jets in e+e- Annihilation."
     Ann.Rev.Nucl.Part.Sci. 38: 279 (1988).

11. L3 Collaboration, (B.Adeva, et.al.), "Studies of Hadronic Event Structure and
     Comparisons with QCD Models at the Z° Resonance." Z.Phys.C 55: 39 (1992).

12. C.Fong, B.Webber, "Jet Fragmentation at Small x." 25th Rencontres De Moriond,
     Les Arcs: 291 (1990).

13. B.Webber, "A QCD Model for Jet Fragmentation Including Soft Gluon Interference."
     Nucl.Phys.B 238: 492 (1984) see p526.

14. G.Ballocchi, R.Odorico, "The String Effect and Independent Fragmentation Models:
     Lore and Facts." Nucl.Phys.B 345: 173 (1990).

15. B.Andersson, G.Gustafson, G.Ingelman, T.Sjöstrand, "Parton Fragmentation and
     String Dynamics." Phys.Rept. 97: 31 (1983).

16. T.Sjöstrand, "The Lund Monte Carlo for Jet Fragmentation and e+ e- Physics –
     JETSET version 6.2." LU-TP-85-10 (1985).

17. OPAL Collaboration, (P.D.Acton, et al.), "A Measurement of Strange Baryon

Production in Hadronic Z0 Decays." Phys.Lett.B 291: 503 (1992).

18. Mark II Collaboration, (S.Klein, et.al.), "Observation of $\Omega-$ Production in e+e-
     Annihilation at 29GeV." Phys.Rev.Lett. 59: 2412 (1987).

19. B.Andersson, "Revisiting the Lund Model." J.Phys.G 17: 1507 (1991).

20. S.Chun, C.Buchanan, "A Simple Relativistic-string Description of Meson and
     Baryon Flavor Formation in e+e- Annihilations." Phys.Lett.B 308: 153 (1993).

21. K.Wilson, "Confinement of Quarks." Phys.Rev.D 10: 2445 (1974).

22. S.Chun, C.Buchanan, "A Simple Powerful Description of Meson and Baryon
     Flavor Formation in e+e- Annihilations." 27th Rencontres De Moriond, Les Arcs
     1992.

23. B.Webber, "A QCD Model for Jet Fragmentation Including Soft Gluon Interference."
     Nucl.Phys.B 238: 492 (1984).

24. G.Marchesini, B.Webber, "Simulation of QCD Jets Including Soft Gluon
     Interference." Nucl.Phys.B 238: 1 (1984).

25. B.Webber, "Jet Fragmentation." J.Phys.G 17: 1492 (1991).

26. G.Marchesini, B.Webber, "Monte Carlo Simulation of General Hard Processes
     with Coherent QCD Radiation." Nucl.Phys.B 310: 461 (1988).

27. G.Marchesini, et.al., "HERWIG 5.1 - a Monte Carlo Event Generator for Simulating
     Hadron Emission Reactions with Interfering Gluons." Comp.Phys.Comm. 67: 465
     (1992).

III. EXPERIMENT

A.   TPC/TWO-GAMMA APPARATUS

The TPC/Two-Gamma Experiment has over a decade's worth of references which explain the accelerator and detector in various degrees of detail. The experiment recorded triggered events from e^+e^- collisions in the center of mass frame. Event triggers were optimized for $q\bar{q}$, $\tau\bar{\tau}$, and 2γ physics (see Figure 6).

The e^+ and e^- were produced and accelerated by the linear accelerator (linac) at the Stanford Linear Accelerator Center (SLAC), which has provided beams for SPEAR (late 1970's and early 1980's), PEP (1978-1990) and SLC (4/89-present). The linac used a thermionic cathode (laser photocathode after 1991) [1,2] system to produce electron clouds, which were immediately accelerated and focused into bunches. These bunches were accelerated in a vacuum of $\sim 10^{-7}$ Torr by 30,000 resonating cavities (see Figure 7) [2]. These cavities transferred energy to the bunches from 238 klystron power supplies with about 1% efficiency. The klystrons operated at a frequency of 2.856 GHz and a peak power of 65MW each [2,3]. The klystrons were pulsed at 120 Hz resulting in $\sim 10^9$ to $\sim 2 \times 10^{10}$ e^-/bunch [4]. Electron bunches could be diverted to hit a tungsten-rhenium target producing 1 to 2 extractable e^+ per incident e^- [5,6]. The e^+ were accelerated to 0.2 GeV before re-injecting into the main accelerator at the appropriate stage. With the SLC construction, damping rings were added for e^+ and e^- at the 1.2 GeV stage [7]. The linac could deliver up to 53 GeV e^- and e^+ with an average accelerating field of 17 MeV/meter [2]. During injection into PEP, the klystrons in the second half of the linac were 180 degrees out of phase, slowing the $\sim$25GeV bunches to 14.5GeV [6].

The linac regularly filled the smooth hexagonal storage ring called PEP (Positron Electron-Project, approved 1976) with e^+ or e^- bunches. The storage ring was an
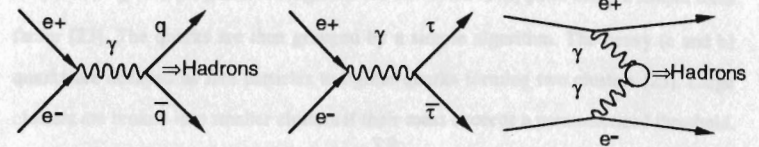
Figure 6. Hadronic, Tau, and 2-photon Events.
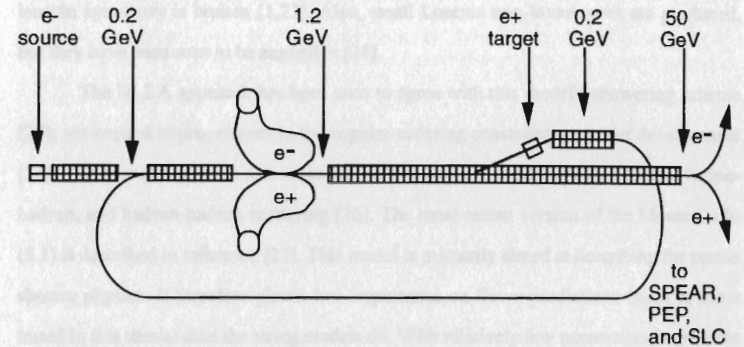
Figure 7. SLAC's 2-mile Long Linear Accelerator.
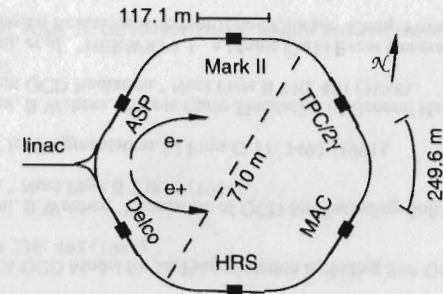
Figure 8. PEP: a 2200.0 meter Circumference Storage Ring, e^+e^- Collider [9,12].

isomagnetic lattice consisting of 192 uniform bending dipole magnets (weighing over 8 tons each), 240 gradient focusing quadrupole magnets, and numerous sextapole, rotated quadrupole, wiggler, and low field dipole magnets (used to form an ideal orbit) [8,9]. The lattice was dynamically tuned to avoid resonance instabilities resulting in a β_y^* of 5.5cm ($2\pi\beta^*$ = the focusing oscillation wavelength at the interaction point) [10]. Bunch injection (upgraded in 1987) was synchronized with 24 five-cell resonating cavities which established counter-rotating electron and positron bunches in stable orbits by (de-) accelerating wayward leptons. Bunches were filled with $\sim10^{12}$ leptons each typically producing currents of about 20 mA/beam after 1987 [11]. PEP ran with 3 e^+ and 3 e^- bunches which collided every 2.44μs (409 kHz) at up to 6 interaction regions where the 6 experiments were done (see Figure 8) [2]. Preparations were being made for increasing the number of bunches just before PEP shut down [11]. The beam energies at PEP were $\sim$13 to 15 GeV. Data was taken at 13.7 GeV (14.5 GeV before 1989) and had dispersions of $\pm$0.3 to 0.5% for e^+ and $\pm$0.15% for e^-, well within design specifications [12]. Beams were occasionally lost due to power supply trips on RF cavities or magnets. Expected beam depletion occurred due to beam-gas scattering, beam-beam scattering, and dynamic aperture losses due to synchrotron radiation. Energy loss due to synchrotron radiation (emittance) and quantum fluctuations (dispersion damping) was $\sim$2.9MW and was compensated for by 12 klystrons which operated at 353 MHz in phase with the 7.3μs/lap orbit time [13]. The bunch size was gradually improved from ($\sim$1000μm x $\sim$100μm x 20mm) to (380μm x $\sim$60μm x 18 mm) in 1987 (radial, vertical, and beam directions) [14]. PEP turned on in 1980 and delivered luminosities $\sim10^{31}$ /cm^{2}s for about a decade. During the 1990 run, PEP and SLC shared the linac with a switching time of $\sim$1 hour [15].

The TPC/Two-Gamma detector recorded maximum luminosities of 1.3×10^{31}, 2.5×10^{31}, and 6.1×10^{31} /cm^{2}s during the running periods: (11/81-6/82, 9/82-6/83, 9/84, 11/84), (12/84, 2/85-5/85, 10/85-2/86), and (10/88-12/88, 10/89-12/89, 4/90-9/90) [16].

Recall that the # events /sec = L (/cm^{2}s) $\cdot$ $\sigma_{event\ type}$ (cm^2) where $\sigma_{e+e^-\to q\bar{q}}$ = 0.4nB (without initial state radiation) at $\bar{E}_{cm}$ = 29 GeV, so $q\bar{q}$ events occurred at $\sim$5-25 mHz [17]. The amount of data recorded for these periods was $\int L dt$ = 77±8, 68±7, and 32±8 pB^{-1} (of the expected 200pB^{-1} from running in parallel with SLD). The TPC's approval in 1/77 led about 100 collaborators from 16 institutions to complete its assembly in 7/81. Since then, about 60 PhD theses, 75 papers, and over 50 conference contributions have come out of the collaboration [18]. The detector configuration was upgraded between each data set. The initial setup used a 3.9kG conventional solenoid due to the accidental destruction of the proposed superconducting magnet. A new superconducting magnet at 13.25kG was installed before the second data set was taken [11]. It was at this time that the Two-Gamma collaboration merged with the TPC collaboration. While waiting for SLC construction, the Inner Drift Chamber, with resolution $\sim$500μm, was replaced by a Vertex Chamber with $\sim$30μm resolution in late 1986 [14]. This thesis contains the only analysis done on the data from the latest detector configuration (see Figure 9). See Table 5 for a brief description of the detector components. The analysis described in Chapter IV relied mainly on measurements from the VC and TPC detectors [for descriptions of the operation of other detector components, see references 19 through 27].

The TPC detector was clearly one of the major achievements of the collaboration. With a pressure more than twice that of current detectors, it has produced the world's first and best dE/dx separation of particle type with simultaneous high quality tracking ($\sim$180 hits per track in the r-z view) [33]. These measurements were done in the following way [34]. Charged particles left a trail of ionized atoms as they interacted with atomic electrons. Particles of measurable momenta were deflected infinitesimally in these interactions, but the occasional nuclear scattering was significant in the solid detector components, which was kept to a minimum (0.0745 radiation lengths before the TPC in
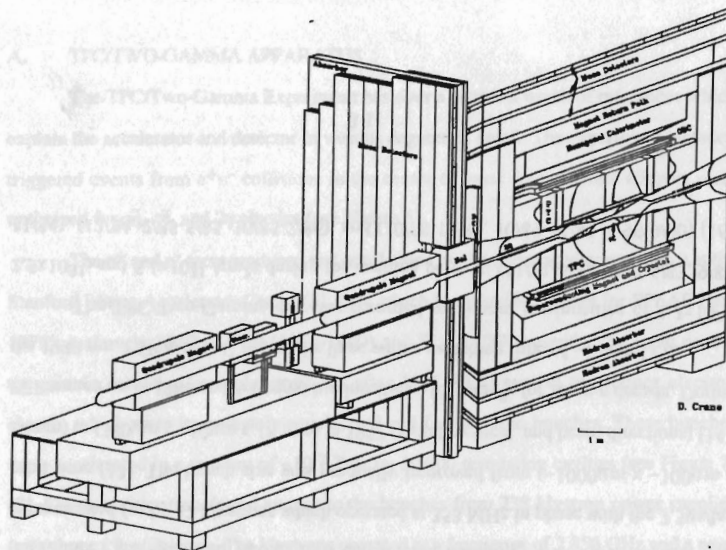
Figure 9. 1988-90 TPC/Two-Gamma Detector Configuration.

Table 5. 1988-90 TPC/Two-Gamma Detector Configuration [11,14,28,29,30,31,32].

BP	Beam Pipe : 3.88cm inner radius	0.0075 radiation lengths of titanium (radially), beryllium, kapton, then beryllium (the VC spreader tube) maintained a vacuum down to 2×10^{-9}Torr. Water cooling compensated for beam induced heating outside the central detector.
VC	Vertex Chamber 4.87-15.11cm radius	0.0190 radiation lengths consisting of 14 layers of aluminum-mylar tubes in 4atm $Ar+CO_2+CH_4$ (49.5:49.5:1.0) surrounding 984 total wires held at 4.0kV. The ~30μm xy position resolution allowed for good xy tracking. No z information was measured.
ODC	Outer Drift Chamber 119-124cm radius	A 0.976 radiation length analysis magnet was inside it. 0.0653 radiation lengths consisting of 216 proportional wire cells were arranged into 3 layers in 1 atm of $Ar+CH_4$ (4:1). The resolution was ~610μm. The ODC was used to detect photon conversions in the magnet coil.
TPC	Time Projection Chamber 22.25-97.05cm radius	A 0.0480 radiation length carbon fiber pressure wall was inside it. A 0.081 radiation length hollow cylinder in 8.5atm of $Ar+CH_4$ (4:1) used field wires at the ends and center to form an E-field of 55kV/m (anti-) parallel to the 13.25kG B-field and beamline. 6 sectors at each end contained 183 sense wires (every 4mm) alternating with field wires, both over 1152 sense pads (7.5mm wide) in rows (every 4.8 or 5.2cm). The average drift time of 30μs gives the 3 dimensional position information. The resolution at the best 70% of the hits (of all the tracks) was 150μm in xy and 205μm in z (for dip angles of -45° to +45°). Tracks with P>150MeV had $(dP/P)^2 = (0.015)^2 + (0.011P)^2$. The TPC cylinder completely covered 2π steradians and partially covered ~1.5π additional steradians, and was used for tracking and particle identification.
HEX	Hexagonal Calorimeter hexagon ~150cm radius	A 10.4 radiation length shower sampling calorimeter operated in limited Geiger mode. Each of 6 sectors consisted of 40 layers of 3.2 mm Pb coated with Al stripes (held at 1.4kV) in 1 atm $Ar+NO_2+methylal$ (92.3%,5.5%,2.2%). γ detection was seen down to 400MeV with ~17mrad average resolution and $(\delta E/E)^2=(0.17(E)^{-0.3})^2+(0.014E)^2$. The ~18% energy resolution for bhabha events in 1986 was found to be the same in 1990. The HEX has been used for energy, position, and direction measurements.
Muon	Muon Barrel and Doors ~2.3 to ~3.3 m radius ~2.8 to ~3.3 m away	4 layers (3 for Muon Doors) of triangular drift tubes in 1 atm $Ar+CH_4$ (4:1) alternated with Fe absorbers. In the last data set these were too noisy to be of use. Previously the resolutions were ~1cm and they were used for muon identification.
PTC	Pole Tip Calorimeter ~1.1 to ~1.5 m away	13.5 radiation lengths consisting of 39 layers of 186 wires and 12 layers of 93 wires, were in proportional mode in 8.5atm $Ar+CH_4$ (4:1). The resolution was found to be ~8mrad in position, and $\delta E/E = 0.11(E)^{-0.5}$ for $E < 10$ GeV and 6% for bhabhas. The PTC was used as a luminosity monitor as well as for energy/position measurements.
NAI	Sodium Iodide Array 45-170mrad at both ends	60 NaI(Tl) crystals at each end had ~4mm resolution and had $\delta E/E = 1.2\%$ for bhabhas. The NAI was used for 2γ analysis.
DC	Drift Chambers 45-220mrad	1 chamber at the South and 1/2 to the North (broken wire) until their destruction in the 1989 earthquake. The resolutions were ~300μm and $(\delta p/p)^2 = (0.026)^2 + (0.008p)^2$. The DCs were used for 2γ analysis.

Figure 10. dE/dx(P) Separation of Particle Mass With the TPC
(tracks with >80 wires and <20% P resolution).
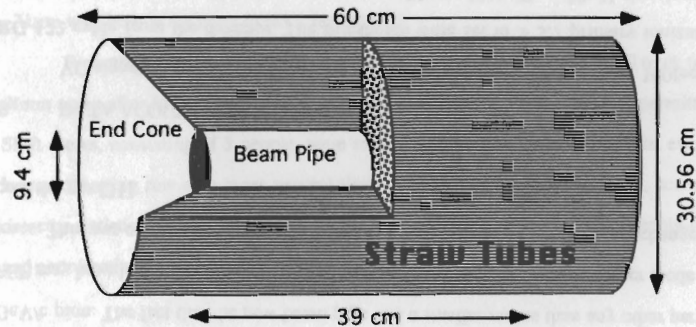
Figure 11. Vertex Chamber Geometry [14,36].

the latest dataset). The ion trails were helical due to the axial magnetic field, with a radius determined by the particle momenta and B-field strength ($R=P_\perp/0.3B$). The ionization electrons drifted towards the endcaps in the TPC's axial E-field where they were recorded by the sense wires and pads. Transverse diffusion of drifting electrons was suppressed by the B-field, increasing resolution. The time dependence was equivalent to z-position information (the z direction was roughly SE parallel to the e⁻ beam, and the y direction was vertical). With the tracks defined in 3 dimensions, the perpendicular momenta could be scaled into total momenta, completing the set of 3 dimensional position and momentum measurements. The dE/dx(P) particle type separation was done by measuring the amount of ionization with the sense wires or pads (the wire measurement was usually better). The observed ionization was linearly fit in both dE/dx and the relativistic parameter $\beta\gamma$ (=P/m) to an assumed shape. Rescaling the resulting curve for different masses led to the predicted ideal distributions of dE/dx(P), where clear differences are seen between particle types except in the crossover regions (see Figure 10)

The main detector difference between previous theses and this one is that the vertexing detector was upgraded before the 3rd data set. The improved resolution made VC tracking possible, increasing considerably the analysis efficiency. The previous chamber, the Inner Drift Chamber, consisted of 4 layers of 60 wires in the TPC gas (total .101 radiation lengths) surrounding a beam pipe (0.026 radiation lengths at 8.5 cm inner radius) from 13.25 to 19.45cm [35]. The new chamber, the Vertex Chamber, was positioned inside the TPC pressure wall (0.0480 radiation lengths) and surrounded a smaller beam pipe (0.0075 radiation lengths at 3.88cm inner radius). Outer layers had more tubes of longer length (36,36,48,48,60,60,72,72,84,84,96,96,96,96 tubes/layer), so ~3.56π steradians were covered by all 14 layers, and an additional ~0.326π steradians were covered by at least one layer (see Figure 11). Each tube consisted of a gold plated tungsten wire of 30μm diameter surrounded by aluminum foil and a mylar straw (2 layers

35   36

of opposite pitch) bonded with polyethylene at a radius of 0.162 to 0.166 inches (~4mm) [31]. The layers were supported at the ends by aluminum eonical endplates. The VC was operated with a nonuniform E-field and unsaturated gas, leading to very nonuniform velocity-time relationships. Additionally, construction and installation alignment tolerances were very relaxed, reducing the cost of the upgrade (to about 10^5). These effects were removed by a detailed software position survey. The observed resolution of ~30μm is smaller than the expected beam pipe multiple scattering contribution of 50μm for a 1 GeV/c pion. The fact that the new beam pipe had a smaller radius than any other part of PEP may have led to the observed 60Watt heating in the detector through higher mode RF loses. This was compensated for by increasing the flow rate and using a heat exchanger to cool the gas [31].

B.   DATA ACQUISITION

VC signals were acquired by preamplifiers and discriminators placed 100feet of RG-172 cable from the detector. The thresholds were set to > 3.7 primary ionization electrons, and the integration times were set to 20nsec [31]. The ~30μV signals were amplified, discriminated, and directed to the TDC and triggering electronics. The digitized TDC outputs were sent to the large data buffer (LDB) and then the VAX where calibration pedestals were subtracted. TPC signals from wires (xy position and ionization magnitude) and pads (xy position and arrival time) were sent to preamps at the edge of the TPC sectors and then to shaper amplifiers 100feet away, in the electronics house. The ~500nsec signals were sent to the triggering electronics as well as sampled by CCD shift registers every 100nsec, producing a 45.5μsec data buffer (large enough to hold an entire event since drift times were <30μsec) [29]. If there was a good trigger, the CCD's were read out to ADC's and TDC's in the electronics house to be digitized and sent to the VAX (via the LDB) where calibration pedestal subtraction occurred.

Triggering occurred in three levels. In order to reduce space charge distortions of the E-field due to ionization prior to the $q\bar{q}$ production, a gated grid was normally on just inside the sense wire planes which prevented ions from passing through. A good pre-pre-trigger (which took up to 0.5μsec to form) switched off the gated grid and allowed complete TPC signals to become available within 1μsec [29]. Pre-pre-triggers occurred when any one of five requirements was met (a minimum energy seen in the PTC or HEX, a PEP9 criterion, a random run setting, or a charged criterion). A charged pre-pre-trigger required two VC tracks and either two VC-TPC coincidences or one VC-ODC coincidence [37]. VC tracks were found by defining azimuthal cells using layers 11+12, 12+13, and 3+4. The cells were one third of a straw across, and right-left ambiguities in the first layer were removed with the second layer's information. A VC track at this level was defined as a coincidence between a cell in layer 11+12 (or 12+13) and the corresponding 3 cell cluster in layer 3+4 [38]. This use of the VC in the pre-pre-trigger was an improvement over the previous IDC and was one of the reasons for the upgrade. The VC track criterion was effectively a transverse momentum cut at about 200MeV/c [36]. The TPC signals came from tracks outside the gated grid, and ODC signals required hits in two of three layers. Coincidences were overlaps in time and angle in the xy plane (the ODC had 15° sections, the TPC had 30° sections) [37]. The second level of triggering was the pre-trigger which also used any of several similar criteria. The charged pre-trigger required two VC-ODC coincidences or two TPC wire group signals (requiring tracks at 45° to ~68° from vertical) or one of each, and took under 7.5μsec to form [29]. The final level of hardware triggering was a set of 7 different track criteria any one of which would form a good trigger (the charged TPC two-ripple trigger was particularly relevant for $q\bar{q}$ event triggering). These 7 were optimized for $q\bar{q}$, $\tau\bar{\tau}$, and 2γ events, and required 35μsec to decide [29]. Since bunch crossings occurred every 2.44μsec the first trigger level can reject an 'event' before the next crossing. Complete event digitization took ~100msec

leading to an observed hardware trigger rate of 1 to 2Hz [30]. Even though deadtime caused 10 to 20% of the bunch crossings to be ignored, the $q\bar{q}$ trigger efficiency was over 99% for the remaining collisions [30].

Each detector was regularly calibrated providing up-to-date channel pedestals, dead channel identification, and individual channel gain factors (the later were adjusted to within a nominal range by tuning the voltage on each channel). The PTC detector, built and maintained by the UCLA group, was software calibrated at least every 2 weeks during data taking. Test pulsing PTC channels was remotely done on both sides of the capacitive coupling between the detector wire and preamp in order to determine the status of each wire. 4.7% of the 1548 channels were inoperative by September 1990 (52 broken wires or capacitors and 20 bad preamps). The TPC pedestals and gain curves were set by test pulsing the shielding grid (wires between the sense wire plane and gated grid that formed the E-field) about once a month. An online monitor program allowed shift operators to adjust individual thresholds as needed. VC thresholds were occasionally adjusted as well. The use of a detailed software position survey improved the VC resolution by removing error contributions from construction uncertainty (~57μm) and tube warpage (~13μm to ~31μm wire bow in the inner to outer layers) [31].

From the LDB, the online data acquisition program stored events to 9 track tapes (8mm tapes after May, 1990) after doing a little software analysis (as time permitted). Shift crews, consisting of 3 people, were responsible for hardware inspections every 4 hours, changing raw data tapes several times a shift (with high luminosity), scanning detector statistics printouts by hand for anomalies, resetting digitizer power supply trips, and coordinating detector turn-on and turn-off with PEP control.

C. DATA PRODUCTION ANALYSIS

Recorded events were labeled by experiment, run, and event number. Experiments 10-13, 14-18, and 19-20 referred to the 1st (low B-field), 2nd (high B-field), and 3rd (vertex chamber) data sets. A typical run consisted of about 1500 to 2000 events. Production analysis of the raw data to form data summary tapes (DST's) included event filtering; various calibrations and corrections; track finding, fitting, and extrapolating; dE/dx(**P**) analysis; interaction point vertexing; and secondary vertex finding (K⁰'s and Λ⁰'s; see chapter IV) [see Figure 12]. Event filtering was done in parallel with data acquisition with the software module *Preanalysis* which looked at TPC pad signals to verify the trigger and rejected 40% of them prior to writing to tape [30]. Calibrations were applied in the modules: *CalibPTC, CalibHEX, DC_Setup, (Pad)Cluster, (Wire)Cluster, VC_Setup, Mu_Setup,* and *PEP9* . The results of ⁵⁵Fe irradiation calibration of the TPC (using permanent sources) formed a monthly gain map which was used in *(Pad)Cluster* and *(Wire)Cluster.* Track finding was performed in the modules *WirePat* and *VCPat* . *VCPat* 's efficiency for finding short tracks in the VC (such as $\Sigma^{\pm}$ decays) was very low, but improving it didn't seem worthwhile. Figure 13 shows two beam's-eye-views of an event, one close up of the VC hits and one showing the HEX showers (both show the fitted track orbits as well). TPC tracks were combined with VC tracks in the module *Combine,* and a final fit to the particle's orbit was done in the module *Fitful . Extrap* was the name of the module that associated these orbits with hits in the PTC, HEX and MUON detectors.

The module *Distort* recalculated the TPC positions using corrections for various distortions including: position corrections for each pad row and azimuthal interval (the angle in the xy plane); curvature and track angle corrections in azimuthal intervals; E-field, B-field, and E-B divergence distortion corrections; time dependent grid potential corrections; time dependent VC-TPC misalignment corrections (rotations and translations
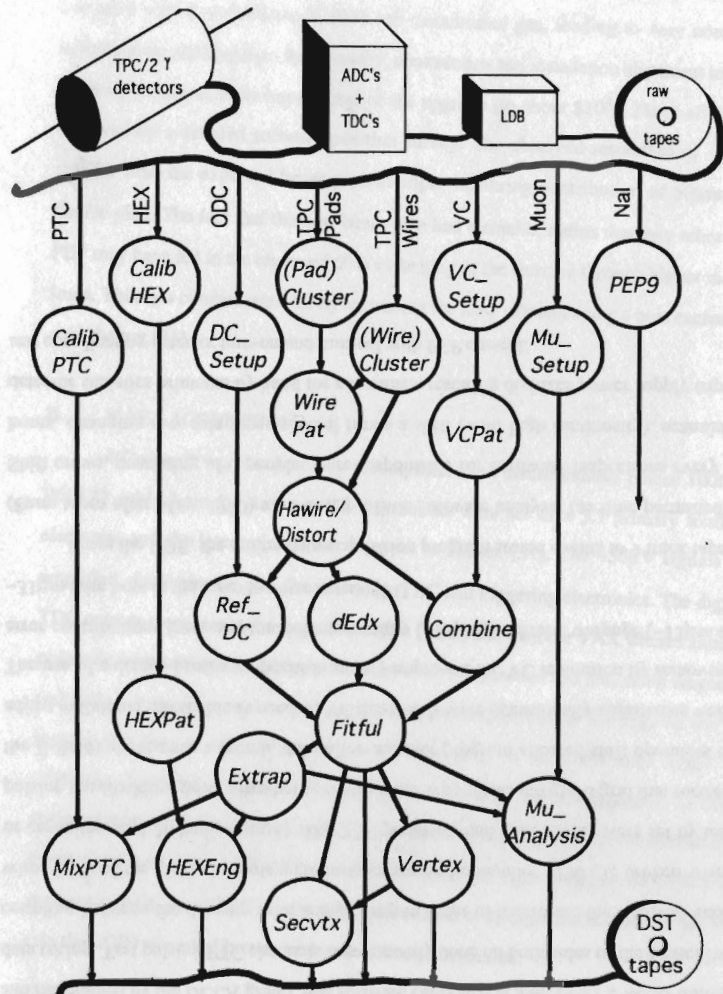
Figure 12. Data Acquisition and Production Analysis Flowchart.
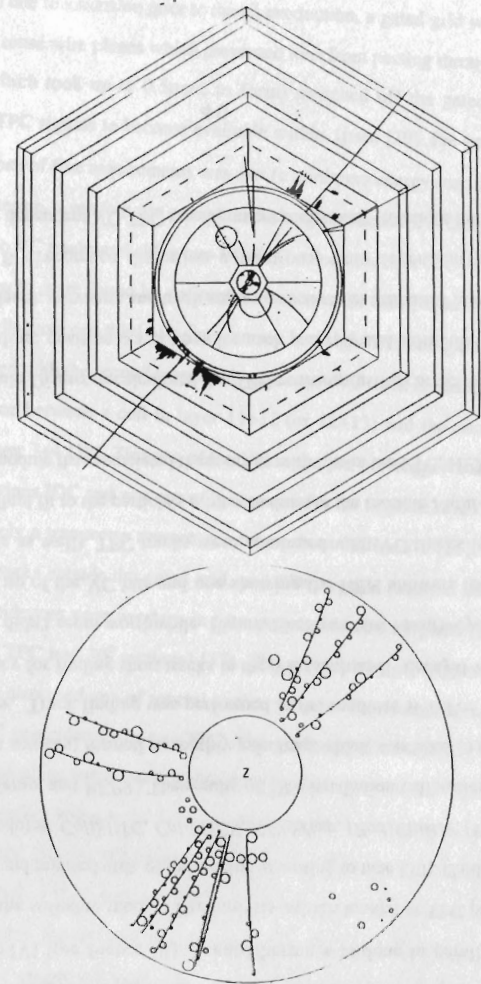
Figure 13. Online Event Displays of a Hadronic Event.

41

42
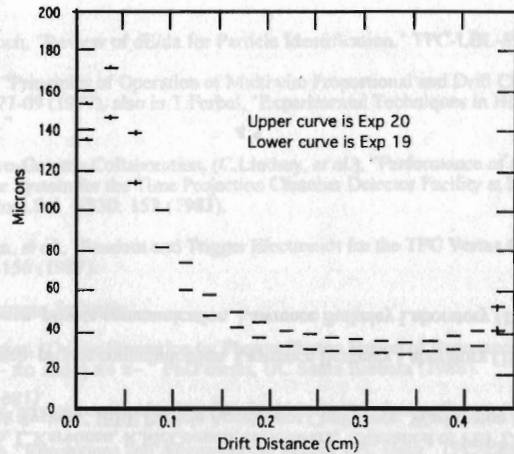
Figure 14. VC Position Resolution as a Function of Drift Distance (bhabha tracks) [39].

about x, y, or z). One end of the TPC showed dip angle dependence of the curvature, the correction of which considerably improved the momentum resolution. After calibrations were completed, the resolution seen in experiment 19 was $(dP/P)^2 = (0.015)^2 + (0.0102P)^2$ where P is in GeV. After combining with VC tracks, this resolution became $(0.015)^2 + (0.0043P)^2$, and became $(0.015)^2 + (0.0040P)^2$ after a primary vertex fit. Experiment 20's corresponding resolution was a little worse: $(0.015)^2 + (0.0110P)^2 \rightarrow +$ $(0.0044P)^2 \rightarrow + \sim(0.0041P)^2$. The 2nd data set, without the benefit of a VC, had a resolution of $(0.015)^2 + (0.012P)^2$ [39]. VC straw-by-straw and run-by-run calibrations (using bhabha events) of the time-to-distance relation, possible tilting of wires in z, and off center wire bending improved the position resolution (see Figure 14). The VC position resolution increase near the anode wires was not completely understood [31]. The observed VC resolution at drift distances of 2-4mm after calibration was 29μm for hits

and 58μm for impact parameters in experiment 19 (for experiment 20 these were 36μm and 71μm, again somewhat worse) [39].

Prior to the TPC's construction, detectors had insufficient sampling density to remove the effects of the long 'Landau tail' from occasional δ-rays on the average dE/dx. The 'truncated mean' Energy (dE/dx) loss for TPC tracks was defined as the average of the lowest 65% of the wire hits (occasionally pad hits) in dE/dx, and was calculated in the module, *Dedx*. 65% was chosen based on early Monte Carlo studies, and gave very good results [14]. The dE/dx distribution was the sum of a Gaussian (from low energy atomic excitations) and a Landau curve (from δ-rays). The number of wires (pads) per unit length was set to minimize the dE/dx width (a Gaussian width increases with the number of measurements/length whereas a Landau curve's width is constant) [14,30]. The resulting dE/dx(P) was compared with the ideal relationship (formed by looking at p$^+$, π$^+$, cosmic μ$^-$, γ → e$^+$e$^-$, and bhabha e$^-$; each in a different βγ interval) and a χ^2 was calculated for e, μ, π, K, and p hypotheses. The truncated means were corrected for time, dip angle (in the $z_\perp$ plane), and measurement-multiplicity-dependent variations. The resulting dE/dx resolution was 3.1% for tracks with over 80 wire hits in the most recent dataset [40].

Primary vertices, where the e$^+$e$^-$ → γ → q$\bar{q}$ occurred, were found with a software module called *Vertex* by fitting all the tracks to a common origin point and then rejecting those with large deviations before refitting. A time dependent average interaction point was calculated and used as a constraint in the vertex fit.

An incredible amount of additional research and programs supported and helped generate the production analysis outlined above.

D.   REFERENCES

Linac and PEP

1. M.James, R.Miller, "A High Current Injector for the Proposed SLAC Linear Collider." IEEE Particle Accelerator Conference, Washington DC 1981: 3461 (1981).

2. Marc Ross and John Seeman, private communication. Stanford Linear Accelerator Center (1993).

3. Z.Farkas, C.Kruse, G.Loew, R.Mcconnell, "Design And Performance Of The SLAC RF Drive System." IEEE Trans.Nucl.Sci. NS14 (3): 223 (1967).

4. J.Clendenin, G.Loew, R.Miller, J.Pellegrin, J.Truher, "Single Bunch Beam Measurements for the Proposed SLAC Linear Collider." IEEE Particle Accelerator Conference, Washington DC 1981: 2452 (1981).

5. H.Wiedemann, "The SLAC Linac Collider (SLC) Project." IEEE Particle Accelerator Conference, Washington DC 1981: 2016 (1981).

6. R.Kofler, private communication. Lawrence Berkeley Laboratory (1990-3).

7. C.S.Fordham, "Neutral Kaon and Lambda Production in Electron-Positron Annihilation at 29GeV and the Z Boson Resonance." PhD Thesis, SLAC-374 (1990).

8. J.Peterson, K.Brown, J.Truher, "Design Features and Operational Characteristics of the PEP Beam Transport and Injection System." IEEE Trans.Nucl.Sci. NS28 (3): 3059 (1981).

9. "The PEP Handbook", a continuously updated ring binder at SLAC, started in 1977.

10. M.Sands, "The Physics of Electron Storage Rings: an Introduction." SLAC-0121 (1970).

11. M.K.Sullivan, private communication. Stanford Linear Accelerator Center (1990-3).

12. T.Jackson, "Design and Performance of PEP DC Power Systems." IEEE Particle Accelerator Conference, Washington DC 1981: 2737 (1981).

13. M.Allen, L.Karvonen, R.McConnell, H.Schwarz, "Operation of PEP Longitudinal Feedback System." IEEE Particle Accelerator Conference, Washington DC 1981: 2317 (1981).

14. G.R.Lynch, private communication. Lawrence Berkeley Laboratory (1990-3).

15. M.T.Ronan, private communication. Lawrence Berkeley Laboratory (1990-3).

TPC /Two-Gamma Hardware

16. TPC/Two-Gamma Collaboration, "TPC/Two-Gamma Tape Log Book". Stanford Linear Accelerator Center (1990).

17. K.Derby, "Integrated Luminosity for Exp. 14-18." TPC/Two-Gamma Internal Note (1987).

18. The SPIRES Database, Stanford Linear Accelerator Center (1991).

19. J. Huth, D.Nygren, "Feasibility Tests of a High Resolution Sampling Radial Drift Chamber." Nucl.Instr.Methods A241: 375 (1985).

20. TPC/Two-Gamma Collaboration, (H.Aihara, *et al.*), "Performance of the Hexagonal Calorimeter at PEP-4." Nucl.Instr.Methods A217: 259 (1983).

21. TPC/Two-Gamma Collaboration, (M.Yamauchi, *et al.*), "Geiger Mode Calorimeter for Pep-4." IEEE Trans.Nucl.Sci. NS30: 117 (1983).

22. TPC/Two-Gamma Collaboration, (J.Bakken, *et al.*), "A Muon Detection System for the PEP-4 Facility." IEEE Trans.Nucl.Sci. NS30: 67 (1983).

23. R.Koda, "A Test of Quantum Electrodynamics at Small Angles Using the PEP-4 Facility." PhD Thesis, UCLA-85-011 (1985).

24. TPC/Two-Gamma Collaboration, (B.Gabioud, *et al.*), "Measurement of Ionization Loss in the Relativistic Rise Region with the Time Projection Chamber." IEEE Trans.Nucl.Sci. NS30: 63 (1983).

25. TPC/Two-Gamma Collaboration, (R.Madaras, *et al.*), "Spatial Resolution of the PEP-4 Time Projection Chamber." IEEE Trans.Nucl.Sci. NS30: 76 (1983).

26. TPC/Two-Gamma Collaboration, (S.Loken, *et al.*), "Performance of the Signal Processing System for the Time Projection Chamber." IEEE Trans.Nucl.Sci. NS30: 162 (1983).

27. C.Buchanan, *et al.*, "Proportional Mode Calorimeters of the TPC Facility." Gas Calorimeter Workshop Proceedings, Batavia 1982: 284 (1982).

28. G.Cowan, "Amount of Material in the PEP-4 TPC (Experiments 13-18)." TPC-LBL-87-23 (1987).

29. T.K.Edberg, "Inclusive Production of Vector Mesons in e^+e^- Annihilation at $\sqrt{s} =$ 29 GeV." PhD Thesis, LBL-25652 (1988).

30. J.W.Gary, "Tests of Models for Parton Fragmentation in e^+e^- Annihilation." PhD Thesis, LBL-20638 (1985).

31. G.L.Godfrey, private communication. Stanford Linear Accelerator Center (1990-3).

32. G.S.Greenbaum, private communication. Stanford Linear Accelerator Center (1993).

33. G.R.Lynch, "Review of dE/dx for Particle Identification." TPC-LBL-89-03 (1989).

34. F.Sauli, "Principles of Operation of Multiwire Proportional and Drift Chambers." CERN-77-09 (1977), also in T.Ferbel, "Experimental Techniques in High Energy Physics."

35. TPC/Two-Gamma Collaboration, (C.Lindsey, *et al.*), "Performance of a Drift Chamber System for the Time Projection Chamber Detector Facility at PEP." IEEE Trans.Nucl.Sci. NS30: 153 (1983).

36. M.Ronan, *et al.*, "Readout and Trigger Electronics for the TPC Vertex Chamber." LBL-24156 (1987).

TPC/Two-Gamma Software

37. A.R.Barker, "On the Formation by Photon-Photon Fusion of Resonances Decaying to $\pi+ \pi- \pi o$ and $\eta \pi+ \pi-$." PhD thesis, UC Santa Barbara (1988).

38. A.Eisner, private communication. Stanford Linear Accelerator Center (1993).

39. G.Lynch, "Resolutions and Alignments in Recent TPC Data." TPC-LBL-91-02 (1991), and G.Lynch, "B Decay Studies with the TPC at PEP." Heavy Quark Physics Conference, Ithaca NY 1989: 130 (1989).

40. D.Lambert, "Dedx Corrections for Experiments 19-20 and Dedx Resolution for Experiments 14-20." TPC-LBL-91-01 (1991) and private communication (1993).

IV. ANALYSIS

A.   EVENT SELECTION

The data summary tapes (DST's) described in Chapter III were a sequential record of events, each containing several data blocks. The DST blocks and the modules which created them were:

0	Event Header Block	Label_Hadron_v2
1	Vertex Block	Vertex
2	Track Block	Fitfull
3	Calorimeter Block	Hex
4	Muon Block	Muon
5	Monte Carlo Block.	the event generator
6	Secondary Vertex Block	Secvtx

The Event Header Block characterized the event as a whole and included trigger information, analysis code versions, and the results of several selection schemes to identify the event type. The Events selected in this analysis used the following selection criteria applied to 'good TPC tracks':

1	≥5 tracks.
2	The total charged energy in the event > 7.25GeV.
3	The total z-momentum/total energy ≤ 0.4 in magnitude.
4	Tau rejection: hemispheric mass > 2.0, hemispheric number of tracks > 3.
5	The number of tracks with non-zero dip angle > 0.
7	The event vertex radius < 2.0cm & z position < 3.5cm relative to nominal values.
8	At least 5 tracks with e- probability < 0.7 or $\chi^2_{dedx}(e-) > 10$.
9.	At least one track with $\chi^2_{dedx}(e-) > 9$.

Events passing these cuts were flagged in bit 11 of the event_class_2 word in the event header block and will be referred to as 'good multihadronic events' following this section. The resulting signal and signal to noise ratio for Λ's found in the data were used to choose between the bit 11 sample and the slightly looser, bit 10 sample. The smaller sample was chosen, which differed in that cuts 8 and 9 were used.

The Vertex and Track blocks contained listings of reconstructed tracks. The subroutines, *Vertex* and *Fitfull* are discussed in Chapter III. Blocks 3 and 4 were not used in this analysis.

The Monte Carlo Block was used in computer generated events to record the actual (generator level) event as opposed to the event as seen by the detector simulation. This kind of event is necessary for any analysis of this type (possibly all high energy experiments, in fact) because the detector inefficiencies aren't known analytically. Comparisons between the data and the Monte Carlo events are very important since differences can manifest as systematic variations of the results. The GEANT Monte Carlo, used for the first time on TPC/Two-Gamma data, was tuned to data characteristics including $\tau\bar{\tau}$ events, e+e- (bhabha) events, general hadronic event characteristics, as well as K° and Λ° mass widths and S/N ratios. The fraction of events accepted as good multihadronic events in the data sample was observed to be 61% (5810/9148 in experiment 19 and 7469/12654 in experiment 20). The Monte Carlo sample had 65% (30897/47993 for experiment 19 and 45721/70267 for experiment 20) good multihadronic events. The ones failing the selection criterion in the Monte Carlo sample were hadronic events which failed to register on the detector adequately. In the data the rejected sample included two-γ events, $\tau\bar{\tau}$ events, e+e- bhabhas, beam-gas collision events, and beam-beampipe collision events. Experiment 20 was observed to have significantly more of the last two types of background events than experiment 19 due to beam dynamics and other accelerator characteristics. The triggering was not adequately simulated in the Monte Carlo, however the purity of both data and Monte Carlo good multihadronic event samples has been estimated to be about 99% [1]. Therefore, results which are normalized to the number of events should be free from systematic variations due to the event selection.

B.   INCLUSIVE SELECTION

K°, Λ°, Ξ⁻, $\Sigma^{*\pm}$, and Ω⁻ inclusive decays have been reconstructed. Based on Monte Carlo studies, it was determined that the vertex chamber track finding routine was not efficient enough to reconstruct $\Sigma^{\pm} \Rightarrow n°\pi^{\pm}$ decays based on the $\Sigma^{\pm}$ and $\pi^{\pm}$ tracks ($c\tau_{+}$=2.4 and $c\tau_{-}$=4.4cm). The reconstruction procedure began with a simple pairing of

K°	$\Rightarrow \pi^{+}\pi^{-}$		weak decay
Λ°	$\Rightarrow p^{+}\pi^{-}$		weak decay
Ξ⁻	$\Rightarrow \Lambda°\pi^{-}$	$\Rightarrow (p^{+}\pi^{-})\pi^{-}$	weak decay
$\Sigma^{*\pm}$	$\Rightarrow \Lambda°\pi^{\pm}$	$\Rightarrow (p^{+}\pi^{-})\pi^{\pm}$	strong decay
Ω⁻	$\Rightarrow \Lambda°K^{-}$	$\Rightarrow (p^{+}\pi^{-})K^{-}$	weak decay
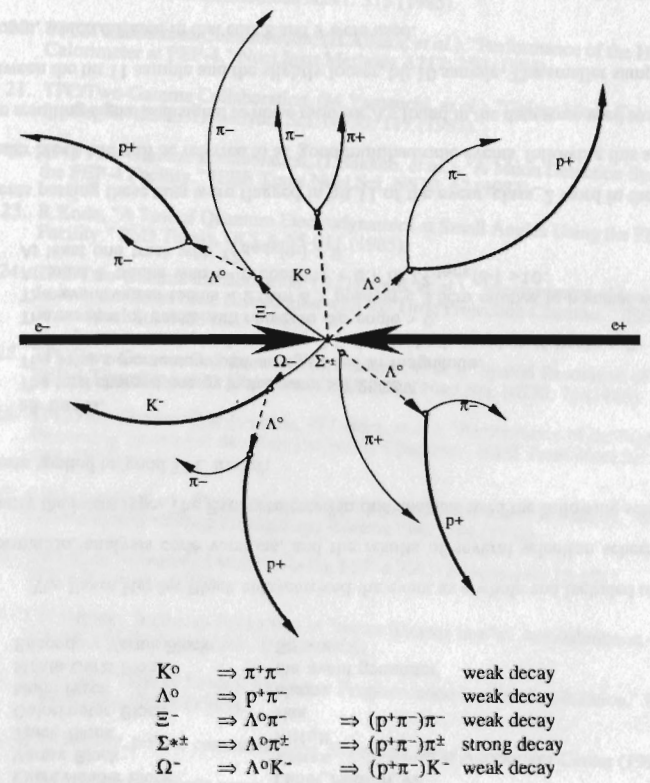
Figure 15. Representation of Various Decay Chains.

Table 6. Reconstruction Cut Table (reject if...).

	K°	Λ°	Ξ⁻	Σ*±	Ω⁻
LIGHT DECAY PRODUCT CUTS:	π	π	π	π	K
dp/p	>0.15	>0.20	>0.05	>0.05	>0.05
dp/p² and	>0.20	>0.20	-	-	-
orbit fit χ^2/degrees of freedom	-	-	>4.5	>2.0	>4.5
dE/dx χ for correct type	>3.0	>4.0	>3.0	>3.0	>3.0
dE/dx $\chi^2_{correct} - \chi^2_{best}$	>5.0	>8.0	>1.5	>1.5	>0.5
impact parameter in σxy	<1.3	<1.5	-	>2.0	-
impact parameter in σz and	<3.0	<1.5	-	-	-
HEAVY DECAY PRODUCT CUTS:	π	p	Λ	Λ	Λ
dp/p	>0.15	>0.20	>0.10	>0.15	>0.10
dp/p² and	>0.20	>0.20	-	-	-
dE/dx χ for correct type	>3.0	>3.5	-	-	-
dE/dx $\chi^2_{correct} - \chi^2_{best}$	>5.0	>1.5	-	-	-
impact parameter in σxy	<1.3	<0.75	-	-	-
impact parameter in σz and	<3.0	<2.0	-	-	-
mass	-	-	>0.009	>0.009	>0.009
mass/err	-	-	>4.0	>4.0	>4.0
3-dimensional deflection	-	-	<0.9	<0.9	<0.9
#wires > 20 or #pads>3	-	on	-	-	-
kinematic fit $\chi 2$	-	-	-	>10.0	-
CANDIDATE CUTS:	K°	Λ°	Ξ⁻	Σ*±	Ω⁻
best ID of tracks is not e+e-	on	-	-	-	-
incoming track length (vertex in VC)	>3.0	>3.0	>13	>13	>13
incoming track length (vertex in TPC)	>3.0	>2.0	>10	>10	>10
daughters miss each other in σxy	-	-	>0.1	>0.1	>0.1
radial vertex separation in cm	-	-	<1.0	<0.0	<1.0
vertex χ^2 in z	>8.0	>8.0	-	-	-
vertex fit χ^2	>8.0	>12.0	>20.0	>20.0	>20.0
max(impact parameter of daughters)	-	-	<2.0	>60.0	<2.0
cos(track deflection angle, 2dim)	<-0.5	<0.0	-	-	-
cos(deflection angle, 3dim)	<0.98†	<0.95†	<0.6	-	<0.6
flight length in σxy	<2.0	<1.5	<0.5	>10.0	<0.5
total P_t/P_Λ	-	-	-	>0.7	-
nonradial $(P_\Lambda/P_t)^2$	-	-	>300.0	-	>300.0
cos(Pgeom•Pmeas) in xy	-	-	<0.96	-	<0.96
(Pg-Pm)/(Pg+Pm) in z	-	-	>20.0	-	>20.0
survival probability (exp-mR/Pτ)	-	-	<0.09	-	<0.09
	-	-	>0.95	-	>0.95
kinematic fit $\chi 2$	>30.0	-	-	-	-

† only applied to vertices inside detector material.

51

any two TPC tracks as hypothetical decay products (see Figure 15). A series of cuts was applied to various parameters to reduce the background levels and minimize the systematic and statistical errors on the resulting rates (see Table 6). Decay products of the $\pi^\pm K^\pm p^\pm$ variety were selected with simple track cuts on momentum resolution, track fit χ^2, dE/dx-probability for particle type, distance of closest approach to the event vertex in standard deviations, and number of TPC hits. The Λ°'s used as hyperon decay products were selected from the reconstructed samples and were required to satisfy mass constraints in GeV and standard deviations, a deflection angle cut, and a kinematic fit χ^2 (assuming the Λ originated at the event vertex). Pairs of decay products formed candidates and were required to satisfy cuts on the χ^2 probability of being an e+e- pair, the length of track hits prior to the decay vertex of the reconstructed hadron, the separation between the Λ and the track at closest approach to each other, the distance between the hyperon decay and Λ decay vertices, a 3-dimensional vertex fit χ^2 and its z-component analog, the maximum impact parameter of the two daughters in xy or z, the tracks' deflection angle as well as the parents', the flight length in standard deviations in the xy plane, the total momentum ratio, the nonradial momentum component ratio squared, the cosine of the angle between the measured momentum and the geometrically determined momentum, the percent difference in the z direction this deviation caused, the survival probability, and a kinematic fit χ^2 assuming the parent originated at the event vertex.

Cut levels were chosen after lengthy consideration. The statistical uncertainty on the extracted efficiencies was minimized while the systematic error was plateaued in terms of a shift in extracted rate. The systematic variations of the most influential cuts used to reconstruct Ξ−, Σ*± and Ω−, are plotted in Figures 16 through 29. The K° and Λ° systematic errors were smaller and their plots are omitted for brevity. Black dots on the axes indicate cut positions.

52
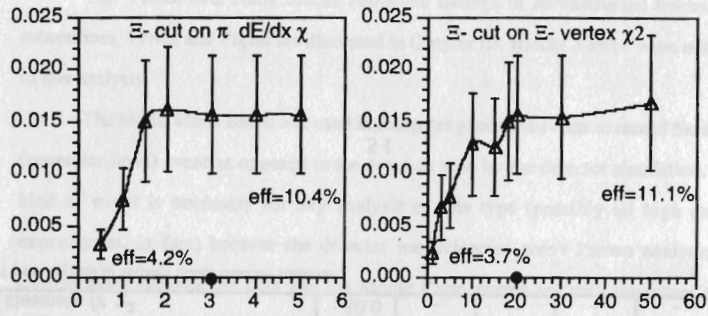
Figure 16. (left) Systematic Variation in the Rate of Ξ^- as a Function of the π dE/dx χ.

Figure 17. (right) Systematic Variation in the Rate of Ξ^- as a Function of its Vertex Fit $\chi 2$.
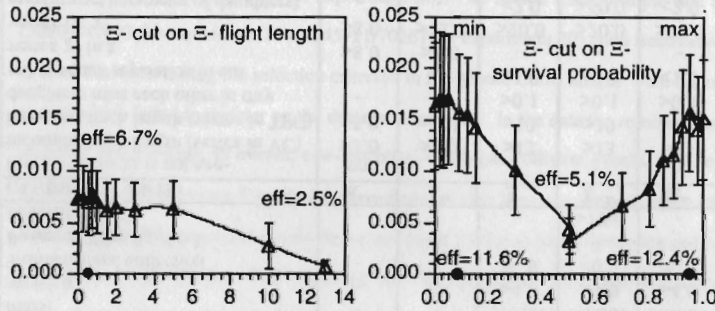
Figure 18. (left) Systematic Variation in the Rate of Ξ^- as a Function of its Flight Length (excluding the good ones >15σ).

Figure 19. (right) Systematic Variation in the Rate of Ξ^- as a Function of its Survival Probability.
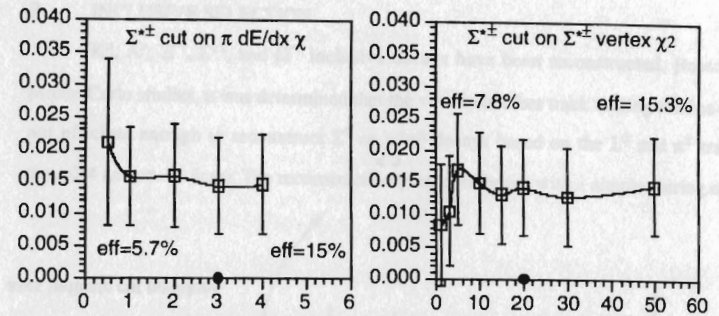
Figure 20. (left) Systematic Variation in the Rate of $\Sigma^{*\pm}$ as a Function of dE/dx χ.

Figure 21. (right) Systematic Variation in the Rate of $\Sigma^{*\pm}$ as a Function of its Vertex Fit $\chi 2$.
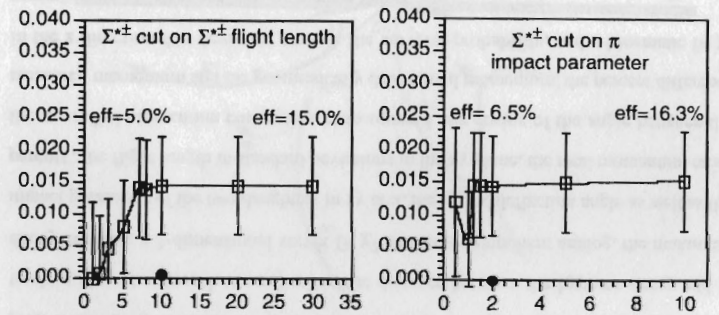
Figure 22. (left) Systematic Variation in the Rate of $\Sigma^{*\pm}$ as a Function of its Flight Length (excluding the good ones >15σ).

Figure 23. (right) Systematic Variation in the Rate of $\Sigma^{*\pm}$ as a Function of the π Impact Parameter.
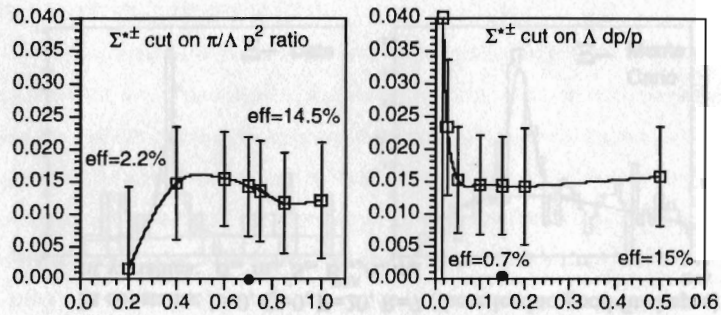
Figure 24. (left) Systematic Variation in the Rate of $\Sigma^{*\pm}$ as a Function of the π/Λ P^2 Ratio.

Figure 25. (right) Systematic Variation in the Rate of $\Sigma^{*\pm}$ as a Function of the Λ dp/p.
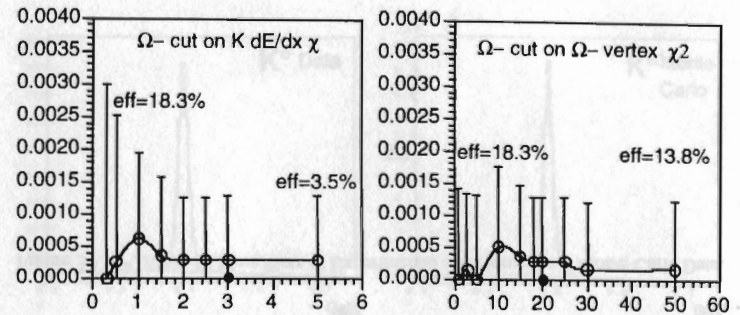
Figure 26. (left) Systematic Variation in the Rate of $\Omega-$ as a Function of the K dE/dx χ.

Figure 27. (right) Systematic Variation in the Rate of $\Omega-$ as a Function of its Vertex Fit $\chi2$.
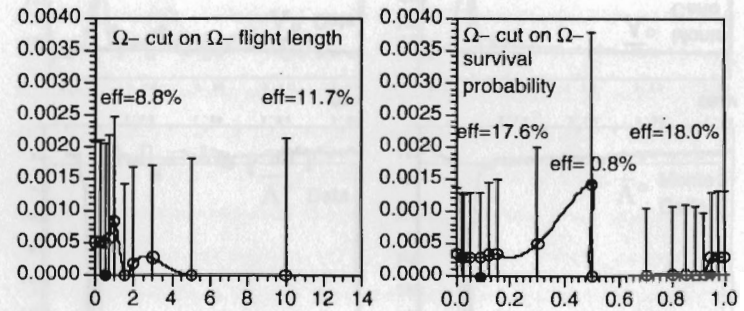
Figure 28. (left) Systematic Variation in the Rate of $\Omega-$ as a Function of its Flight Length (excluding the good ones >15σ).

Figure 29. (right) Systematic Variation in the Rate of $\Omega-$ as a Function of its Survival Probability.

55

56

The Monte Carlo event sample was divided into 'tune' and 'measurement' subsets to avoid false efficiency enhancement due to cut selection. A comparison of extracted efficiencies between the subsets showed no bias and the entire sample was used for efficiency determination. The extracted rates for Λ and $\bar{\Lambda}$ differed considerably (Λ=0.0839±.0061, $\bar{\Lambda}$ =0.1094±.0079, a 2.6σ difference), and so an in-depth search for a systematic bias was performed. The observed data were about the same, but the efficiency was larger for Λ than for $\bar{\Lambda}$. No other systematic bias was found, and there is a 1% chance of such a difference being a statistical fluctuation. There was no way of knowing whether the nuclear interaction cross sections in the GEANT Monte Carlo subprograms FLUKA and GEISHA (both showed similar $\Lambda/\bar{\Lambda}$ bias) were too large for production of Λ or absorption of $\bar{\Lambda}$. In order to minimize the bias, half the Monte Carlo sample was generated by each.

The 4-vectors of the decay products were added and the measured mass and momentum of the parent particles were calculated. The mass distributions show peaks at the expected masses: (K°, Λ°, Ξ^-, $\Sigma^{*\pm}$, Ω^-) = (0.4977, 1.1156, 1.321, 1.385, and 1.672) GeV. Maximum log-likelihood fits were made using generalized Gaussians for the signals and a polynomial distributions for the backgrounds (See Equation 18), and values for the signals were extracted (see Figures 30 and 31).

$$S(m) = \frac{S_o \sigma_1 \sigma_2}{(\sigma_2 - \sigma_1)\,(m-m_o)^2}\left[e^{(m-m_o)^2/2\sigma_2^2} - e^{(m-m_o)^2/2\sigma_1^2}\right]$$
$$B(m) = B_o m^A \left(1+Lm+Qm^2\right)\left(m_B-m\right)^E \qquad (18)$$

where $\sigma_1 = \sigma_o\sqrt{(R^3-1)/(3*R^2(R-1))}$ and $\sigma_2 = R\sigma_1$

fit constants: L=0, Q=0, E=20, R=7 (these lead to good fit shapes)

fit variables: σ_o, m_o, S_o, B_o, A, m_B
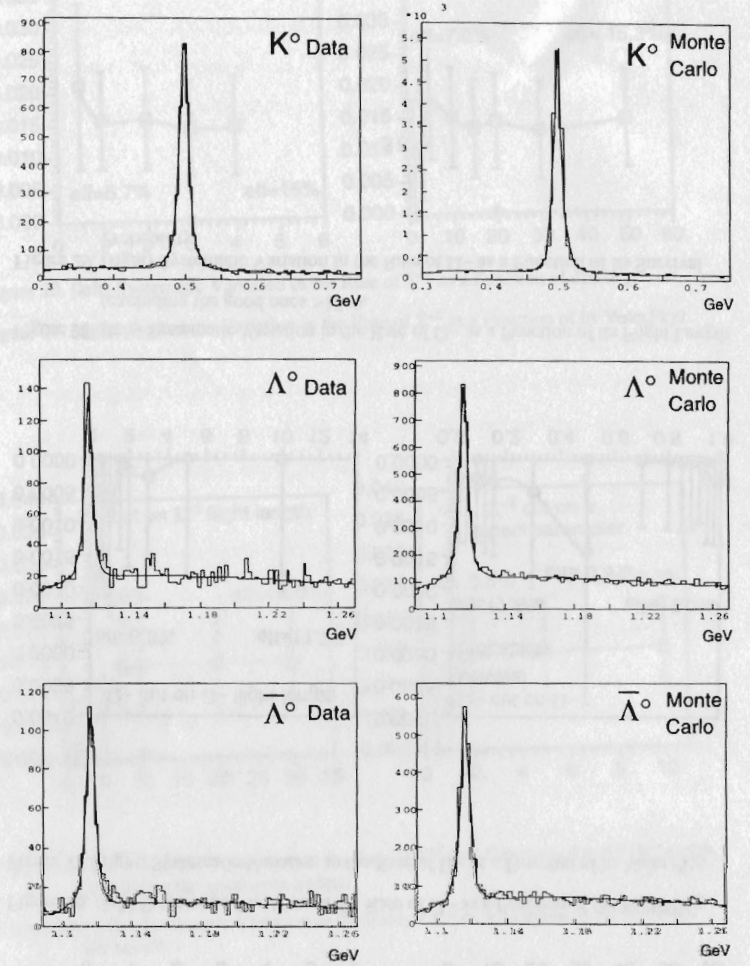
Figure 30. K°, Λ° & $\bar{\Lambda}^\circ$ Mass Plots of Experimental and Normalized Monte Carlo Data.
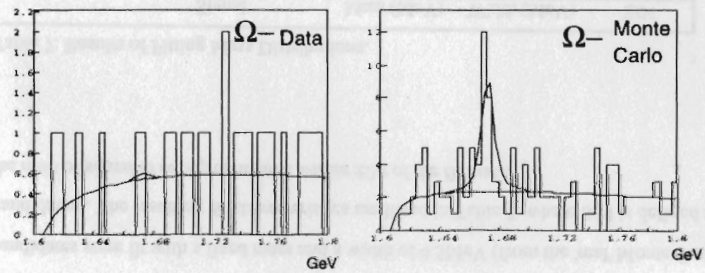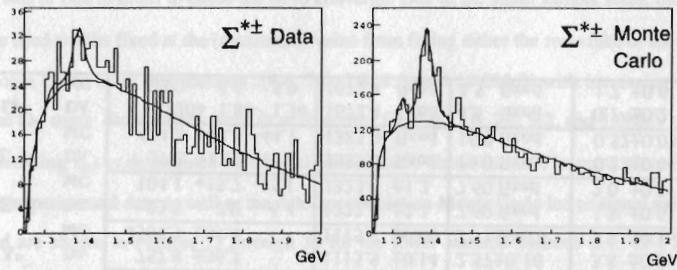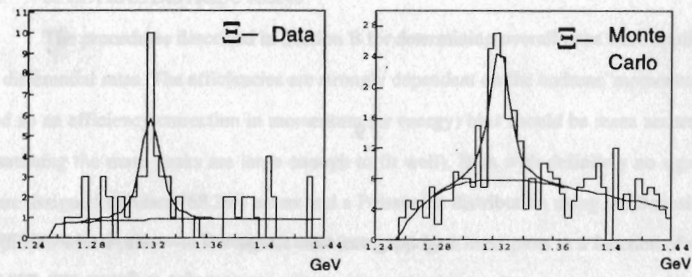
Figure 31. Ξ⁻, Σ*±, and Ω⁻ Mass Plots of Experimental and Normalized Monte Carlo Data.
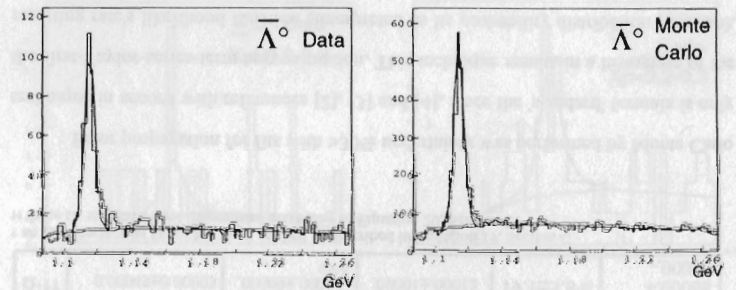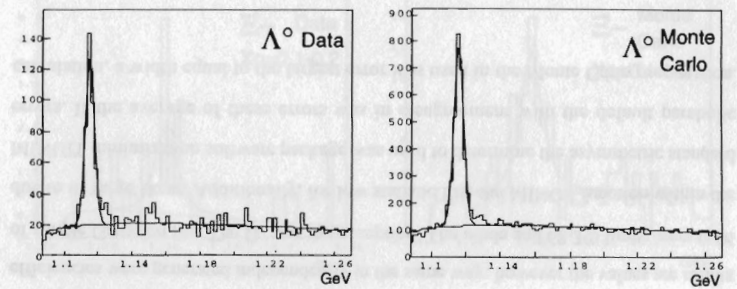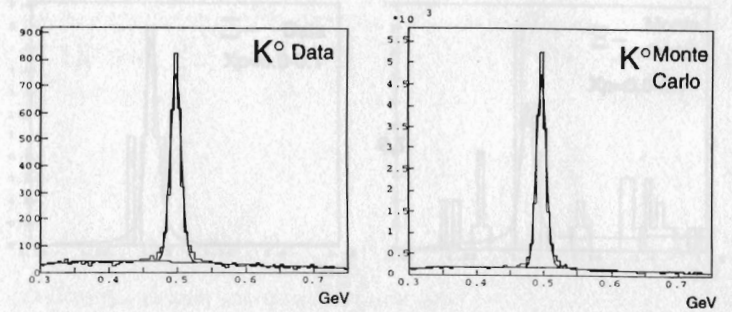
Figure 32. Several Mass Plots Fit with a Single Gaussian.

This generalized Gaussian is the result of a simple integration in $d\sigma$ over a Gaussian with a width distribution of $1/\sigma^3$ (a continuous function chosen for it's integration properties). A single Gaussian fit was studied as well and was shown to form poorer fits (see Figure 32). The K° and Λ° threshold effects were a source of systematic bias in the fitting and so the mass regions were restricted to 0.3-0.75GeV and 1.09-1.27GeV. The $\Xi-$ mass distributions were fit with a width fixed at the value determined from the Monte Carlo distribution (7.6 ± 0.1MeV). The $\Sigma^{*\pm}$ candidates were fit with two generalized Gaussians (background Ξ^- and $\Sigma^{*\pm}$) with fixed masses and widths (7MeV and 16MeV). The $\Omega-$ candidates were fit with a fixed mass and a width of 4.5MeV (from the 'real' Monte Carlo candidates). The resulting fit characteristics are listed in Table 7, where S/N is defined as the ratio of signal to background area within $\pm 2\sigma$ of the fit mass.

Table 7. Results of Fitting Mass Distributions.

		Signal	Mass (MeV)	Width (MeV)	S/N
K°	DA	3089.8 ±62.2	497.72±0.17	7.18±0.18	12.8 ±0.9
	MC	17459.4 ±144.5	497.23±0.06	6.26±0.06	18.6 ±0.7
Λ°	DA	757.8 ±36.3	1115.5 ±0.14	2.57±0.16	3.8 ±0.3
	MC	4567.3 ±89.4	1115.5 ±0.06	2.71±0.07	3.8 ±0.1
$\Xi-$	DA	23.5 + 7.0 - 6.4	1322.4 ±2.2	7.60 fixed	1.8 ±0.6
	MC	104.1 +15.7 -15.1	1323.6 ±1.2	7.60 fixed	2.0 ±0.3
$\Sigma^{*\pm}$	DA	37.2 +17.9 -17.2	1385.0 fixed	16.0 fixed	0.22±0.04
	MC	464.2 +44.8 -44.1	1385.0 fixed	16.0 fixed	0.52±0.03
$\Omega-$	DA	0.20+ 1.88- 1.34	1672.4 fixed	4.5 fixed	0.1 ±0.2
	MC	22.0 + 6.6 - 5.9	1672.4 fixed	4.5 fixed	1.7 ±0.6

When this fitting is repeated for Monte Carlo events, an overall efficiency can be calculated using the event generator's rates (see Table 8).

Table 8. Overall Efficiencies and Rates Therefrom (statistical errors only).

	Generator Rate (499995 $q\bar{q}$)	#/$q\bar{q}$ for MC (76618 $q\bar{q}$)	#/$q\bar{q}$ for Exp (13279 $q\bar{q}$)	Efficiency[†]	Rate
K°	1.3152±0.0016	0.2279±0.0019	0.2327±0.0047	17.0±0.1%	1.373±.030
Λ°	0.19064±0.00062	0.0596±0.0012	0.0571±0.0027	30.3±0.6%	.1884±.0098
$\Xi-$	0.01260±0.00016	0.0014±0.0002	0.0018±0.0008	10.3±1.6%	.0171+.0062 -.0054
$\Sigma^{*\pm}$	0.03314±0.00026	0.0061±0.0006	0.0028±0.0013	17.9±1.8%	.0157+.0076 -.0075
$\Omega-$[††]	0.00045±0.00003	.00009±.00004	.00001±.00012	19.1±5.8%	0.00007 +.00068 -.00065

† an Ecm correction factor has been applied as described in Equation 19, Section C.
†† these $\Omega-$ statistics were determined according to Equation 20, Section C.

Error propagation for fits with >30% uncertainty was performed by Monte Carlo technique in accord with references [2], [3] and [4], since the 'standard' formula is only the first-Taylor-series-term approximation. This technique results in a histogram of the resulting rate's likelihood function (interpreted as its probability distribution function), from which median and (68.3%) standard asymmetric errors were directly extracted. The efficiencies were generated independently in the same way; however the values are results of simple Gaussian fits. The $\Omega-$ was the exception. The mode and 68.3% limits were used due to its large skew. Additionally, for low statistic fits, the MINOS function within the MINUIT minimization software package was used to determine the asymmetric standard errors. If the average of these errors was in disagreement with the default parabolic calculation, a width equal to the largest error was used in the Monte Carlo propagation.

C. SPECTRAL DISTRIBUTIONS

The procedures described in Section B for determining overall rates were applied to differential rates. The efficiencies are strongly dependent on the hadrons' momentum, and so an efficiency correction in momentum (or energy) bins should be more accurate (assuming the mass peaks are large enough to fit well). Bins with definitely no signal were assigned standard (68.3%) errors and a Poissonian distribution using the Bayesian approach with a prior = 1. The signals were extracted from mass plots as a function of x_p, $-\ln(x_p)$, and x_E, where in some cases the number of background parameters was reduced to two or one in order to cause the fit to converge. Due to the small sample sizes, the $\Xi-$ fits used widths fixed at the (maximum) value from fitting either the real+fake or the real Monte Carlo mass distributions (4.1, 7.6, 7.8, 8.0, and 10.0MeV with increasing x_p). The $\Omega-$ mass distributions were fit with widths fixed at (1.0, 2.8, 9.2, and 1.0MeV with increasing x_p) as determined by the real Monte Carlo distributions. The mass plots from the experimental data as well as the detector simulation Monte Carlo led to signal values, and are shown in Figures 33 through 38 for the lower statistic hadrons (i.e.: $\Xi-$, $\Sigma^{*\pm}$, and $\Omega-$).
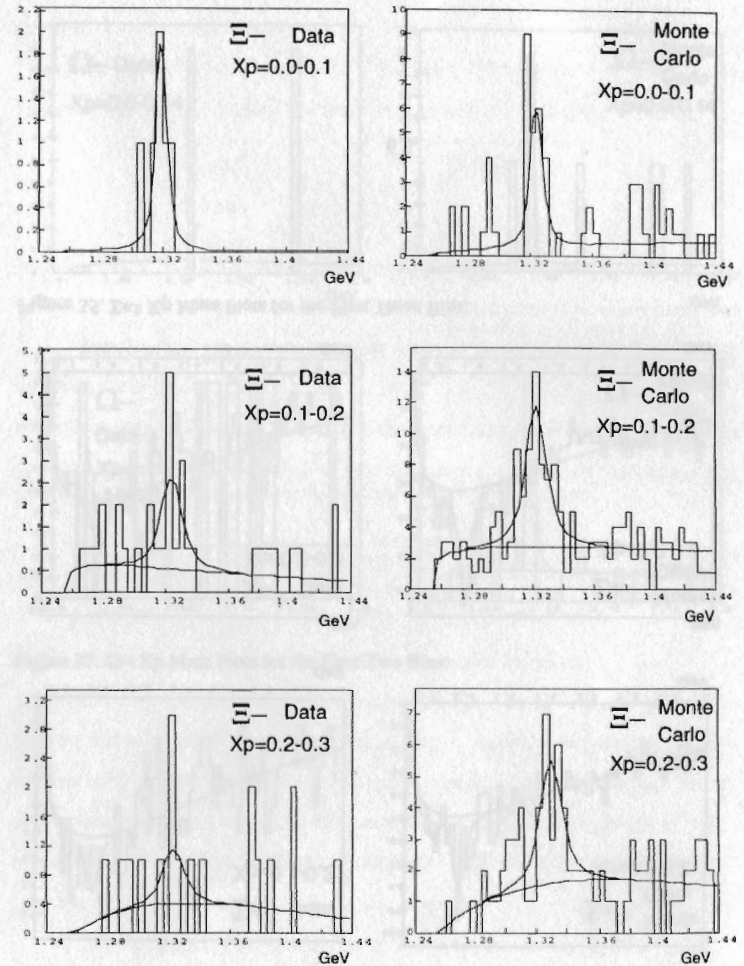
Figure 33. $\Xi-$ Xp Mass Plots for the First Three Bins.
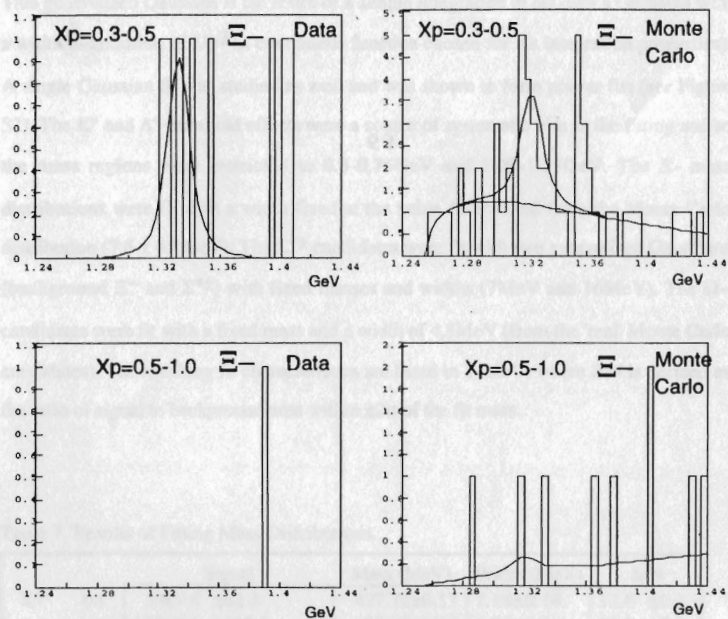
Figure 34. Ξ− Xp Mass Plots for the Last Two Bins.
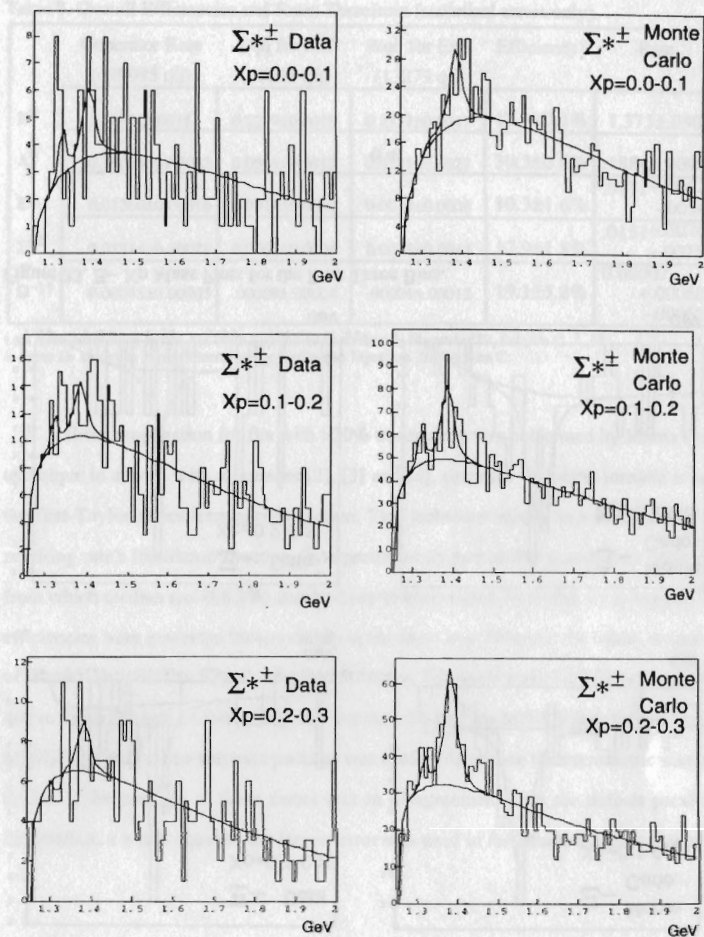
Figure 35. Σ*± Xp Mass Plots for the First Three Bins.
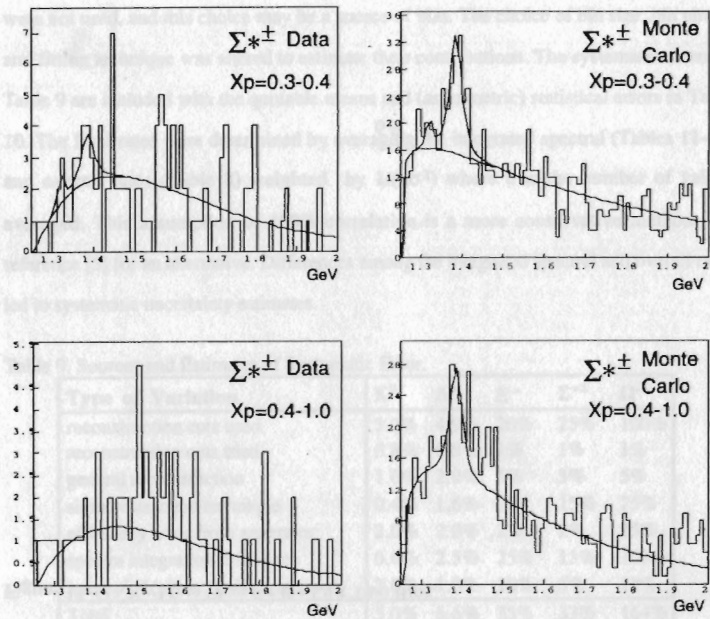
Figure 36. $\Sigma*^{\pm}$ Xp Mass Plots for the Last Two Bins.
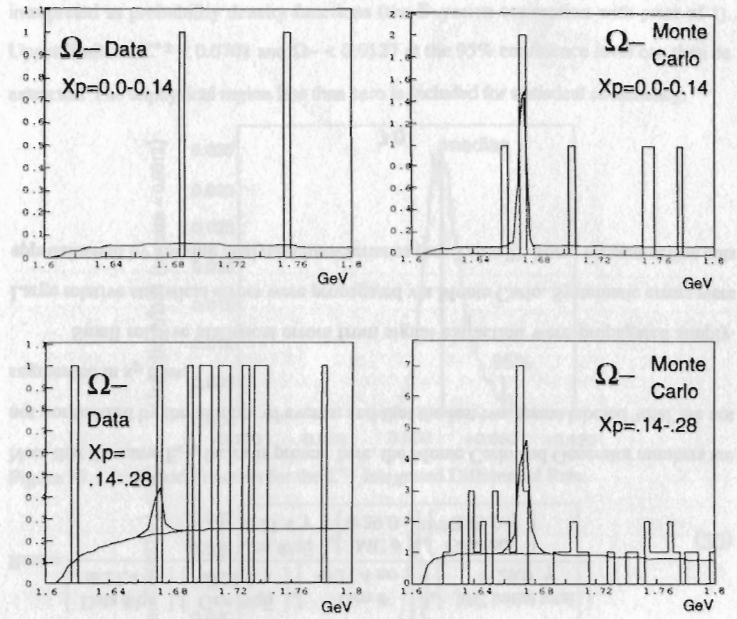
Figure 37. $\Omega-$ Xp Mass Plots for the First Two Bins.
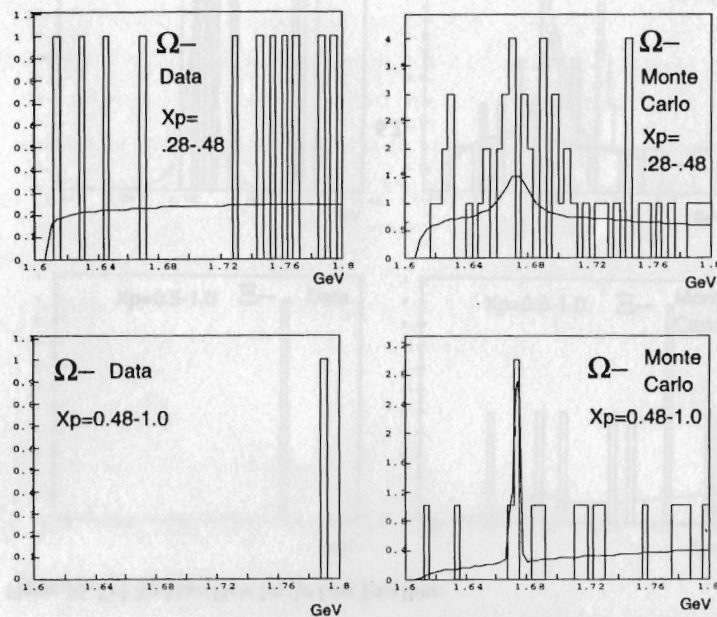
Figure 38. Ω– Xp Mass Plots for the Last Two Bins.

The generator-level rate was measured in the same variables from a sample of 499,995 events statistically independent of the detector simulated events. The measured results were calculated with Equation 19 where each term was measured at either 27.38GeV or 29.0GeV, and the values either include or exclude the effects of initial state radiation (γ indicates initial state radiation).

$$\text{Rate} = \frac{\left[\begin{array}{c}\text{Data \#/q}\bar{\text{q}}\\ @27.4\,\gamma\end{array}\right] * \left[\begin{array}{c}\text{Gen \#/q}\bar{\text{q}}\\ @29.0\,\gamma\end{array}\right] * \left[\begin{array}{c}\text{Gen \#/q}\bar{\text{q}}\\ @27.4\,\text{no}\,\gamma\end{array}\right]}{\left[\begin{array}{c}\text{Gen \#/q}\bar{\text{q}}\\ @27.4\,\gamma\end{array}\right] * \left[\begin{array}{c}\text{MC \#/q}\bar{\text{q}}\\ @29.0\,\gamma\end{array}\right]} \qquad (19)$$

The ratio of the two generator level terms with initial state radiation compensated for the center-of-mass energy discrepancy between the data and the Monte Carlo (this approximation was used rather than re-generating the entire Monte Carlo sample), and is referred to as the 'E$_{cm}$ factor' below. The Ω– rate determination differed because the Monte Carlo sample was too small. An additional 300 events were generated using an event filter such that each event contained an Ω-. In order to calculate the Ω– rate independent of this filter, Equation 20 was used to approximate the rate.

$$\text{Rate} = \frac{\left[\begin{array}{c}\text{Data \#/q}\bar{\text{q}}\\ @27.4\,\gamma\end{array}\right] * \left[\begin{array}{c}\text{Gen \#/q}\bar{\text{q}}\\ @29.0\,\gamma\end{array}\right] * \left[\begin{array}{c}\text{Gen \#}\\ @27.4\,\text{no}\,\gamma\end{array}\right] * \left[\begin{array}{c}\text{MC initial total}\\ @29.0\,\gamma\end{array}\right]}{\left[\begin{array}{c}\text{Gen \#/q}\bar{\text{q}}\\ @27.4\,\gamma\end{array}\right] * \left[\begin{array}{c}\text{MC \#}\\ @29.0\,\gamma\end{array}\right] * \left[\begin{array}{c}\text{Gen total}\\ @29.0\,\gamma\end{array}\right]} \qquad (20)$$

Note that the same E$_{cm}$ factor is present here, the Monte Carlo and Generator numbers are not normalized by the number of events, and that the last two terms labeled 'total' are not segmented in x_p bins.

Small relative statistical errors from signal extraction were propagated simply. Large relative statistical errors were propagated via Monte Carlo. Systematic errors were approximated by varying analysis characteristics (see Table 9). Some reconstruction cuts

were not used, and this choice may be a source of bias. The choice of bin size, bin phase, and fitting technique was altered to estimate their contributions. The systematic errors of Table 9 are included with the quotable means and (asymmetric) statistical errors in Table 10. The final rates were determined by averaging the integrated spectral (Tables 11-19) and overall rates (Table 8) weighted by $1/(n\sigma^2)$ where n is the number of values averaged. This assumption of 100% correlation is a more conservative method; see reference [5] for an alternative. Differences among the integrated spectral and overall rates led to systematic uncertainty estimates.

Table 9. Sources and Estimates of Systematic Error.

Type of Variation	K^0	Λ^0	Ξ^-	$\Sigma^{*\pm}$	Ω^-
reconstruction cuts used	3.2%	4.9%	20%	25%	100%
reconstruction cuts tried	0.8%	0.8%	1%	1%	1%
general reconstruction	1.0%	2.0%	5%	5%	5%
signal extraction technique	0.4%	1.6%	7%	15%	75%
efficiency error from generator	2.0%	2.0%	2%	2%	25%
spectra integration difference	0.6%	2.5%	25%	13%	103%
mass plot (s/n,m,σ) differences	3.0%	1.0%	10%	5%	10%
Total	5.0%	6.6%	35%	33%	164%

Table 10. Final Measurement Results.

	Rate	Statistical Error	Systematic Error
K^0	1.370	±0.030	±0.069
Λ^0	0.1825	±0.0095	±0.0120
Ξ^-	0.0179	+0.0065 / -0.0057	±0.0063
$\Sigma^{*\pm}$	0.0183	+0.0089 / -0.0087	±0.0060
Ω^-	0.00012	+0.00050 / -0.00047	±0.00020

Figures 39 and 40 are the previously discussed likelihood functions for the $\Sigma^{*\pm}$ and Ω^- integrated differential rates where Table 9's systematic uncertainties have been included separately (first four → DA & MC, last three → Generator). They can be

interpreted as probability density functions (the Bayesian convention with prior of 1). Upper limits of $\Sigma^{*\pm} < 0.0701$ and $\Omega^- < 0.0127$ at the 95% confidence level can then be extracted. The unphysical region less than zero is included for statistical consistency.
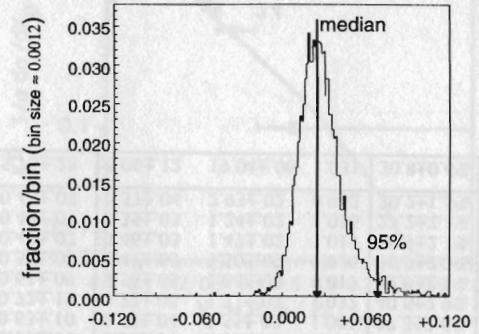
Figure 39. Likelihood Function for the $\Sigma^{*\pm}$ Integrated Differential Rate.
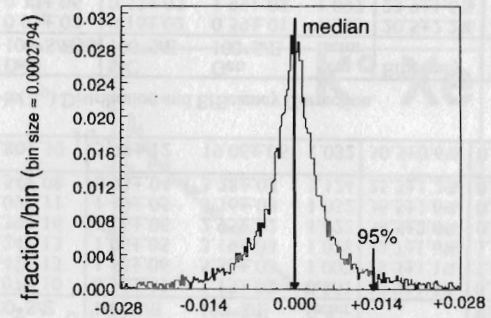
Figure 40. Likelihood Function for the Ω^- Integrated Differential Rate.

The signals, efficiencies, and rates are tabulated in x_p, $-\ln(x_p)$, and x_E bins in Tables 11 through 19 and plotted in Figures 41 through 49 with the LUND prediction (JETSET version 6.3 with the version 7.3 decay table) for comparison.

Table 11. K^o X$_p$ Distribution and Efficiency Correction.

Range	Data 100*S/E	MC 100*S/E	Generator 100*S/E	Ecm factor	Efficiency	Differential Rate
.000-.025	0.28±.05	0.36±.03	6.82±.04	0.997	5.3±0.4%	2.133±.438
.025-.045	1.70±.13	1.50±.05	15.06±.05	1.000	9.9±0.3%	8.565±.695
.045-.065	2.09±.14	2.10±.06	15.79±.06	0.995	13.4±0.4%	7.800±.567
.065-.085	2.11±.14	2.22±.06	13.73±.05	0.997	16.2±0.4%	6.511±.462
.085-.105	2.11±.14	2.15±.06	11.56±.05	0.998	18.6±0.5%	5.666±.405
.105-.125	2.22±.14	1.93±.05	9.94±.04	1.002	19.4±0.6%	5.726±.403
.125-.145	1.89±.14	1.95±.06	8.59±.04	0.994	22.8±0.7%	4.153±.328
.145-.165	1.55±.12	1.59±.05	7.37±.04	0.998	21.7±0.7%	3.576±.296
.165-.185	1.27±.12	1.38±.05	6.49±.04	1.017	21.0±0.7%	3.021±.297
.185-.205	1.37±.11	1.25±.04	5.38±.03	1.023	22.7±0.8%	3.006±.271
.205-.225	1.27±.11	0.98±.04	4.63±.03	1.051	20.2±0.8%	3.129±.296
.225-.245	0.93±.09	0.87±.04	3.94±.03	1.050	21.1±0.9%	2.212±.244
.245-.265	0.81±.08	0.68±.03	3.35±.03	1.052	19.2±0.8%	2.095±.213
.265-.285	0.62±.08	0.61±.03	2.85±.02	1.089	19.8±1.0%	1.578±.208
.285-.305	0.55±.07	0.50±.03	2.40±.02	1.064	19.7±1.2%	1.397±.200
.305-.405	1.65±.13	1.60±.05	7.67±.04	1.105	18.9±0.6%	0.870±.074
.405-1.00	0.99±.11	1.20±.05	5.96±.03	1.200	16.8±0.7%	0.099±.011
total	23.41±.47	22.89±.19	131.52±.16	1.022	17.0±0.1%	1.368±.032

Table 12. K^o X$_F$ Distribution and Efficiency Correction.

Range	Data 100*S/E	MC 100*S/E	Generator 100*S/E	Ecm factor	Efficiency	Differential Rate
.00-.05	0.98±.10	0.99±.04	12.54±.05	1.000	7.9±0.3%	2.499±.264
.05-.10	6.25±.24	6.16±.10	43.17±.09	0.998	14.3±0.2%	8.728±.366
.10-.15	5.29±.22	5.16±.09	25.56±.07	0.996	20.3±0.4%	5.221±.239
.15-.20	3.57±.19	3.68±.08	17.02±.06	1.009	21.4±0.5%	3.338±.188
.20-.25	2.88±.17	2.46±.06	11.21±.05	1.048	21.0±0.6%	2.753±.174
.25-.30	1.67±.12	1.62±.05	7.46±.04	1.064	20.4±0.7%	1.636±.133
.30-.40	1.77±.14	1.66±.05	8.19±.04	1.106	18.3±0.6%	0.969±.081
.40-.60	0.94±.10	1.11±.04	5.40±.03	1.156	17.8±0.7%	0.265±.030
.60-1.00	0.16±.04	0.20±.02	0.97±.01	1.402	14.4±1.6%	0.028±.008
total	23.51±.47	23.02±.19	131.52±0.16	1.022	17.1±0.2%	1.371±.031

Table 13. K^o -ln(X$_p$) Distribution and Efficiency Correction.

Range	Data 100*S/E	MC 100*S/E	Generator 100*S/E	Ecm factor	Efficiency	Differential Rate
.00-.60	0.26±.05	0.31±.03	1.63±.02	1.312	14.4±1.3%	.045±.010
.60-1.0	1.35±.11	1.38±.05	6.75±.04	1.136	18.0±0.7%	.188±.016
1.0-1.3	2.02±.14	2.01±.06	9.30±.04	1.090	19.8±0.6%	.340±.026
1.3-1.6	3.50±.18	2.99±.07	14.07±.05	1.053	20.2±0.5%	.577±.033
1.6-1.8	2.42±.15	2.44±.06	11.56±.05	1.019	20.7±0.5%	.585±.040
1.8-2.0	2.45±.15	2.52±.06	11.10±.05	0.991	22.9±0.6%	.535±.036
2.0-2.2	2.54±.16	2.37±.06	12.00±.05	1.001	19.7±0.5%	.645±.043
2.2-2.4	2.09±.14	2.10±.06	10.74±.05	0.997	19.6±0.5%	.532±.038
2.4-2.6	1.82±.13	1.84±.05	11.08±.05	1.000	16.6±0.5%	.547±.042
2.6-2.8	1.52±.12	1.51±.05	9.48±.04	0.992	16.1±0.5%	.473±.040
2.8-3.0	1.10±.10	1.12±.04	9.09±.04	0.994	12.4±0.5%	.441±.045
3.0-3.2	1.00±.10	0.88±.04	7.03±.04	1.002	12.4±0.5%	.401±.043
3.2-3.4	0.59±.07	0.62±.03	5.96±.03	0.999	10.4±0.5%	.284±.038
3.4-4.0	0.80±.09	0.75±.03	8.83±.04	1.005	8.4±0.4%	.158±.019
4.0-6.0	0.07±.03	0.11±.01	2.82±.02	0.989	3.9±0.6%	.009±.004
total	23.53±0.47	22.94±0.19	131.46±.16	1.022	17.1±0.1%	1.370±.032

Table 14. Λ^o X$_p$ Distribution and Efficiency Correction.

Range	Data 100*S/E	MC 100*S/E	Generator 100*S/E	Ecm factor	Efficiency	Differential Rate
.00-.05	0.17±.05	0.33±.03	2.04±.02	0.959	16.9±1.7%	.2029±.0673
.05-.10	1.30±.13	1.30±.05	4.35±.03	1.017	29.3±1.2%	.8861±.0931
.10-.15	1.31±.13	1.12±.05	3.34±.03	1.020	33.0±1.6%	.7931±.0899
.15-.20	0.99±.13	0.89±.05	2.35±.02	1.012	37.5±2.2%	.5279±.0773
.20-.25	0.72±.09	0.69±.04	1.70±.02	1.068	37.9±2.2%	.3786±.0542
.25-.30	0.56±.08	0.49±.03	1.35±.02	0.983	37.1±2.4%	.3037±.0460
.30-.35	0.27±.05	0.39±.03	1.06±.01	1.058	34.6±2.6%	.1585±.0327
.35-.40	0.19±.04	0.26±.02	0.85±.01	1.039	29.8±2.7%	.1269±.0310
.40-.50	0.16±.04	0.31±.02	1.09±.01	1.104	25.7±2.1%	.0638±.0175
.50-.70	0.06±.02	0.21±.02	0.82±.01	1.223	21.2±1.9%	.0136±.0059
.70-1.0	0.00±.02 Bayesian	0.02±.01	0.12±.005	1.498	10.5±3.7%	.0000±.0120
total	5.73±0.28	6.01±0.12	19.06±.06	1.032	30.6±0.6%	.1780±.0102

Table 15. Λ^o X$_E$ Distribution and Efficiency Correction.

Range	Data 100*S/E	MC 100*S/E	Gen 100*S/E	Ecm factor	Efficiency	Differential Rate
.00-.09	0.07±.10	0.12±.01	1.13±.02	0.961	10.9±1.2%	0.2250±.3344
.09-.13	1.47±.13	1.53±.06	5.36±.03	1.007	28.3±1.1%	2.0436±.2033
.13-.17	1.24±.13	1.06±.05	3.19±.03	1.018	32.7±1.6%	1.1376±.1336
.17-.23	1.39±.16	1.16±.06	2.95±.02	1.022	38.5±2.0%	0.6625±.0812
.23-.34	1.09±.11	1.19±.05	3.16±.03	1.032	36.5±1.6%	0.2841±.0311
.34-1.00	0.54±.08	0.93±.04	3.28±.03	1.124	25.3±1.2%	0.0327±.0050
total	5.80±.30	5.99±.12	19.06±.06	1.032	30.5±0.6%	0.1834±.0133

Table 16. Λ^o -ln(X$_p$) Distribution and Efficiency Correction.

Range	Data 100*S/E	MC 100*S/E	Gen 100*S/E	Ecm factor	Efficiency	Differential Rate
.00-.60	0.03±.02	0.16±.02	0.59±.01	1.293	20.5±2.2%	.0024±.0015
.60-1.00	0.32±.06	0.52±.03	1.99±.02	1.097	23.9±1.6%	.0332±.0070
1.00-1.30	0.58±.08	0.79±.04	2.10±.02	1.022	36.7±1.9%	.0528±.0076
1.30-1.60	0.99±.11	0.88±.04	2.28±.02	1.048	36.8±1.9%	.0896±.0106
1.60-1.80	0.63±.10	0.58±.04	1.55±.02	1.001	37.3±2.6%	.0847±.0150
1.80-2.00	0.72±.12	0.72±.05	1.71±.02	1.032	40.6±2.9%	.0884±.0159
2.00-2.20	0.61±.09	0.56±.03	1.68±.02	1.017	32.9±2.1%	.0925±.0151
2.20-2.40	0.53±.08	0.47±.03	1.50±.02	1.026	30.7±2.0%	.0863±.0142
2.40-2.60	0.45±.07	0.46±.03	1.47±.02	1.019	30.9±2.1%	.0726±.0127
2.60-2.80	0.43±.07	0.35±.03	1.24±.02	1.036	27.2±2.1%	.0797±.0138
2.80-6.00	0.45±.08	0.57±.04	2.93±.02	0.962	20.2±1.5%	.0069±.0014
total	5.73±.28	6.06±.12	19.04±.06	1.031	30.8±0.6%	.1804±.0097

Table 17. Ξ^- X_p Distribution and Efficiency Correction.

Range	Data in 100*S/E	MC in 100*S/E	Gen in 100*S/E	Ecm factor	Efficiency	Differential Rate
0.0-0.1	0.040±.020	0.022±.007	0.339±.008	0.970	6.7±2.1%	0.0596+.0409 -.0318
0.1-0.2	0.088±.032	0.055±.012	0.360±.008	1.029	14.9±3.4%	0.0591+.0288 -.0228
0.2-0.3	0.038±.023	0.026±.009	0.215±.007	1.040	11.8±4.2%	0.0321+.0281 -.0196
0.3-0.5	0.030±.018	0.022±.008	0.233±.007	1.063	9.1±3.2%	0.0329+.0281 -.0200
0.5-1.0	0.000±.017 Bayesian	0.001±.002	0.112±.005	1.332	0.7±1.7%	0.0028+.0185 -.0168
total	0.205±.048	0.127±.018	1.260±.016	1.047	9.6±1.4%	0.0218+.0141 -.0111

Table 18. $\Sigma^{*\pm}$ X_p Distribution and Efficiency Correction.

Range	Data 100*S/E	MC 100*S/E	Gen 100*S/E	Ecm factor	Efficiency	Differential Rate
0.0-0.1	0.084±.054	0.059±.021	0.972±.014	0.964	6.4±2.3%	0.1293+.1180 -.0853
0.1-0.2	0.132±.090	0.184±.034	1.019±.014	1.035	17.5±3.3%	0.0753+.0560 -.0520
0.2-0.3	0.082±.066	0.182±.030	0.532±.010	1.067	32.2±5.4%	0.0255+.0217 -.0208
0.3-0.4	0.050±.046	0.101±.021	0.300±.008	0.976	34.5±7.5%	0.0146+.0144 -.0134
0.4-1.0	0.000±.027	0.047±.019	0.491±.010	1.115	14.4±3.6%	0.0000+.0032 -.0032
total	0.348±.133	0.605±.058	3.314±.026	1.025	17.8±1.7%	0.0254+.0140 -.0111

Table 19. Ω^- X_p Distribution and Efficiency Correction.

Range	Data 100*S/E	MC 100*S/E	Gen 100*S/E	Ecm factor	Efficiency	Differential Rate
.00-.14	0.000±.017 Bayesian	0.004±.004	0.010±.001	1.196	9 +12 -5%	0.0024+.0073 -.0023
.14-.28	0.003±.008	0.011±.005	0.010±.001	0.929	28.9+20.8 -12.4%	0.0007+.0021 -.0018
.28-.48	0.000±.027	0.006±.010	0.014±.002	1.075	9.9+16.9 -8.7%	0.0001+.0095 -.0097
.48-1.0	0.000±.017 Bayesian	0.008±.010	0.010±.001	0.931	19 +22 -10%	0.0004+.0010 -.0003
total	0.018±.030	0.029±.010	0.045±.003	1.030	18.5±7.2%	0.0002+.0009 -.0009
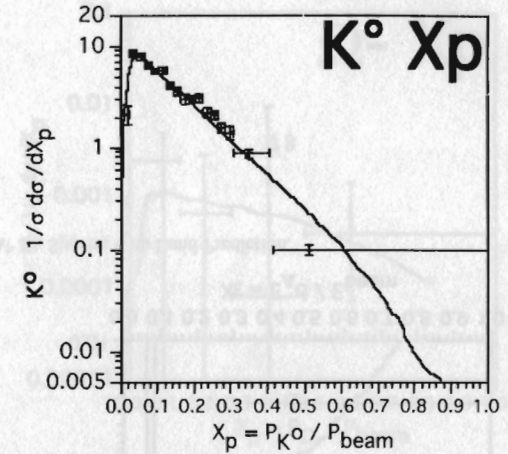
Figure 41. K° X_p Spectra with Lund Prediction.
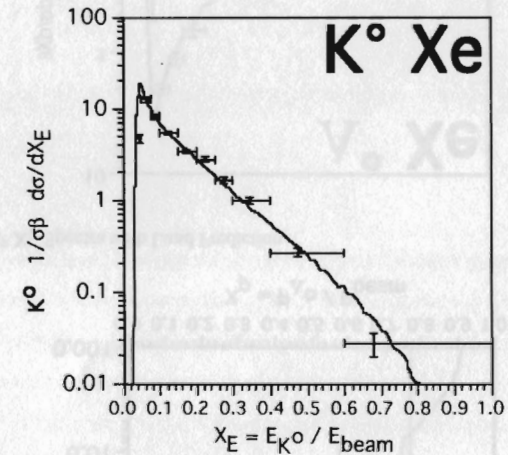
Figure 42. K° X_E Spectra with Lund Prediction.
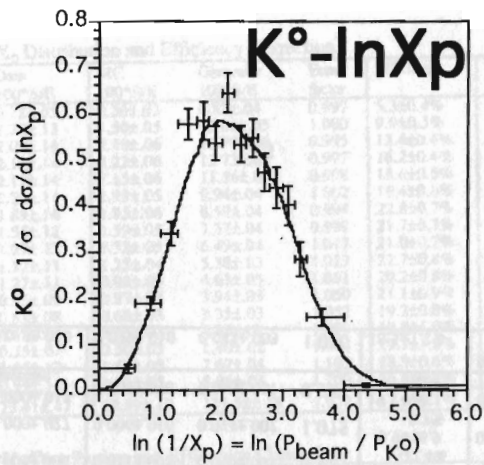
Figure 43. K° -lnX$_p$ Spectra with Lund Prediction.
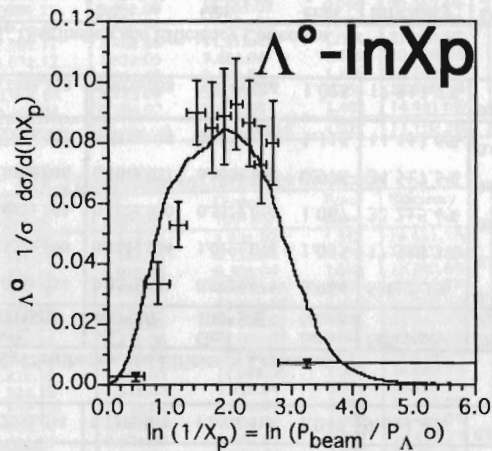
Figure 44. Λ° -lnX$_p$ Spectra with Lund Prediction.
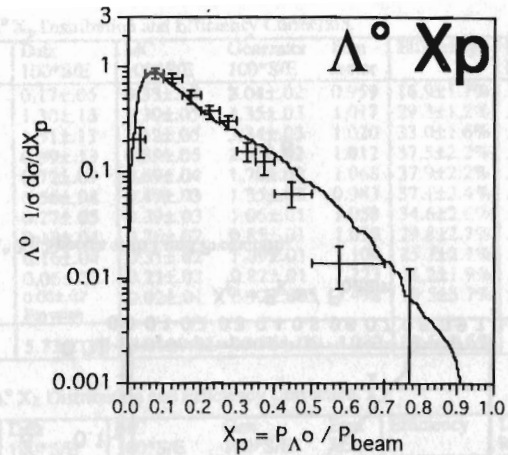
Figure 45. Λ° X$_p$ Spectra with Lund Prediction.
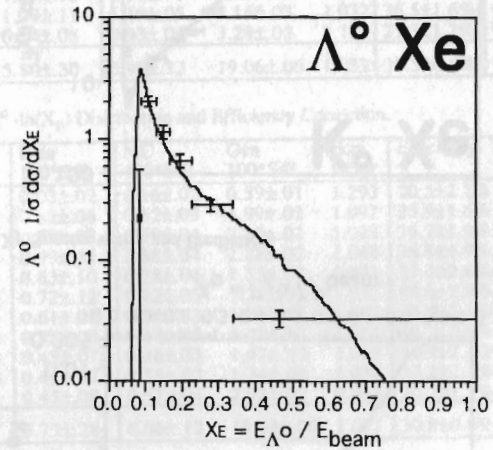
Figure 46. Λ° X$_E$ Spectra with Lund Prediction.

77

78
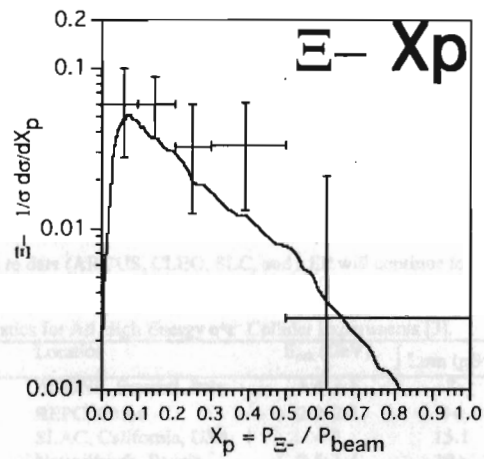
Figure 47. Ξ− X_p Spectra with Lund Prediction.
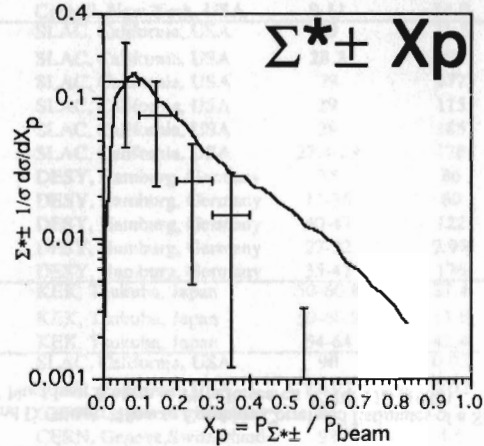
Figure 48. Σ*± X_p Spectra with Lund Prediction.
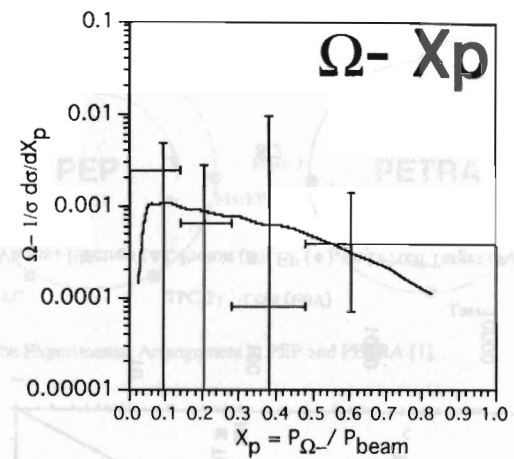
Figure 49. Ω− X_p Spectra with Lund Prediction.

D.   REFERENCES

1. G.Cowan, "Inclusive p±, K±, p,p Production in e+e- Annihilation at sqrt(s) =
    29GeV." LBL-24715: 90-94 (1988).

2. Particle Data Group, "Review of Particle Properties."
    Phys.Rev.D 50: 1271-1282 (1994).

3. F.James, "Determining the Statistical Significance of Experimental Results." CERN-
    Data Handling Division DD/81/02, (1981).

4. F.James, "Interpretation of the Shape of the Likelihood Function Around its
    Minimum." Computer Physics Communications 20: 29 (1980).

5. L.Lyons and D.Gibaut, "How to Combine Correlated Estimates of a Single Physical
    Quantity." Nucl.Instr.&Meth.in Phys.Research A270: 110 (1988).

V. SURVEY

A.   THE EXPERIMENTS

Many High Energy experiments have been constructed in the last 30 years using particle accelerators. Prior to this the required engineering for high intensity collimated beams was not available and physicists relied on cosmic rays, x-ray tubes, and naturally occurring radiation sources to explore the behavior of subatomic particles. Technology took another step in 1960's with the first colliding storage ring (at Frascati, Italy) [1]. Today's technology tends to limit the maximum achievable luminosity for a given collider according to $L \sim E_{cm}^2$, whereas fixed target experiments have different constraints. Figure 50 is a summary of various colliders (the ones in parentheses are in the design or construction stage). Notice that PEP and PETRA have been the only ones at ~30GeV.
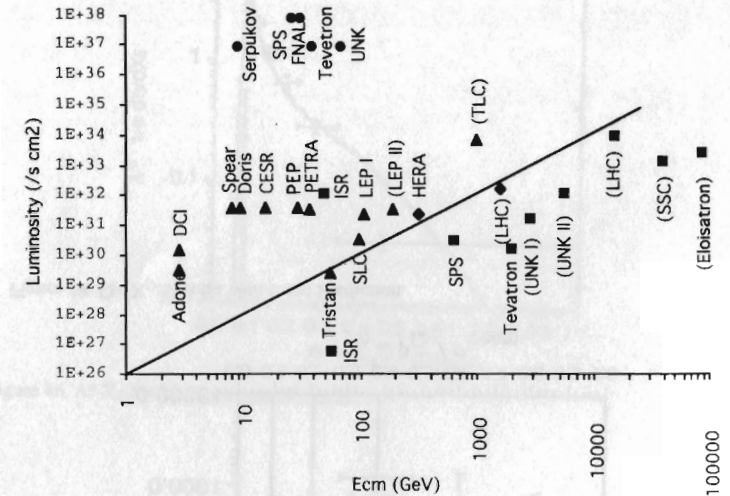
Figure 50. Various Electron (▲), Proton (■), EP (♦), and Fixed Target (●) Colliders [2].

TRISTAN at 60GeV is the next higher step in energy, and CESR and DORIS at 10GeV are the next lower step in energy. As Table 20 shows, no more e+e- collider data is expected from any experiment at ~30GeV because PETRA turned off in 1986 [1] and PEP's last run ended in 1990 (with the TPC/Two-Gamma detector alone). The production rates of various particles at each of the PEP and PETRA experiments (see Figure 51) are compared and averaged in Sections B and C. Similar tabulations are made for 10GeV and 91GeV results to date (ARGUS, CLEO, SLC, and LEP will continue to run).

Table 20. Statistics for All High Energy e+e- Collider Experiments [3].

Collaboration	Location	E$_{cm}$ (GeV)	∫ Lum (pB^{-1})	Status
PSI,...	ADONE, Frascati, Italy	1.4-3.1	?	on
BES	BEPC, China	2.2-2.8	0+	on
SPEAR	SLAC, California, USA	4-7	15.1	off
VEPP	Novosibirsk, Russia	0.5-1.4	19+	on
ARGUS	DESY, Hamburg, Germany	9-10	520	off
PLUTO	DESY, Hamburg, Germany	9-12	0.45	off
CLEO	Cornell, New York, USA	9-11	20.7	on
CUSB	Cornell, New York, USA	9-11	14.0	off
DELCO	SLAC, California, USA	29	21.5	off
HRS	SLAC, California, USA	28.3	291	off
MAC	SLAC, California, USA	29	177	off
ASP	SLAC, California, USA	29	115	off
MARK II	SLAC, California, USA	29	185	off
TPC/2γ	SLAC, California, USA	27.4-29	178	off
CELLO	DESY, Hamburg, Germany	35	86	off
JADE	DESY, Hamburg, Germany	12-36	60	off
MARK J	DESY, Hamburg, Germany	40-47	122	off
PLUTO	DESY, Hamburg, Germany	27-32	2.98	off
TASSO	DESY, Hamburg, Germany	35-42	176	off
AMY	KEK, Tsukuba, Japan	50-60.8	27.4	on
TOPAZ	KEK, Tsukuba, Japan	50-60.8	13.6	on
VENUS	KEK, Tsukuba, Japan	54-64	42.4	on
SLD	SLAC, California, USA	90	0.02	on
MARK II	SLAC, California, USA	89-93	0.02	off
ALEPH	CERN, Geneve,Switzerland	91	5.2	on
DELPHI	CERN, Geneve,Switzerland	91	4.6	on
L3	CERN, Geneve,Switzerland	91	4.7	on
OPAL	CERN, Geneve,Switzerland	88-95	6.5	on
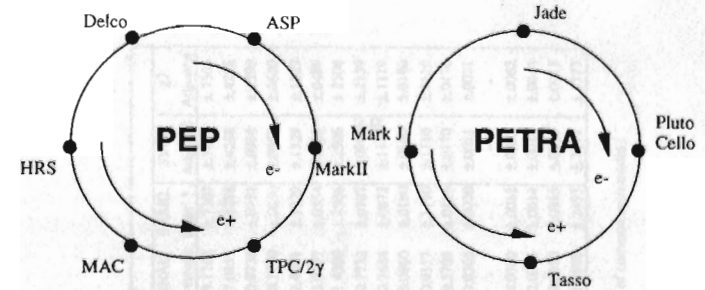
Figure 51. The Experimental Arrangement at PEP and PETRA [1].

B.   TABULATION OF RESULTS

In Section C, production rate measurements are tabulated at various center-of-mass energies for π°, π±, η, η', K±, K°, ρ°, K*-, K*°, φ, p±, Λ, Ξ⁻, Δ++, Σ*+ or Σ*-, Ξ*°, Ω⁻, and all charged particles, followed by reference tabulations for D°, D*±, and Λ$_c$. Included in each table is a weighted average over the independent measurements which have been published in refereed journals (non-refereed yet believable results which are averaged are footnoted). A summary of these averages is presented at the end of this section.

The simple weighted averages in the tables of Section C neglect several characteristics of the experimenter's domain, but it is a starting point. A weighted average is calculated using Equation 21, where the weights (w_i) are a measure of the influence a value (x_i) has on the result ($\bar{x}$).

$$\bar{x} = \frac{\sum_i x_i w_i}{\sum_j w_j} \tag{21}$$

The averages in the tables of Section C use the inverse of the square of the total scaled error for the weight, as seems reasonable. The uncertainty of the average, given the uncertainties of each value, is simplified in this case (see Equation 22).

$$\sigma_{\bar{x}}^2 = \sum_i (\frac{\partial \bar{x}}{\partial x_i}\sigma_i)^2 + 2\sum_{ik}^{i>k} \frac{\partial \bar{x}}{\partial x_i}\frac{\partial \bar{x}}{\partial x_k}\sigma_{ik}^2 = \frac{\sum_i (\sigma_i w_i)^2}{(\sum_j w_j)^2} \Rightarrow \frac{1}{\sum_j w_j} \tag{22}$$

The first characteristic of the measurements to account for in order to improve the value's accuracy is the common systematic errors among measurements from the same source or using the same techniques. The direct and rigorous approach to this would derive a generalized equation for $\bar{x}$ by minimizing the χ^2 in Equation 23, where $\sigma_{ii}^2 = \sigma_i^2$ and $\sigma_{ij}^2 (i \neq j)$ are the correlations.

$$\chi^2 = (x_i-\bar{x})(\sigma_{ij}^2)^{-1}(x_j-\bar{x}) \tag{23}$$

The corresponding formula for $\sigma_{\bar{x}}^2$ would follow from $\bar{x}$ by using Equation 22. To avoid the difficulty of minimizing the χ^2 in Equation 23, a basic weighted average is calculated for measurement subsets (with the same detector) with their common systematic errors removed (assumed to be 60% of the systematic error). The subsets are then combined using another basic weighted average assuming 40% common systematic error (due to the analysis approach).

The second characteristic to consider is that published uncertainties may be poor estimates of the actual uncertainties. This is only a significant problem when the quoted error is too small, of course. To account for this effect, the square root of the total χ^2 per degree of freedom is recalculated after taking common systematics into account (see Equation 24).

$$\sqrt{\chi^2/(n-1)} = \sqrt{\sum_i [(x_i-\bar{x})/\sigma_i]^2/(n-1)} \tag{24}$$

If the result is greater than 1.0 then the resulting uncertainty of the average is increased by this factor. It should be noted that this use of the goodness-of-fit information to increase the average's error bar is a way of combining separate pieces of information when several inclusive rates are compared to a model's predictions simultaneously. Both the average and χ^2 per degree of freedom should be quoted.

The third point to consider also depends on how these averages are used. If the average is compared with the prediction of a model (see chapter VI), then the prediction's uncertainty should be included. Specifically, most models use a decay table as the last step in generating a production rate, and these branching ratios are determined experimentally with some uncertainty. The difference between the average rate and predicted rate, divided by the sum of the errors of each in quadrature, is the number of standard deviations they differ by (assuming small errors). In order to simplify matters the predicted rate uncertainty is added to the average uncertainty in quadrature. Other comparisons will differ. For example, the ratio of two rates would include the model's decay table uncertainty only once. The decay table uncertainties quoted here are simple estimates.

The contributions from these three uncertainties are summarized in Table 21 by center-of-mass energy and particle type. The relative uncertainties are not cumulative in that they are the contributions to the uncertainty from each process. Table 22 summarizes the world averages and cumulative absolute uncertainties for each case. The integer following the particle type labeled by "#" is the number of measurements which contributed to that average.

Table 21.   Summary of Contributions to Relative Uncertainties (D=detector 60%, A=analysis 40% †).

10 GEV

	#	BASIC Error	COMMON Type	COMMON Error	χ2 †† Factor	χ2 †† Error	DECAY TABLE
π0	3	7.14%	A	3.84%	0.69	0.00%	3%
π±	2	1.76%	A	1.00%	4.37	8.60%	3%
η0	2	18.11%	A	4.86%	0.40	0.00%	7%
η0'	1	32.35%	-	0.00%	0.00	0.00%	6%
K±	2	3.31%	A	3.47%	1.94	7.96%	4%
K0	6	5.29%	DA	6.16%	0.64	0.00%	4%
ρ0	2	10.44%	A	4.22%	1.67	15.15%	4%
K*±	2	11.36%	A	4.77%	2.25	24.18%	10%
K*0	2	9.41%	A	4.89%	0.84	0.00%	8%
φ	2	6.73%	A	6.74%	1.67	12.88%	8%
p±	3	6.15%	A	5.30%	1.99	13.97%	4%
Λ	2	8.04%	A	2.54%	2.17	16.09%	4%
Ξ-	2	11.48%	A	3.36%	1.36	10.62%	7%
Δ++	1	25.00%	-	0.00%	0.00	0.00%	5%
Σ*±	1	18.18%	-	0.00%	0.00	0.00%	7%
Ξ*0	1	33.33%	-	0.00%	0.00	0.00%	10%
Ω-	1	52.78%	-	0.00%	0.00	0.00%	10%
Nch	8	1.65%	DA	1.52%	1.56	2.62%	3%

29 GEV

	#	BASIC Relative	COMMON Type	COMMON Error	χ2 †† Factor	χ2 †† Error	DECAY TABLE
π0	4	4.59%	A	3.47%	0.46	0.00%	3%
π±	3	3.04%	DA	1.55%	0.15	0.00%	3%
η0	4	11.96%	A	7.02%	0.12	0.00%	7%
η0'	1	39.62%	-	0.00%	0.00	0.00%	6%
K±	3	4.80%	DA	3.11%	1.01	0.81%	4%
K0	11	2.22%	DA	4.13%	0.68	0.00%	4%
ρ0	4	4.75%	A	4.33%	1.31	5.44%	4%
K*±	2	8.83%	A	2.76%	1.09	4.02%	10%
K*0	6	6.41%	DA	5.31%	0.65	0.00%	8%
φ	2	16.24%	DA	10.25%	0.29	0.00%	8%
p±	4	5.67%	DA	3.20%	0.92	0.00%	4%
Λ	8	4.20%	DA	4.75%	0.51	0.00%	4%
Ξ-	5	14.56%	A	10.24%	1.24	13.09%	7%
Δ++	1	Limit	-	0.00%	0.00	0.00%	5%
Σ*±	1	28.59%	-	0.00%	0.00	0.00%	7%
Ξ*0	2	68.95%	A	18.48%	1.14	39.41%	10%
Ω-	2	45.98%	A	17.66%	1.28	39.20%	10%
Nch	11	1.41%	DA	2.20%	1.09	1.12%	3%

91 GEV

	#	BASIC Relative	COMMON Type	COMMON Error	χ2 †† Factor	χ2 †† Error	DECAY TABLE
π0	1	7.95%	-	0.00%	0.00	0.00%	3%
π±	1	2.52%	-	0.00%	0.00	0.00%	3%
η0	2	9.44%	A	3.60%	1.41	10.06%	7%
η0'	1	37.14%	-	0.00%	0.00	0.00%	6%
K±	1	5.50%	-	0.00%	0.00	0.00%	4%
K0	4	1.70%	A	1.62%	0.47	0.00%	4%
ρ0	1	17.55%	-	0.00%	0.00	0.00%	4%
K*±	2	10.17%	A	7.28%	2.21	24.67%	10%
K*0	2	11.36%	A	9.13%	0.58	0.00%	8%
φ	1	20.93%	-	0.00%	0.00	0.00%	8%
p±	1	12.12%	-	0.00%	0.00	0.00%	4%
Λ	4	3.13%	A	3.34%	0.81	0.00%	4%
Ξ-	2	9.80%	A	3.50%	0.11	0.00%	7%
Δ++	0	-	-	-	--	-	-
Σ*±	1	16.32%	-	0.00%	0.00	0.00%	7%
Ξ*0	1	22.22%	-	0.00%	0.00	0.00%	10%
Ω-	1	30.00%	-	0.00%	0.00	0.00%	10%
Nch	6	1.19%	DA	1.08%	0.64	0.00%	3%

†   The systematic error is assumed to equal the statistical error in cases where only the total is quoted.

††   These factors are from the initial basic weighted average. Values ≥ 1.0 are recalculated with the final average and applied to Table 3.

Table 22.   Summary of Survey Results.

10 GEV

	#	FINAL Average	BASIC Error †	SYST Adjusted	χ2 Adjusted
π0	3	3.3252	±.2373	±.2695	±.2695
π±	2	6.5356	±.1149	±.1321	±.5773
η0	2	0.2067	±.0375	±.0388	±.0388
η0'	1	0.0340	±.0108	±.0108	±.0108
K±	2	0.8974	±.0297	±.0430	±.0834
K0	6	0.8984	±.0475	±.0730	±.0730
ρ0	2	0.3532	±.0370	±.0400	±.0668
K*±	2	0.2759	±.0315	±.0342	±.0770
K*0	2	0.2995	±.0282	±.0318	±.0318
φ	2	0.0457	±.0031	±.0044	±.0073
p±	3	0.2746	±.0169	±.0223	±.0444
Λ	2	0.0802	±.0064	±.0067	±.0145
Ξ-	2	0.0058	±.0007	±.0007	±.0009
Δ++	1	0.0400	±.0100	±.0100	±.0100
Σ*±	1	0.0107	±.0020	±.0020	±.0020
Ξ*0	1	0.0015	±.0005	±.0005	±.0005
Ω-	1	0.0007	±.0004	±.0004	±.0004
Nch	8	8.5632	±.1381	±.1877	±.2928

29 GEV

	#	FINAL Average	BASIC Error †	SYST Adjusted	χ2 Adjusted
π0	4	5.8369	±.2678	±.3355	±.3355
π±	3	10.5982	±.3222	±.3618	±.3618
η0	4	0.5933	±.0710	±.0823	±.0823
η0'	1	0.2600	±.1030	±.1030	±.1030
K±	3	1.4468	±.0691	±.0823	±.0831
K0	11	1.3955	±.0311	±.0658	±.0658
ρ0	4	0.8455	±.0401	±.0542	±.0710
K*±	2	0.6413	±.0567	±.0594	±.0647
K*0	6	0.5755	±.0366	±.0475	±.0475
φ	2	0.0787	±.0128	±.0151	±.0151
p±	4	0.5697	±.0323	±.0371	±.0371
Λ	8	0.2090	±.0088	±.0133	±.0133
Ξ-	5	0.0175	±.0026	±.0031	±.0038
Δ++	1	<.094	95%	-	-
Σ*±	1	0.0330	±.0094	±.0094	±.0094
Ξ*0	2	0.0050	±.0035	±.0036	±.0041
Ω-	2	0.0053	±.0025	±.0026	±.0033
Nch	11	12.5753	±.1757	±.3248	±.3540

91 GEV

	#	FINAL Average	BASIC Error †	SYST Adjusted	χ2 Adjusted
π0	1	9.1765	±.7303	±.7303	±.7303
π±	1	17.0455	±.4288	±.4288	±.4288
η0	2	0.9738	±.0921	±.0986	±.1390
η0'	1	0.1750	±.0650	±.0650	±.0650
K±	1	2.4201	±.1329	±.1329	±.1329
K0	4	2.0797	±.0354	±.0489	±.0489
ρ0	1	1.4300	±.2506	±.2506	±.2506
K*±	2	0.7732	±.0787	±.0968	±.2139
K*0	2	0.7684	±.0872	±.1119	±.1119
φ	1	0.0860	±.0180	±.0180	±.0180
p±	1	0.9157	±.1110	±.1110	±.1110
Λ	4	0.3705	±.0116	±.0170	±.0170
Ξ-	2	0.0205	±.0020	±.0021	±.0021
Δ++	0	-	-	-	-
Σ*±	1	0.0380	±.0062	±.0062	±.0062
Ξ*0	1	0.0063	±.0014	±.0014	±.0014
Ω-	1	0.0050	±.0015	±.0015	±.0015
Nch	6	21.0598	±.2493	±.3377	±.3377

†   The error from the initial basic average on that average, not on the final average (which includes the effects of common systematics).

C. SUMMARY TABLES

Tables 23 through 43 list production rate measurements in the following format. Each line consists of publication year, collaboration name, reference number (see the Appendix: Key to Tables), quoted rate and uncertainty (#/event), experimental center-of-mass energy (GeV), the resulting scaling factor to account for differences in E_{cm}, scaled rate and uncertainty (#/event), values for the basic weighted average (see below), luminosity recorded (pB^{-1}), observed signal and background, and an identification number that shows which entries are results from the same dataset. Measurement entries are ordered by experiment and date.

The quoted uncertainty is either the total error or the statistical then systematic error. A question mark indicates that the publication neglected to specify if systematic errors were included, whereas a hyphen indicates that the article specified that the error includes systematics. The energy scaling factor is $\ln(E_{cm}/2M_{hadron})$ ($\pm30\%$ of the deviation from 1.0) and is the predicted QCD scaling violation [4]. This is a very good approximation among measurements at similar energies. The mass used for the scaling of the $N_{charged}$ measurements (193.4MeV) was found to be uniform from 10 to 91GeV by summing the $\pi^{\pm}$, $K^{\pm}$, and $p^{\pm}$ contributions. The tables are broken into sections corresponding to measurements around 10, 29, or 91GeV center-of-mass energy. The sum of the weights and weighted values, square root of χ^2 per degree of freedom (i.e.: # of measurements -1), weighted average and resulting uncertainty (including both statistical and systematic) appear at the bottom of each group of similar entries. These tables are rather complete† as of October 31, 1993, and include many of the main publications between then and September, 1994. Each table concludes with a list of additional relevant publications which do not quote production rates. A cross reference table is provided at the end (Table 44).

† An "♠" symbol identifies publications that could not be located.

89

Table 23 πo Production Rate Measurements.

Yr	Exper	Ref	Value			Ecm	ln(E/2m)	Scaled		weight	w*value	$\chi2$	Lu	Sig	Bck
90	Cello	34	6.430	±.600	±.860	35	0.961	6.181	±1.011	.979	6.050	0.12	87	1267	-
90	Jade	123	6.400	±.100	±.400	34.9	0.962	6.156	±0.403				176	-	-
90	Jade	123	7.000	±.250	±.450	43.8	0.919	6.433	±0.503				43	-	-
85	Jade	119	6.100	±.100	±.300	34	0.967	5.899	±0.312	10.293	60.722	0.05	-	-	-
85	Jade	119	5.500	±.400	±.300	22	1.063	5.845	±0.541				-	-	-
89	Tasso	208	5.400	±1.000	?	44	0.918	4.958	±0.928				34	-	-
86	Tasso	205	5.800	±.900	-	34.6	0.964	5.589	±0.870	1.322	7.391	0.08	67	-	1
84	Tasso	196	6.100	±2.000	(±.2)†	34	0.967	5.899	±1.935					-	1
85	Tpc	225	5.300	±.700	(±.5)††	29	1.000	5.300	±0.860	1.351	7.162	0.38	49	-	2
85	Tpc	226	5.300	±.700	-	29	1.000	5.300	±0.700				-	-	2
								5.832	±0.268	13.946	81.326	0.46			
90	Argus	20	3.220	±.070	±.310	10	1.000	3.220	±0.318	9.901	31.881	0.11	37	-	-
85	Cleo	44	3.000	±.700	-	10.5	0.987	2.961	±0.691	2.095	6.202	0.28	17	-	-
91	CryBa	68	3.640	±.210	±.360	10	1.000	3.640	±0.417	5.757	20.956	0.57	42	-	3
86	CryBa	66	3.700	±.600	?	10	1.000	3.700	±0.600				-	-	3
85	Jade	119	4.700	±.200	±.200	14	0.915	4.299	±0.285				-	-	-
								3.326	±0.237	17.753	59.039	0.69			
94	L3‡	301	9.180	±.030	±.730	91.2	1.000	9.177	±0.730	1.8748	17.204	0.00	35	-	4
91	L3	124	6.400	±.100	±.400	91.2	1.000	6.398	±0.412		‡‡		-	31.3k	4
91	L3	‡‡	9.877	±.805	-	91.2	1.000	9.873	±0.805				-	31.3k	4
								9.177	±0.730	1.8748	17.204	0.00			
87	Argus	12				10									
86	Argus	11				10									
83	Cello	33				14,22,34									
82	Cello	32				34									
85	Hrs	95				29									
83	Jade	113				14-35									
78	Lgw	128				4.9-7.4									
82	Mark2	136				29									
83	Tasso	190				14,34									
82	Tasso	185				14,34									1

Note: The numbers under "Ref" refer to the articles listed in the Appendix: Key to Tables.

† Systematic error is not quoted; syst = stat is assumed.
†† Estimate of additional systematic error due to spectral extrapolation from 2.0±.3 by C.D.Buchanan.
‡ Submitted to Phys.Lett.B.
‡‡ Extrapolation from (.0075 to .065GeV) based on: Lund(6.3 to 9.7) & Herwig(6.4 to 9.9) by L3.

90

Table 24 π± Production Rate Measurements.

Yr Exper	Ref	Value			Ecm	ln(E/2m)	Scaled		weight	w*value	χ2	Lu	Sig	Bck
89 Tasso	208	10.900	±.500	?†	34	0.967	10.54	±.50	4.0742	42.94	0.02	77	-	- 1
89 Tasso	208	11.100	±.500	?	44	0.918	10.19	±.53				34	-	- -
85 Tasso	203	10.300	±.400	?	34	0.967	9.96	±.40				-	-	- 1
85 Tasso	203	8.800	±1.000	?	22	1.063	9.36	±1.08				-	-	- 1
85 Tasso	202	10.900	±.300	?	34	0.967	10.54	±.31				-	-	- ?
83 Tasso	190	10.300	±.400	(±.4)††	34	0.967	9.96	±.40				-	-	- 1
84 Tpc	215	10.700	±.600	-	29	1.000	10.70	±.60	2.7778	29.72	0.03	-	-	- 2
88 Tpc‡	233	10.600	±.600	-	29	1.000	10.60	±.60	2.7778	29.44	0.00	68	-	- -
85 Tpc	226	10.700	±.600	-	29	1.000	10.70	±.60				-	-	- 2
83 Hrs	89	●												
85 Hrs	94	●												
77 Pluto	165	●												
76 Spear	246	●												
							10.60	±.32	9.6298	102.11	0.15			
89 Argus	17	6.380	±.120	-	9.98	1.001	6.38	±.12	69.36	442.8	1.60	3	-	- -
85 Cleo	44	8.300	±.400	-	10.5	0.987	8.19	±.40	6.37	52.2	17.46	17	-	- -
79 Dasp	76	3.000	to	4.000	4.4	1.298	3.89	±.70				8	13k	- -
85 Tasso	203	7.200	±.600	?	14	0.914	6.58	±.58				-	-	- -
83 Tasso	190	7.200	±.600	?	14	0.914	6.58	±.58				-	-	- -
							6.54	±.11	75.74	495.0	4.37			
94 Opal	158	17.052	±.429	-	91.2	1.000	17.046	±.429				25	-	- -
87 Argus	12				10									
81 Dasp	77				3.1-5.2									
77 Dasp	70				3.1-5.2									
87 Hrs	103				29									
83 Jade	113				12,30,35									
81 Jade	114				33									
85 Mac	129				29									
85 Mark2	141				29									
78 Spear	176				7.28									
75 Spear	172				4-7.									
82 Tasso	186				14,22,34									
80 Tasso	181				12,30									
88 Tpc	232				29									
87 Tpc	230				29									

Note: The numbers under "Ref" refer to the articles listed in the Appendix: Key to Tables.

† Systematic error inclusion is not specified; assumed included.
†† Systematic error is not quoted; syst = stat is assumed.
‡ LBL Publication

Table 25 ηo Production Rate Measurements.

Yr Exper	Ref	Value			Ecm	ln(E/2m)	Scaled		weight	w*value	χ2	Lu	Sig	Bck
90 Cello	34	.630	±.120	±.1500	35	0.946	.596	±.182	30.2	18.0	0.00	87	272	- -
88 Hrs	108	.580	±.100	-	29	1.000	.580	±.100	100.0	58.0	0.02	300	-	- 2
87 Hrs	107	.370	±.080	?	29	1.000	.370	±.080				300	-	- 2
90 Jade	123	.640	±.090	±.0600	34.9	0.946	.606	±.103				176	-	- 1
85 Jade	119	.640	±.150	-	34.4	0.950	.608	±.143	49.0	29.8	0.01	-	-	- 1
83 Jade	115	.720	±.100	±.1800	34	0.954	.687	±.197				-	694	- 1
88 Mark2	147	.620	±.170	±.1500	29	1.000	.620	±.227	19.5	12.1	0.01	208	-	- -
							.593	±.071	198.6	117.9	0.12			
90 Argus	20	.190	±.040	±.0400	10	1.000	.190	±.057	312.5	59.4	0.09	37	-	- -
87 Argus	13	.420	±.160	?	10	1.000	.420	±.160				37	-	- -
91 CryBa	68	.220	±.040	±.0300	10	1.000	.220	±.050	400.0	88.0	0.07	42	-	- ?
86 CryBa	66	.390	±.080	?	10	1.000	.390	±.080				-	-	- ?
							.207	±.037	712.5	147.4	0.40			
92 Aleph	4	.298	±.023	±.021	91	1.000	.298	±.031	†			-	-	- -
92 Aleph	†	1.117	±.088	±.137	91	1.000	1.117	±.163	37.7	42.1	1.62	-	-	- -
94 L3 ††	301	.910	±.020	±.110	91.2	1.000	.910	±.112	80.1	72.8	0.35	35	-	- -
							.976	±.092	117.8	115.0	1.41			
83 Cello	33				14,22,34									
82 Cello	32				34									
81 CryBa	65				10									
79 Dasp	74				3.1-5.2									
79 Dasp	75				3.1-5.2									
77 Dasp	72				3.1-5.2									
88 Hrs	109				29									
92 L3	125				91.2									

Table 26 ηo' Production Rate Measurements.

Yr Exper	Ref	Value			Ecm	ln(E/2m)	Scaled		weight	w*value	χ2	Lu	Sig	Bck
88 Mark2	147	.260	±.090	±.050	29	1.000	.260	±.103	94.34	24.53	0.00	208	45	- -
							.260	±.103	94.34	24.53	0.00			
92 Argus	30	.034	±.010	±.004	10	1.000	.034	±.011	8621	293.1	0.00	-	-	- -
92 Argus	24	.034	±.010	±.004	10	1.000	.034	±.011				-	-	- -
86 CryBa	66	.100	±.500	?	10	1.000	.100	±.500				-	-	- -
							.034	±.011	8621	293.1	0.00			
92 Aleph	4	.068	±.018	±.016	91	1.000	.068	±.024	†			-	-	- -
92 Aleph	†	.175	±.047	±.045	91	1.000	.175	±.065	236	41.3	0.00	-	-	- -
							.175	±.065	236	41.3	0.00			

Note: The numbers under "Ref" refer to the articles listed in the Appendix: Key to Tables.

† Extrapolations from (0.1 to 1.0 XE) with LUND by E.C.Berg.
†† Submitted to Phys.Lett.B.

Table 27 K± Production Rate Measurements.

Yr Exper	Ref	Value			Ecm	ln(E/2m)	Scaled		weight	w*value	χ2	Lu	Sig	Bck
89 Tasso	208	1.760	±.200	?†	34	0.955	1.681	±.192	26.99	45.37	1.57	77	-	-	2
85 Tasso	203	2.000	±.200	(±.2)††	34	0.955	1.910	±.193				-	-	-	2
85 Tasso	203	1.500	±.200	?	22	1.089	1.634	±.221				-	-	-	2
83 Tasso	190	2.000	±.200	(±.2)††	34	0.955	1.910	±.193				-	-	-	2
85 Tasso	202	1.740	±.140	?	34	0.955	1.662	±.136				-	-	-	2
88 Tpc‡	233	1.430	±.090	-	29	1.000	1.430	±.090	123.46	176.54	0.01	68	-	-	-
85 Tpc	226	1.350	±.130	-	29	1.000	1.350	±.130				-	-	-	1
84 Tpc	215	1.350	±.130	-	29	1.000	1.350	±.130	59.17	79.88	0.48	-	-	-	1
85 Hrs	94	♠													
77 Pluto	165	♠													
76 Spear	246	♠													
							1.440	±.069	209.62	301.80	1.01				
85 Cleo	44	1.300	±.200	-	10.5	0.980	1.274	±.196	26	33	3.68	17	-	-	-
79 Dasp	76	.500	to	.600	4.4	1.549	.852	±.124				8	890	-	-
85 Tasso	203	1.200	±.140	?	14	0.873	1.048	±.130				-	-	-	-
89 Argus	17	.888	±.018	±.024	9.98	1.001	.889	±.030	1109	986	0.09	3	-	-	-
81 Cleo	37	♠													
							.898	±.030	1135	1019	1.94				
94 Opal	158	2.421	±.133	-	91.2	1.000	2.420	±.133				25	-	-	-
85 Mark2	141				29										
87 Hrs	103				29										
84 Tpc	216				29										
88 Tpc	232				29										
75 Spear	172				4-7.										
80 Tasso	181				22-44										
87 Argus	12				10										
83 Jade	114				33										
85 Mac	129				29										
81 Dasp	77				3.1-5.2										
77 Dasp	70				3.1-5.2										
77 Dasp	71				3.1-5.2										

Note: The numbers under "Ref" refer to the articles listed in the Appendix: Key to Tables.

† Systematic error inclusion is not specified; assumed included.
†† Systematic error is not quoted; syst = stat is assumed.
‡ LBL Publication

Table 28. Ko Production Rate Measurements.

Yr Exper	Ref	Value			Ecm	ln(E/2m)	Scaled		weight	w*value	χ2	Lu	Sig	Bck
90 Cello	35	1.420	±.090	±.180	35	0.947	1.345	±.192	27.14	36.5	0.09	86	-	-	-
90 Hrs	111	1.427	±.021	±.097	29	1.000	1.427	±.099	101.52	144.9	0.06	291	7155	-	-
87 Hrs	103	1.580	±.030	±.080	29	1.000	1.580	±.085				185	-	-	1
87 Jade	122	1.800	±.140	-	44	0.890	1.602	±.138	52.48	84.1	2.06	-	-	-	-
83 Jade	113	1.270	±.160	±.130	22	1.089	1.383	±.227				-	-	-	-
83 Jade	113	1.490	±.220	±.150	30	0.990	1.475	±.264	14.39	21.2	0.07	-	-	-	-
83 Jade	113	1.450	±.080	±.150	35	0.947	1.373	±.163	37.80	51.9	0.03	-	-	-	-
90 Mark2	152	1.260	±.040	±.140	29	1.000	1.260	±.146				25	1442	31	-
85 Mark2	141	1.270	±.030	±.150	29	1.000	1.270	±.153	42.74	54.3	0.76	105	4200	-	-
81 Pluto	171	1.460	±.300	(0.3)†	29.6	0.994	1.451	±.422	5.62	8.2	0.01	3.0	-	-	-
90 Tasso	211	1.280	±.110	±.080	21.5	1.097	1.405	±.154				3	292	55	2
90 Tasso	211	1.490	±.040	±.050	34.5	0.951	1.417	±.065	238.80	338.4	0.04	78	3426	289	3
90 Tasso	211	1.480	±.030	±.030	35	0.947	1.402	±.047	461.91	647.5	0.00	111	4766	175	-
90 Tasso	211	1.520	±.050	±.050	42.6	0.898	1.364	±.079				4	1262	90	-
85 Tasso	203	1.480	±.050	?	34	0.955	1.413	±.052				-	-	-	3
85 Tasso	203	1.170	±.130	?	22	1.089	1.274	±.145				-	-	-	2
84 Tasso	196	1.600	±.100	(±.1)†	34	0.955	1.528	±.098				-	-	-	3
80 Tasso	180	1.400	±.300	±.140	30	0.990	1.386	±.328	9.31	12.9	0.00	-	90	26	-
85 Tpc	226	1.220	±.150	-	29	1.000	1.220	±.150				-	-	-	4
84 Tpc	218	1.220	±.030	±.150	29	1.000	1.220	±.153	42.74	52.1	1.44	77	2076	-	4
85 Hrs	94	♠													
75 None	243	♠													
82 Tasso	184	♠													
							1.404	±.031	1034.4	1452.0	0.68				
89 Argus	17	0.910	±.050	±.034	9.98	1.001	0.911	±.061	273.0	248.7	0.04	2.6	-	-	-
85 Cleo	44	0.920	±.120	-	10.5	0.980	0.901	±.118	72.2	65.1	0.00	17	-	-	-
82 Cusb	69	0.820	±.090	±.090	10	1.000	0.820	±.127	61.7	50.6	0.38	-	-	-	-
83 Jade	113	1.140	±.270	±.110	12	0.927	1.057	±.271	13.6	14.3	0.34	-	-	-	-
83 Jade	113	1.050	±.100	±.110	14	0.873	0.916	±.136				-	-	-	-
81 Pluto	171	0.730	±.160	(.16)†	9.37	1.029	0.751	±.233	18.4	13.8	0.40	35	-	-	-
81 Pluto	171	1.500	±.400	(.40)†	12	0.927	1.390	±.525	3.6	5.0	0.88	10	-	-	-
90 Tasso	211	1.170	±.090	±.070	14.8	0.855	1.000	±.110				2	396	39	5
85 Tasso	203	1.150	±.100	?	14	0.873	1.004	±.098				-	-	-	5
							0.898	±.048	442.6	397.6	0.64				
94 Aleph††	300	2.061	±.047	?††	91	1.000	2.061	±.047	452.69	933.00	0.16	-	-	-	-
92 Delphi	85	2.120	±.050	±.040	91	1.000	2.120	±.064	243.90	517.07	0.39	-	9.4k	-	-
94 L3 ‡	301	(1.02	±.010	±.07)*2‡	91.2	1.000	2.039	±.141	50.05	102.05	0.08	35	-	-	-
90 Mark2	152	1.540	±.210	±.180	91	1.000	1.540	±.277				02	60.2	5.2	-
91 Opal	157	2.100	±.020	±.140	91.3	0.999	2.098	±.141	50.07	105.08	0.02	-	13.8k	-	-
							2.080	±.035	796.72	1657.20	0.47				
87 Argus	12				10										
84 Cleo	40				10.5										
85 Mark2	142				29										
93 Opal	162				91.3										
77 Pluto	166				9-12.										
76 Pluto	164				9-12.										
77 Spear	173				4-7.										
81 Tasso	182				33.3										

Note: The numbers under "Ref" refer to the articles listed in the Appendix: Key to Tables.

† Systematic error is not quoted; syst = stat is assumed.
†† Systematic Inclusion not stated; assumed included; submitted to Z.Phys.C.
‡ Only quoted K0s rate; submitted to Phys.Lett.B.

Table 29 ρo Production Rate Measurements.

Yr Exper	Ref	Value			Ecm	ln(E/2m)	Scaled		weight	w*value	χ2	Lu	Sig	Bck
85 Hrs	97	.950	±.090	?	29	1.000	.950	±.090				185	-	- 1
89 Hrs	110	.900	±.050	-	29	1.000	.900	±.050	400.0	360.000	1.27	291	-	- 1
84 Jade	116	.980	±.090	±.150	35	0.940	.921	±.165	36.6	33.686	0.22	61	-	- -
85 Tasso	203	.730	±.060	(±.06)†	34	0.949	.693	±.081	151.4	104.831	3.45	-	-	- 2
84 Tasso	199	.730	±.060	(±.06)†	34	0.949	.693	±.081				-	-	- 2
88 Tpc ††	234	.770	±.080	±.150	29	1.000	.770	±.170	34.6	26.644	0.19	68	-	- -
84 Mark2	138	●												
							.844	±.040	622.6	525.2	1.31			
93 Argus‡	29	.326	±.015	±.038	10	1.000	.326	±.041	599.2	195.327	0.49	17	-	- -
85 Cleo	44	.500	±.090	-	10.5	0.975	.488	±.088	129.6	63.190	2.29	17	-	- -
							.355	±.037	728.8	258.5	1.67			
93 Delphi	87	1.430	±.120	±.220	91	1.000	1.430	±.251	15.9	22.771	0.00	-	-	- -
							1.430	±.251	15.9	22.8	0.00			
84 Hrs	91				29									
85 Mark2	141				29									
84 Mark2	137				29									
82 Tasso	189				22-44									2

Table 30 K*± Production Rate Measurements.

Yr Exper	Ref	Value			Ecm	ln(E/2m)	Scaled		weight	w*value	χ2	Lu	Sig	Bck
87 Hrs	105	.620	±.045	±.0400	29	1.000	.620	±.060	275.9	171.0	0.13	300	970	- -
84 Jade	116	.870	±.160	±.0800	35	0.937	.815	±.168	35.3	28.7	1.05	61	-	- -
							.642	±.057	311.1	199.8	1.09			
93 Argus‡	29	.246	±.015	±.031	10	1.000	.246	±.034	843	207.4	0.83	17	-	- -
85 Cleo	44	.450	±.080	-	10.5	0.973	.438	±.078	165	72.1	4.24	17	-	- -
							.277	±.031	1008	279.5	2.25			
92 Delphi	85	1.330	±.110	±.2400	91	1.000	1.33	±.264	14.35	19.08	4.43	17	-	- -
93 Opal	163	.720	±.020	±.0800	91	1.000	0.72	±.082	147.06	105.88	0.43	17	-	- -
							0.77	±.079	161.41	124.96	2.21			
89 Hrs	110				29									
84 Mark2	137				29									
87 Tpc	229				29									

Note: The numbers under "Ref" refer to the articles listed in the Appendix: Key to Tables.

Table 31. K*o Production Rate Measurements.

Yr Exper	Ref	Value			Ecm	ln(E/2m)	Scaled		weight	w*value	χ2	Lu	Sig	Bck
90 Cello	35	.770	±.170	±.140	35	0.937	.721	±.207	23.4	16.9	0.53	86	-	- -
89 Hrs	110	.590	±.050	-	29	1.000	.590	±.050	400.0	236.0	0.15	291	-	- 1
85 Hrs	97	.630	±.100	?	29	1.000	.630	±.100				185	-	- 1
90 Tasso	211	.510	±.180	±.070	35	0.937	.478	±.181	30.5	14.6	0.26	-	219	- -
90 Tasso	211	.660	±.120	±.040	34.5	0.941	.621	±.120	69.9	43.4	0.18	-	643	- -
90 Tasso	211	.770	±.170	±.080	42.6	0.879	.677	±.167				-	190	- -
88 Tpc †	234	.580	±.050	±110	29	1.000	.580	±.121	68.5	39.7	0.01	68	-	- -
85 Tpc	226	.490	±.080	-	29	1.000	.490	±.080				-	-	- 2
84 Tpc	218	.490	±.040	±.070	29	1.000	.490	±.081	153.8	75.4	1.01	77	2750	- 2
84 Mark2	138	●												
							.571	±.037	746.1	425.9	0.65			
93 Argus††	29	.292	±.007	±.029	10	1.000	.292	±.030	1124	328.1	0.07	-	-	- -
85 Cleo	44	.380	±.090	-	10.5	0.973	.370	±.088	130	48.2	0.63	17	-	- -
							.300	±.037	1254	376.2	0.84			
93 Delphi	87	.970	±.180	±.310	91	1.000	.970	±.358	7.8	7.55	0.32	-	-	- -
92 Opal	160	.755	±.067	±.060	91	1.000	.755	±.090	123.6	93.34	0.02	-	-	- -
							.768	±.087	131.4	100.89	0.58			
87 Argus	12				10									
87 Hrs	105				29									
84 Jade	116				22,30,35									
83 Jade	113				22,30,35									
85 Mark2	141				29									
85 Mark2	142				29									
84 Mark2	137				29									
81 Pluto	171				9-12.									
82 Tasso	189				22-44									
80 Tasso	180				30									

Note: The numbers under "Ref" refer to the articles listed in the Appendix: Key to Tables.

Table 32. φ Production Rate Measurements.

Yr Exper	Ref		Value		Ecm	ln(E/2m)	Scaled		weight	w*value	χ2	Lu	Sig	Bck
88 Tpc †	234	.076	±.010	±.0120	29	1.000	.076	±.016	4098	311.5	0.03	68	-	-	-
85 Tpc	226	.084	±.022	-	29	1.000	.084	±.022				-	-	-	1
84 Tpc	216	.084	±.013	±.0180	29	1.000	.084	±.022	2028	170.4	0.06	69	62	-	1
							.079	±.013	6127	481.9	0.29				
89 Argus	19	.041	±.002	±.0021	9.46	1.036	.0428	±.0030				37	-	-	-
89 Argus	19	.045	±.002	±.0024	10	0.999	.0447	±.0032	98613	4411	0.07	37	-	-	-
93 Argus	29	.044	±.002	±.0020	10	1.000	.0440	±.0028				37	-	-	-
85 Cleo	44	.080	±.020	-	10.5	0.971	.0777	±.0194	2649	206	2.72	17	-	-	-
? Argus	31	¢													
							.0456	±.0031	101262	4617	1.67				
92 Opal	160	.086	±.015	±.0100	91	1.000	.0860	±.0180	3077	264.6	0.00	-	-	-	-
93 Aleph	6	¢													
							.0860	±.0180	3077	265	0.00				
85 Hrs	96				27.2										

Note: The numbers under "Ref" refer to the articles listed in the Appendix: Key to Tables.

97

Table 33. p± Production Rate Measurements.

Yr Exper	Ref		Value		Ecm	ln(E/2m)	Scaled		weight	w*value	χ2	Lu	Sig	Bck
81 Jade	114	(.27	±.030	)*2†	33	0.955	.516	±.058	299.7	154.6	0.86	-	-	-	-
89 Tasso	208	.670	±.060	?††	34	0.945	.633	±.058	299.6	189.7	1.23	77	-	-	2
85 Tasso	203	.800	±.100	(±.1)‡	34	0.945	.756	±.095				-	-	-	2
85 Tasso	203	.620	±.060	?	22	1.112	.690	±.070				-	-	-	2
85 Tasso	202	.680	±.060	?	34	0.945	.643	±.058				-	-	-	2
85 Tasso	201	.680	±.080	-	34	0.945	.643	±.076				-	-	-	2
83 Tasso	190	.800	±.100	(±.1)‡	34	0.945	.756	±.095				-	-	-	2
88 Tpc ‡‡	233	.530	±.070	-	29	1.000	.530	±.070	204.1	108.2	0.31	68	-	-	-
85 Tpc	226	.600	±.080	-	29	1.000	.600	±.080				-	-	-	1
84 Tpc	215	.600	±.080	-	29	1.000	.600	±.080	156.3	93.8	0.15	-	-	-	1
84 Tpc	219	.600	±.080	-	29	1.000	.600	±.080				-	-	-	1
77 Pluto	165	¢													
76 Spear	246	¢													
							.569	±.032	959.7	546.2	0.92				
89 Argus	17	(0.271	0.018)†	-	9.98	1.001	.271	±.018	3079	835.4	0.03	3	-	-	-
85 Cleo	44	.400	±.060	-	10.5	0.972	.389	±.058	293	113.9	3.82	17	-	-	-
81 Dasp	77	(.050±.03	(±.03)‡)*2†		9.74	1.016	.102	±.086	135	13.7	4.03	1	-	-	?
79 Dasp	76	.050	to	±.080	4.4	1.963	.098	±.033				8	130	-	?
85 Tasso	203	.420	±.060	?	14	0.833	.350	±.054				-	-	-	3
83 Tasso	190	.420	±.060	?	14	0.833	.350	±.054				-	-	-	3
							.275	±.017	3506	963.0	1.99				
94 Opal	158	0.916	±.111	-	91.2	1.000	0.916	±.111				25	-	-	-
88 Argus	14				10										
87 Argus	12				10										
84 Cleo	40				10.5										
77 Dasp	70				3.1-5.2										
87 Hrs	103				29										
83 Jade	113				12-35.										
85 Mark2	140				29										
85 Mark2	141				29										
82 Mark2	133				29										
78 Spear	176				4-7.										
77 Spear	174				4-7.										
75 Spear	172				4-7.										
84 Tasso	197				34										
83 Tasso	192				22-44										
82 Tasso	186				22-44										
81 Tasso	182				33.3										
80 Tasso	181				30										
88 Tpc	232				29										
87 Tpc	230				29										
85 Tpc	224				29										

Note: The numbers under "Ref" refer to the articles listed in the Appendix: Key to Tables.

98

Table 34 Λo Production Rate Measurements.

Yr Exper	Ref	Value			Ecm	ln(E/2m)	Scaled		weight	w*value	χ2	Lu	Sig	Bck	
90 Cello	35	.211	±.027	±.027	35	0.932	.197	±.036	779	153	0.12	86	220	-	-
87 Hrs	103	.217	±.009	±.022	29	1.000	.217	±.024	1770	384	0.11	185	-	-	1
86 Hrs	99	.220	±.007	±.022	29	1.000	.220	±.023				256	-	-	1
85 Jade	121	.247	±.014	±.030	34	0.942	.233	±.031				-	-	-	?
81 Jade	114	(0.117	±.032	)*2†	33	0.952	.223	±.122	67	15	0.01	-	-	-	?
90 Mark2	152	.170	±.015	±.018	29	1.000	.170	±.023				25	245	63	-
85 Mark2	142	.213	±.012	±.018	29	1.000	.213	±.022	2137	455	0.03	205	1610	-	-
89 Tasso	210	.256	±.030	±.025	42.1	0.873	.224	±.035				-	-	-	4
89 Tasso	210	.218	±.011	±.021	34.8	0.934	.204	±.023	1966	400	0.06	-	-	-	5
88 Tasso	207	.218	±.011	±.021	34.8	0.934	.204	±.023				-	-	-	5
88 Tasso	207	.256	±.030	±.025	42.1	0.873	.224	±.035				-	-	-	4
85 Tasso	203	.310	±.030	?	34	0.942	.292	±.029				-	-	-	5
85 Tasso	203	.220	±.050	?	22	1.121	.247	±.057	343	91	1.13	-	-	-	2
83 Tasso	190	.280	±.040	±.040	33	0.952	.267	±.054				-	-	-	2
81 Tasso	182	.280	±.040	±.040	33	0.952	.267	±.054				-	-	-	2
92 Tpc ††	236	.211	±.010	±.014	29	1.000	.211	±.017	3378	713	0.01	68	1038	-	3
91 Tpc	237	.211	±.009	±.014	29	1.000	.211	±.017				68	1038	-	3
90 Tpc	235	.211	±.009	±.014	29	1.000	.211	±.017				70	1038	-	3
85 Tpc	223	.197	±.012	±.017	29	1.000	.197	±.021	2309	455	0.34	-	-	-	6
85 Tpc	226	.200	±.020	-	29	1.000	.200	±.020				-	-	-	6
84 Tpc	219	.216	±.013	±.018	29	1.000	.216	±.022				-	-	-	6
86 Mark2	144	♠													
84 Mark2	138	♠													
88 Tasso	206	♠													
84 Tasso	200	♠													
							.209	±.009	12749	2667	0.51				
88 Argus	14	.092	±.003	±.008	10	1.000	.092	±.009	13699	1260	2.05	42	-	-	-
85 Cleo	44	.066	±.010	-	10.5	0.969	.064	±.010	10606	678	2.65	17	-	-	-
85 Tasso	203	.130	±.040	?	14	0.817	.106	±.033							
							.080	±.006	24304	1939	2.17				
94 Aleph ‡	300	.386	±.016	-	91	1.000	.3860	±.0160	3906	1508	0.86	-	-	-	-
93 Delphi	302	.357	±.017	?	91	1.000	.3570	±.0170				-	-	-	-
92 Delphi	85	.360	±.030	±.060	91	1.000	.3600	±.0671	222	80	0.03	-	1915	-	
94 L3 ‡‡	301	.370	±.010	±.040	91.2	0.999	.3698	±.0412	589	218	0.00		25	6	-
90 Mark2	152	.470	±.100	±.050	91	1.000	.4700	±.1118				0	25	6	-
92 Opal	161	.351	±.003	±.019	91	1.000	.3510	±.0192	2703	949	1.10	-	17.5K	7.5K	-
93 Aleph	6	♠													
							.3712	±.0116	7420	2754	0.81				
87 Argus	12				10										
86 Argus	11				10										
85 Argus	8				10										
84 Cleo	40				10.5										
86 Hrs	101				29										
85 Mark2	141				29										
82 Mark2	133				29										
82 Mark2	134				29										
81 Pluto	171				9-12.										
77 Spear	174				4-7.										
90 Tasso	211				22-44										
84 Tasso	198				22-44										
83 Tasso	192				22-44										

Note: The numbers under "Ref" refer to the articles listed in the Appendix: Key to Tables.

† This measurement is of Lambda-Bar only.
†† TPC/Two-Gamma paper to be submitted.
‡ Submitted to Z.Phys.C.
‡‡ Submitted to Phys.Lett.B.

Table 35 Ξ− Production Rate Measurements.

Yr Exper	Ref	Value			Ecm	ln(E/2m)	Scaled		weight	v*value	χ2	Lu	Sig	Bck	
87 Hrs	106	.0160	±.004	±.004	29	1.000	.0160	±.0057	31250	500	0.08	300	-	-	-
87 Jade	122	.0500	±.010	±.010	34	0.949	.0474	±.0134	5535	263	4.94	-	-	-	-
88 Mark2	148	.0170	±.004	±.004	29	1.000	.0170	±.0057				207	41	14	1
87 Mark2	145	.0170	±.004	±.004	29	1.000	.0170	±.0057	31250	531	0.01	207	41	14	1
89 Tasso	210	.0140	±.003	±.004	34.8	0.942	.0132	±.0047	44971	593	0.86	-	-	-	2
88 Tasso	207	.0111	±.003	±.002	34.8	0.942	.0105	±.0034				-	-	-	2
85 Tasso	203	.0260	±.008	(±.009)†	34	0.949	.0247	±.0076				-	-	-	2
84 Tasso	196	.0260	±.008	±.009	34	0.949	.0247	±.0114				-	-	-	2
83 Tasso	192	.0260	±.008	±.009	34	0.949	.0247	±.0114				-	16	4	2
92 Tpc ††	236	.0200	±.004	±.003	29	1.000	.0200	±.0050	40000	800	0.24	68	50.6	-	3
91 Tpc	237	.0200	±.004	±.003	29	1.000	.0200	±.0050				68	53	-	3
90 Tpc	235	.0200	±.004	±.003	29	1.000	.0200	±.0050				70	53	-	3
85 Tpc	226	.0200	±.009	-	29	1.000	.0200	±.0090				-	-	-	4
85 Tpc	227	.0200	±.008	±.004	29	1.000	.0200	±.0089				77	17.3	-	4
84 Tpc	219	.0250	±.009	±.006	29	1.000	.0250	±.0108				-	16	-	4
84 Tpc	220	.0250	±.009	±.008	29	1.000	.0250	±.0120				-	16	-	4
82 Mark2	133	♠													
							.0176	±.0026	153006	2687	1.24				
85 Cleo	44	.0050	±.0010	-	10.5	0.975	.00488	±.00098	1050E+3	5119	0.97	17	-	-	-
88 Argus	14	.0067	±.0006	±.0007	10	1.000	.00670	±.00092	1176E+3	7882	0.87	42	-	-	-
							.00584	±.00067	2226E+3	13002	1.36				
92 Delphi	85	.0200	±.0040	±.0030	91	1.000	.020	±.005	40000	800	0.01	42	-	-	-
92 Opal	161	.0206	±.0011	±.0019	91	1.000	.021	±.002	207469	4274	0.00	20	726	388	-
92 Aleph	5	♠													
							.021	±.002	247469	5074	0.11				
87 Argus	12				10										
86 Argus	11				10										
85 Argus	8				10										
84 Cleo	40				10.5										
84 Cleo	43				10.5										
83 Jade	114				12-35.										
84 Mark2	139				29										
78 Spear	175				4-7.										
83 Tasso	190				22-44										
81 Tasso	182				22-44										
84 Tpc	217				29										

Note: The numbers under "Ref" refer to the articles listed in the Appendix: Key to Tables.

† Systematic error is not quoted; syst = other reference is assumed.
†† TPC/Two-Gamma paper to be submitted.

Table 36 Δ++ Production Rate Measurements.

Yr Exper	Ref	Value			Ecm	ln(E/2m)	Scaled		weight	w*value	χ2	Lu	Sig	Bck
84 Tasso	198	<.10	95%	-	34.4	0.935	.094	-				73	-	-
							<.094	95%.						
89 Argus	18	.040	±.008	±.006	10	1.000	.040	±.010	10000	400 0.00	45 1185	-
85 Cleo	45	¢											
							.040	±.010	10000	400 0.00		
92 Aleph	6	¢			91								
? Opal	?	¢			91								
84 Cleo	40				10.5								

Table 37 Σ*± Production Rate Measurements.

Yr Exper	Ref	Value			Ecm	ln(E/2m)	Scaled		weight	w*value	χ2	Lu	Sig	Bck
87 Hrs	106	.0330	±.0080	±.005	29	1.000	.033	±.009	11236	370.8 0.00	300	-	-
89 Tasso	210	<.053	95%	-	34.8	0.928	.049	±.009			-	-	- 2
88 Tasso	207	<.053	95%	-	34.8	0.928	.049	-			-	-	- 2
84 Tasso	198	<.09	95%	-	34.4	0.932	.084	-			73	-	-
85 Tpc	227	.0730	±.0320	±.017	29	1.000	.073	±.036			77 39.4	τ	1
85 Tpc	226	.0730	±.0360	-	29	1.000	.073	±.036			77	-	- 1
						†	.033	±.009	11236	370.8 0.00		
88 Argus	14	.00513	±.00095	±.00092	10	1.000	.005	±.001			42	-	- 3
88 Argus	14	.00553	±.00109	±.00098	10	1.000	.006	±.001			42	-	- 3
- sum -		.01066	±.00197	-	10	1.000	.011	±.002	256581	2735 0.00	42	-	- 3
							.011	±.002	256581	2735 0.00		
92 Opal	161	.0380	±.0038	±.0049	91	1.000	.0380	±.0062	26008	988.3 0.00	20 2480	-	-
							.0380	±.0062	26008	988.3 0.00		
87 Argus	12				10								
86 Argus	11				10								
85 Argus	8				10								
85 Cleo	44				10.5								

Note: The numbers under "Ref" refer to the articles listed in the Appendix: Key to Tables.

Table 38 Ξ*0 Production Rate Measurements.

Yr Exper	Ref	Value			Ecm	ln(E/2m)	Scaled		weight	w*value	χ2	Lu	Sig	Bck
88 Mark2	148	<.006	90%	-	29	1.000	.0060	-				207	-	1
87 Mark2	145	<.006	90%	-	29	1.000	.0060	-				207	-	1
87 Mark2	†	.0010	±.0050	-	29	1.000	.0010	±.0050	40000	40.0 0.67	207	.8	5.3 1
92 Tpc ††	236	.0090	±.0038	±.0031	29	1.000	.0090	±.0049	41580	374.2 0.64	68	9.7	- 2
91 Tpc	237	.0100	±.0050	±.0030	29	1.000	.0100	±.0058			68	11.7	- 2
90 Tpc	235	.0097	±.0039	±.0043	29	1.000	.0097	±.0058			68	11.5	- 2
85 Tasso	204	¢											
							.0051	±.0035	81580	414.2 1.14		
88 Argus	14	.0015	±.0005	±.0002	10	1.000	.0015	±.0005	3844675	5613 0.00	-	-	-
							.0015	±.0005	3.8E+6	5613 0.00		
92 Opal	161	.0063	±.0010	±.0010	91	1.000	.0063	±.0014	500000	3150 0.00	-	-	-
							.0063	±.0014	500000	3150 0.00		
87 Argus	12				10								
86 Argus	11				10								
85 Argus	8				10								
85 Cleo	44				10.5								
84 Cleo	40				10.5								
84 Cleo	43				10.5								

Table 39 Ω± Production Rate Measurements.

Yr Exper	Ref	Value			Ecm	ln(E/2m)	Scaled		weight	w*value	χ2	Lu	Sig	Bck
88 Mark2	148	.0140	±.0060	±.0040	29	1.000	.01400	±.00721			207	14	9 3
87 Mark2	146	.0140	±.0060	±.0040	29	1.000	.01400	±.00721	19231	269.2 1.44	207	16	7 3
88 Tasso	207	<.013	95%	-	34.8	0.922	.01199	-			-	-	-
92 Tpc ††	236	.0042	±.0022	±.0014	29	1.000	.00420	±.00261	147059	617.6 0.19	68	8.8	- 1
91 Tpc	237	.0042	±.0022	±.0014	29	1.000	.00420	±.00261			68	8.8	- 1
90 Tpc	235	.0037	±.0018	±.0014	29	1.000	.00370	±.00228			70	10	- 1
85 Tpc	226	.0270	±.0170	-	29	1.000	.02700	±.01700			-	-	- 2
85 Tpc	227	.0270	±.0120	±.0090	29	1.000	.02700	±.01500			77	-	- 2
							.00533	±.00245	166290	887 1.28		
88 Argus	14	.0007	±.0004	±.0001	10	1.000	.00072	±.00038	6825939	4915 0.00	42	-	-
							.00072	±.00038	683E+4	4915 0.00		
92 Opal	161	.0050	±.0012	±.0009	91	1.000	.00500	±.00150	444444	2222 0.00	20	-	-
							.00500	±.00150	444444	2222 0.00		
87 Argus	12				10								
86 Argus	11				10								
85 Argus	8				10								
85 Cleo	44				10.5								

Note: The numbers under "Ref" refer to the articles listed in the Appendix: Key to Tables.

Table 40 Nch Production Rate Measurements (includes K°ς & Λ° decay products).

Yr Exper	Ref	Value			Ecm	ln(E/2m)†	Corrected ††		weight	w*value	χ2	Lu	K	Λ
86 Hrs	100	11.34	±.03	±.30	29	1.000	12.56	±.30	10.797	135.66	0.22	185.	x	x	-
86 Hrs	95	13.10	±.05	±.60	29	1.000	13.10	±.60	2.759	36.138	1.27	.2	-	-	1
85 Hrs	98	13.10	±.05	±.60	29	1.000	13.10	±.60				-	?	?	1
87 Jade	122	11.80	±.40	±.70	34	.964	11.38	±.79				.1	?	?	?
83 Jade	113	11.40	±.40	±.70	30	.992	12.54	±.80	1.556	19.511	0.02	-	x	x	?
83 Jade	113	11.87	±.40	±.70	35	.958	12.60	±.79	1.598	20.136	0.05	-	x	x	?
79 Jade	112	11.60	±.50	?	27.7	1.011	11.72	±.51				.2	?	?	?
79 Jade	112	10.10	±.70	?	22	1.068	10.79	±.78				.04	?	?	-
79 Jade	112	11.70	±.50	?	30	.992	11.61	±.50				.4	?	?	-
79 Jade	112	10.90	±.60	?	31.6	.980	10.69	±.59				.1	?	?	?
85 Mark2	143	12.90	±.10	±.60	29	1.000	12.90	±.61	2.703	34.865	0.62	205	-	-	-
80 Pluto	170	9.70	±.70	(±7%)‡	22	1.068	11.32	±1.07				-	x	-	-
80 Pluto	170	10.40	±.30	(±7%)‡	27.6	1.012	11.48	±.80	1.568	18.003	1.39	-	x	-	-
80 Pluto	170	10.40	±.20	(±7%)‡	30.2	.991	11.26	±.75	1.779	20.037	2.39	-	x	-	-
80 Pluto	170	10.60	±.30	(±7%)‡	30.7	.987	11.42	±.79	1.593	18.196	1.60	-	x	-	-
80 Pluto	170	11.00	±.30	(±7%)‡	31.3	.983	11.77	±.82	1.504	17.698	0.64	-	x	-	-
80 Pluto	170	10.60	±.10	(±7%)‡	30.9	.986	11.41	±.74	1.822	20.787	1.87	-	x	-	-
89 Tasso	209	11.30	±.08	±.46	22	1.068	12.07	±.55				-	-	-	2
89 Tasso	209	13.59	±.02	±.46	34.8	.959	13.04	±.47	4.495	58.614	1.72	-	-	-	2
89 Tasso	209	15.08	±.06	±.47	43.6	.914	13.78	±.58				-	-	-	2
84 Tasso	197	11.22	±.07	(±3%)‡‡	22	1.068	11.99	±.45				90	-	-	2
84 Tasso	197	11.69	±.24	(±3%)‡‡	25	1.036	12.11	±.47				-	-	-	2
84 Tasso	197	12.79	±.13	(±3%)‡‡	30.5	.988	12.64	±.42				-	-	-	2
84 Tasso	197	13.48	±.03	(±3%)‡‡	34.5	.961	12.96	±.43				-	-	-	2
84 Tasso	197	14.41	±.24	±.45	41.5	.923	13.31	±.58				-	-	-	2
80 Tasso	179	11.20	±.70	±.80	22	1.068	11.97	±1.16				-	?	?	-
80 Tasso	179	12.10	±.30	±.80	27.6	1.012	12.24	±.87				-	?	?	-
80 Tasso	179	13.40	±.20	±.90	30.3	.990	13.27	±.91				-	?	?	-
80 Tasso	179	13.10	±.30	±.90	31.2	.983	12.88	±.94				-	?	?	-
83 Tpc	214	12.00	±.30	±1.00	29	1.000	12.00	±1.04				68	?	?	-
85 Delco	79	•													
79 None	252	•													
78 None	250	•													
88 None	267	•													
							12.42	.18	32.18	399.6	1.09				
90 Aleph	2	21.30	±.10	±.60	91.2	1.000	21.29	±.61	2.704	57.584	0.19	-	-	-	-
91 Delphi	83	20.71	±.04	±.77	91.3	.999	20.70	±.77	1.684	34.853	0.18	-	-	-	?
90 Delphi	82	20.60	±1.00	-	91.3	.999	20.59	±1.00				-	?	?	?
92 L3	126	20.79	±.52	-	91.2	1.000	20.78	±.52	3.701	76.915	0.23	-	-	-	-
91 L3	124	20.70	±.70	-	91.2	1.000	20.69	±.70	2.042	42.261	0.23	-	-	-	-
90 Mark2	151	20.10	±1.00	±.90	91.1	1.000	20.10	±1.35				.02	-	-	8
90 Mark2	153	20.10	±1.00	±.90	91.1	1.000	20.10	±1.35	.553	11.107	0.48	.02	-	-	8
92 Opal	159	21.40	±.02	±.43	91.2	1.000	21.39	±.43	5.401	115.53	0.71	3.5	-	-	?
90 Opal	156	21.28	±.04	±.84	91.3	.999	21.27	±.84				1.3	?	?	?
90 Delphi	81	•													
							21.03	±.25	16.085	338.25	0.64				

Note: The numbers under "Ref" refer to the articles listed in the Appendix: Key to Tables.

† all scaling based on an average mass of 193.4MeV.
†† corrected to include decay products < K°ς & Λ° if x'd in corresponding column.
‡ systematic error inclusion not specified, 7% assumed.
‡‡ syst not included: 3% assumed.

Table 40 Nch Production Rate Measurements (continued).

Yr Exper	Ref	Value			Ecm	ln(E/2m)†	Corrected ††		weight	w*value	χ2	Lu	K	Λ
92 Argus	26	8.35	±.02	±.20	10.5	.986	8.95	±.21	23.712	212.29	7.73	43	x	x	-
82 Cleo	38	8.10	±.10	±.30	10.6	.982	7.96	±.31	10.169	80.918	1.83	5.5	-	-	-
83 Jade	113	7.20	±.50	±.70	12	.947	7.54	±.83	1.468	11.066	1.05	-	x	x	-
81 Lena	127	6.32	±.08	±10%	9.5	1.016	6.42	±.65				.1	?	?	-
81 Lena	127	6.42	?	?	10	1.000	6.42	?				0.4	?	?	-
81 Pluto	171	6.90	±.10	±7%	9.4	1.020	7.66	±.51	3.893	29.809	2.04	.4	x	-	3
81 Pluto	171	7.40	±.20	±7%	12.0	.947	7.62	±.54	3.397	25.901	1.95	.1	x	-	4
80 Pluto	170	6.90	±.10	±7%	9.4	1.019	7.65	±.51				-	x	-	3
80 Pluto	170	7.40	±.20	±7%	12.0	.947	7.62	±.54				-	x	-	4
80 Pluto	170	7.40	±.30	±7%	13.0	.925	7.46	±.58	2.933	21.895	2.47	-	x	-	-
80 Pluto	170	8.00	±.30	±7%	17.0	.860	7.49	±.66				-	x	-	-
89 Tasso	209	9.30	±.06	±.41	14	.906	8.43	±.46	4.775	40.242	0.01	-	-	-	5
84 Tasso	197	8.48	±.21	±.25	12	.947	8.03	±.34				90	-	-	5
84 Tasso	197	9.08	±.05	(±3%)‡	14	.906	8.23	±.36				90	-	-	5
80 Tasso	179	9.00	±.40	±.60	13.0	.925	8.33	±.70	2.058	17.14	0.01	-	-	-	-
80 Tasso	179	10.70	±.60	±.70	17.0	.860	9.20	±.91				-	-	-	-
							8.382	±.14	52.4	439.26	1.56				
90 Amy	7	17.19	±.07	±.48	57	1.000	17.19	±.49	4.250	73.056	0.00	-	-	-	-
							17.19	±.49	4.250	73.06	0.00				

Yr Exper	Ref	Value	Ecm
79 Adone	1		<2GeV
79 Dasp	76		3.6
77 Dasp	70		3.6-5
92 Delphi	86		91
91 Delphi	84		91
86 Hrs	102		29
85 Mac	129		29
82 Mark1	130		2.6-5.1
82 Mark2	136		5,7,and 29
79 Mark3	154		12-45.
89 None	268		-
90 Opal	155		91
79 Pluto	169		12-45.
79 Pluto	256		12-45.
78 Pluto	167		12-45.
85 Spear	264		2.6-7.8
76 Spear	246		2.4-7.8
75 Spear	242		2.4-5.0
90 Tasso	212		12-45.
82 Tasso	188		12-45.
82 Tasso	187		12-45.
79 Tasso	178		13.2
88 Tpc	233		29
88 Tpc	231		29
87 Tpc	232		29
84 Tpc	215		29
93 Venus	240		58

Note: The numbers under "Ref" refer to the articles listed in the Appendix: Key to Tables.

† all scaling based on an average mass of 193.4MeV.
†† corrected to include decay products < K°ς & Λ° if x'd in corresponding column.
‡ syst not included: 3% assumed.

Table 41. References Relevant to Production of Do.

Yr Exper	Ref	Ecm	Channel	Lum	Comments	Yr Exper	Ref	Ecm	Channel	Lum	Comments
88 Hrs	108	29	–	·	·	92 Argus	27	10	–	·	·
87 Hrs	104	29	–	·	·	92 Argus	22	10	–	·	·
85 Hrs	96	29	–	·	Ds	92 Argus	23	10	–	·	·
84 Hrs	91	29	–	·	·	85 Argus	9	10	–	·	·
85 Jade	120	12-45.	–	·	·	85 Argus	8	10	–	·	·
88 Mark2	147	29	–	·	Ds	92 Cleo	59	10.6	–	·	·
85 ♣	265	-				91 Cleo	53	10.6	–	·	·
76 ♣	248	-				84 Cleo	42	10.6	–	·	·
87 ♣	266	-				76 Mark I	247	2-10.	–	·	·
80 ♣	259	-									

Table 42. References Relevant to Production of D*±.

Yr Exper	Ref	Ecm	Channel	Lum	Comments	Yr Exper	Ref	Ecm	Channel	Lum	Comments
86 Delco	78	29	–	·	·	92 Argus	28	10	–	·	D
85 Delco	80	29	–	·	·	92 Argus	27	10	–	·	D*
88 Hrs	109	29	–	·	·	92 Argus	25	10	–	·	D±
86 Hrs	101	29	–	·	·	85 Argus	10	10	–	·	·
84 Hrs	93	29	–	·	·	85 Argus	9	10	–	·	·
84 Hrs	92	29	–	·	·	85 Argus	8	10	–	·	D*,D*±
84 Hrs	90	29	–	·	·	93 Cleo	64	10.6	–	·	D
85 Jade	120	12-45.	–	·	·	93 Cleo	63	10.6	–	·	D* BR
84 Jade	118	12-45.	–	·	·	93 Cleo	62	10.6	–	·	Ds
84 Jade	117	12-45.	–	·	·	93 Cleo	61	10.6	–	·	D BR
84 Jade	116	12-45.	–	·	·	93 Cleo	60	10.6	–	·	D±
82 Mark2	135	29	–	·	·	92 Cleo	58	10.6	–	·	D* BR
84 Tasso	196	12-45.	–	·	·	92 Cleo	57	10.6	–	·	Ds
84 Tasso	195	12-45.	–	·	·	92 Cleo	56	10.6	–	·	Ds
83 Tasso	194	12-45.	–	·	·	92 Cleo	55	10.6	–	·	Ds
83 Tasso	193	12-45.	–	·	·	92 Cleo	54	10.6	–	·	D*
83 Tasso	191	12-45.	–	·	·	91 Cleo	53	10.6	–	·	D
86 Tpc	228	29	–	·	D*,D*±	88 Cleo	50	10.6	–	·	·
85 Tpc	226	29	–	·	·	84 Cleo	42	10.6	–	·	·
85 ♣	265	-				84 Cleo	41	10.6	–	·	·
83 ♣	263	-				82 Cleo	39	10.6	–	·	·
82 ♣	262	-				77 Cleo	36	10.6	–	·	·
81 ♣	260	-				82 Spear	177	2-10.	–	·	·
79 ♣	255	-				93 Topaz	213	58±	–	·	·
77 ♣	249	-				93 Venus	239	58±	–	·	·
						91 Aleph	3	91	–	·	D
						93 Delphi	88	91	–	·	D

Note: The numbers under "Ref" refer to the articles listed in the Appendix: Key to Tables.

Table 43. References Relevant to Production of Λc±.

Yr Exper	Ref	Ecm	Channel	Lum	Comments	Yr Exper	Ref	Ecm	Channel	Lum	Comments
89 Mark2	149	29	εΛX,μΛX	207		91 Argus	21	10	εΛX,μΛX	494	s=~2000
88 Mark2	148	29	εΛX,μΛX	207	s/n=11/3,6/2	88 Argus	15	10	PKπ,Λππ,PK	219	s=480/10/73
92 Tpc	238	29	PKπ	70	s=16	85 Argus	8	10.2	PKπ	·	
90 Tpc	235	29	PKπ	70	different BR	91 Cleo	52	10.6	PKπ,PK,PKππ,Λπ		
90 Mark2	150	29	≈	·		86 Cleo	48	10.6	PKπ	·	
82 Mark2	134	29	≈	·		85 Cleo	46	10.5	Λππ	·	
82 Mark2	132	29	≈	·		85 Cleo	47	10.6	Λππ	·	BR only
						80 Mark2	131	5.2	PKπ	9	
						90 Cleo	51	10.6	≈	·	
						88 Argus	16	10	≈	·	
						80 Cleo	50	10.5	≈	·	
						87 Cleo	49	10.5	≈	·	

Note: The numbers under "Ref" refer to the articles listed in the Appendix: Key to Tables.

Table 44. Cross Referencing Table (overlapping datasets are grouped in '[ ]').

π^0	10 GeV	20,44,[68,66],119	
	29 GeV	34,119,123,[196,205],208,[225,226]	
	91 GeV	124,301	
$\pi^\pm$	10 GeV	17,44,76,190,203	
	29 GeV	[190,203,208],202,[215,226],233	
$\eta^0\ \eta'$	10 GeV	13,20,66,68;	24,30,66
	29 GeV	34,[107,108],[115,119,123],147;	147
	91 GeV	4,301;	4
$K^\pm$	10 GeV	17,37,44,76,203	
	29 GeV	[190,202,203,208],[215,226],233	
K^0	10 GeV	17,44,69,113,171,[203,211]	
	29 GeV	35,[103,111],113,122,141,152,171,180,[196,203,211],218,226	
	91 GeV	85,152,157,300,301	
$\rho^0\ K^{*\pm}$	10 GeV	29,44;	29,44
	29 GeV	[97,110],116,[199,203],234;	105,116
	91 GeV	87;	85,163
K^{*0}	10 GeV	29,44	
	29 GeV	35,[97,110],211,[218,226],234	
	91 GeV	87,160	
ϕ^0	10 GeV	19,29,44	
	29 GeV	[216,226],234	
	91 GeV	160	
$p^\pm$	10 GeV	17,44,76,77,[190,203]	
	29 GeV	114,[190,201,202,203,208],[215,219,226],233	
Λ^0	10 GeV	14,44,203	
	29 GeV	35[99,103]114,121,142,152[182,190][203,207,210][219,223,226][235,236,237]	
	91 GeV	85,152,161,300,301,302	
Ξ^-	10 GeV	14,44	
	29 GeV	106,[122,192,196,203,207,210][145,148][219,220,226,227,235,236,237]	
	91 GeV	85,161	
$\Delta^{++}\Sigma^{*\pm}$	10 GeV	18;	14
	29 GeV	198;	106,198,[207,210],[226,227]
	91 GeV		161
$\Xi^{*0}\Omega^-$	10 GeV	14;	14
	29 GeV	[145,148],[235,236,237];	[146,148],207,[226,227],[235,236,237]
	91 GeV	161;	161
Ncharged	10 GeV	26,38,113,127,[170,171],179,[197,209]	
	29 GeV	[95,98],100,[112,113,122?],143,170,179,[197,209],214	
	57 GeV	7	
	91 GeV	2,82,83,124,126,[151,153],[156,159?]	

Note: The numbers listed here refer to the articles listed in the Appendix: Key to Tables.

107

D.   REFERENCES

1. R.Marshall, "e+e- Annihilation at High Energies." RAL-89-021 (1989).

2. Herwig Schopper, ICFA Seminar on Future Perspectives in HEP, Brookhaven: 1987: 299 (1987).

3. Various references in the Appendix as well as:

    ASP Collaboration, (A.S.Johnson, *et al.*), 22nd Rencontre De Moriond, Gif-sur-Yvette 1987: 119 (1989).

    BES Collaboration, (M.S.Chanowitz, et al.), "Prospects for the Study of Gluonic States at BEPC." LBL-26484 (1989). Heavy Flavor Symp, Beijing 1988.

    MARK II Collaboration, (A.Petersen, *et al.*), at SLC. Phys.Rev.D 37: 1 (1988).

    SLD Collaboration, SLAC realtime beam monitor, Stanford Linear Accelerator Center (1993).

    VEPP Collaboration, (S.I.Dolinsky, *et al.*), Phys.Rep. 202: 99 (1991).

4. F.Halzen, A.D.Martin, Quarks and Leptons. Wiley: 231 and 370 (1984).

108

VI. DISCUSSION

A. COMPARISONS AMONG RATE MEASUREMENTS

The inclusive production rates of K°, Λ°, Ξ^-, $\Sigma^{*\pm}$, and Ω^- measured herein improve the accuracy of the world-averaged rates as displayed in Table 45.

Table 45. Improvements in the World-averaged Rate Accuracies.

ID	#	Rate	Absolute Error	Relative Error	Common Systematics: % of error	Type	$\sqrt{\chi^2/dof}$	error due to $\sqrt{\chi^2/dof}$	error including $\sqrt{\chi^2/dof}$	Decay Table Error
K°	11	1.396	±.066	±4.7%	88%	DA	0.68	+0.0%	±4.7%	4%
	+1	1.370	±.075	±5.5%	0%	-	0.00	+0.0%	±5.5%	4%
	12	1.402	±.063	±4.5%	89%	DA	0.65	+0.0%	±4.5%	4%
Λ°	8	0.2090	±.0133	±6.4%	75%	DA	0.51	+0.0%	±6.4%	4%
	+1	0.1825	±.0153	±8.4%	0%	-	0.00	+0.0%	±8.4%	4%
	9	0.2051	±.0125	±6.1%	84%	DA	0.65	+0.0%	±6.1%	4%
Ξ^-	5	0.0175	±.0031	±17.7%	58%	A	1.24	+13.1%	±22.1%	7%
	+1	0.0179	±.0088	±49.0%	0%	-	0.00	+0.0%	±49.0%	7%
	6	0.0174	±.0032	±18.3%	64%	DA	1.11	+8.8%	±20.3%	7%
$\Sigma^{*\pm}$	1	0.0330	±.0094	±28.6%	0%	-	0.00	+0.0%	±28.6%	7%
	+1	0.0183	±.0107	±58.2%	0%	-	0.00	+0.0%	±58.2%	7%
	2	0.0269	±.0073	±27.2%	22%	A	0.99	+0.0%	±27.2%	7%
Ω^-	2	.00534	±.00263	±49.2%	36%	A	1.28	+39.3%	±63.0%	10%
	+1	.00012	±.00052	±437.2%	0%	-	0.00	+0.0%	±437.2%	10%
	3	.00042	±.00098	±236.6%	86%	DA	1.71	+328.1%	±404.5%	10%

This experiment's K° measurement weakens the previous very low TPC measurement's influence and the world average actually increases. The uncertainty decreases as one would expect by adding another measurement. The Λ° measurement brings the world average and it's relative error down a little at the expense of a slightly increased disagreement figure ($\sqrt{\chi^2/dof}$). The Ξ^- measurement similarly weakens the influence of the previous high valued TPC measurement and decreases the world average. The increased common systematic error actually increases the total uncertainty slightly, but improves the agreement among measurements. The $\Sigma^{*\pm}$ measurement slightly decreases the relative error and significantly reduces the world average as expected since the previous average is but one measurement. The Ω^- measurement is very much in disagreement with the previous world average, and the $\sqrt{\chi^2/dof}$ increases reflecting this. The average drops dramatically and the relative uncertainty increases just as dramatically. Figures 52 through 56 show the published measurements on the left and the independent conference and thesis measurements on the right for a visual comparison (see Chapter V for references).
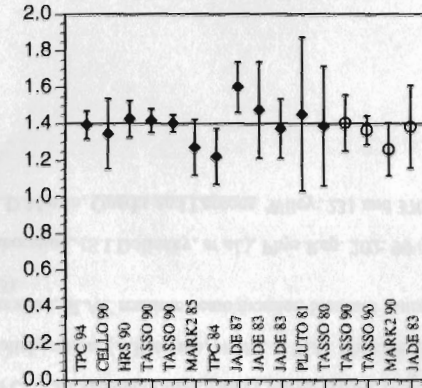
Figure 52. K° Measurements from Table 28.
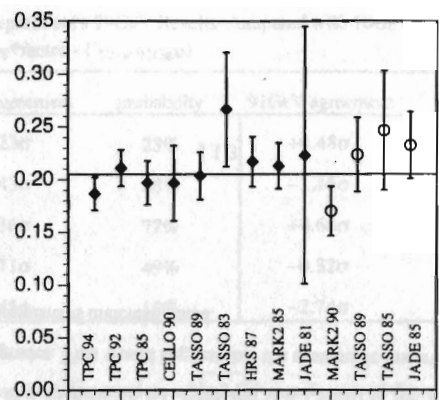
Figure 53. Λ° Measurements from Table 34.
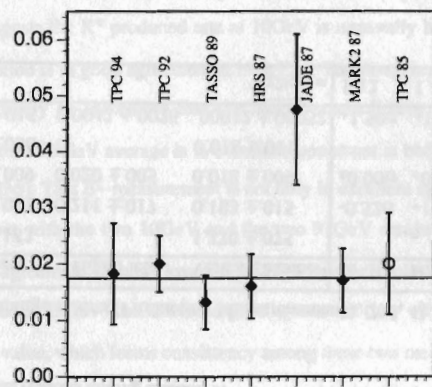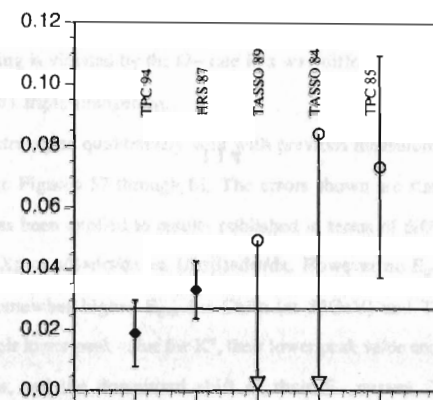

Figure 54. Ξ^- Measurements from Table 35.
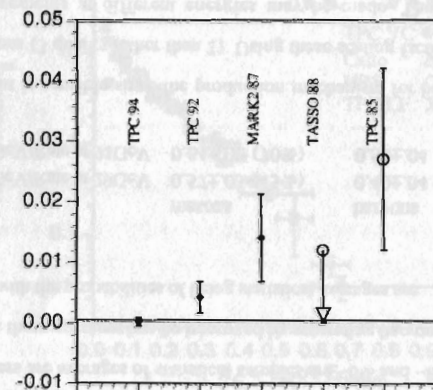

Figure 55. $\Sigma^{*\pm}$ Measurements from Table 37.

Figure 56. Ω^- Measurements from Table 39.

As one can see, the K° and Λ° measurements look well behaved. The Ξ− measurements, with the exception of one old and poorly measured result, also convince one of the average value's accuracy. The Σ*± measurements however, are meager yet consistent, and the average value is somewhat uncertain. The Ω− measurements are quite scattered and uncertain, and the current average would move quite a bit with any new measurement.

It's interesting to compare the previous TPC measurements with those reported here. Table 46 shows the rate results from all three data sets at the TPC/Two-Gamma detector, and the deviations among them.

Table 46. TPC Strange Hadron Production Measurements [1, 2, 3, 4].

ID	Low Field	High Field	Vertex Chamber	LF-HF	HF-VC	LF-VC
K°	1.220 ±.153	-	1.370 ±.075	-	-	-0.88σ
Λ°	0.197 ±.021	0.211 ±.017	0.183 ±.015	-0.52σ	+1.24σ	+0.54σ
Ξ−	0.020 ±.009	0.020 ±.005	0.018 ±.009	±0.00σ	+0.19σ	+0.16σ
Σ*±	0.073 ±.036	-	0.018 ±.011	-	-	+1.46σ
Ω−	0.027 ±.015	0.0042 ±.0026	.00012 ±.00052	+1.50σ	+1.54σ	+1.79σ
			$\sqrt{\chi^2/dof} =$	1.12	1.40	1.27

A systematic variation can be seen between baryon measurements from this dataset and the previous two, with the newer measurements at lower values. This variation is only significant for the Σ*± and Ω− results and is ascribed to differences in either the reconstruction code and cuts (which were previously constructed by H.Yamamoto and J.Oyang, and in this analysis by E.C.Berg and G.R.Lynch) or the vertex chamber and Monte Carlo upgrades. This would suggest that the systematic uncertainty of a subset of these five measurements is underestimated.

A comparison of rates between center-of-mass energies reveals that, as expected, more hadrons are produced as E_{cm} increases. Approximating this behavior with a simple multiplicative factor and allowing the factor to be different between the 10-29GeV and 29-91GeV comparisons is equivalent to making a local linear scaling violation assumption. A weighted average over all species from Table 22 except η, η' and Ω- (due to their large deviation), Δ++ and $N_{charged}$, results in scaling ratios of 0.53±.02 and 0.63±.02 for the two comparisons. Note that the 'χ² Adjusted' errors are used. The probabilities that the above two numbers are averages of statistical samples are ~6% and ~80%. The degree of agreement within these averages can be improved by separating baryons from mesons, the results of which with the probabilities of being statistical averages are:

	mesons	baryons
Rate at 10GeV/Rate at 29GeV	0.57±.03 (45%)	0.40±.04 (90%)
Rate at 29GeV/Rate at 91GeV	0.64±.02 (70%)	0.58±.04 (72%)

The improvement is sensible since the production mechanism for baryons is known to differ from mesons (3 quarks rather than 2). Using these scaling factors, the consistency between measurements at different energies may be made. The results of such a comparison (made by scaling this experiment's results to higher and lower energies, and then comparing with the world averages) are presented in Table 47.
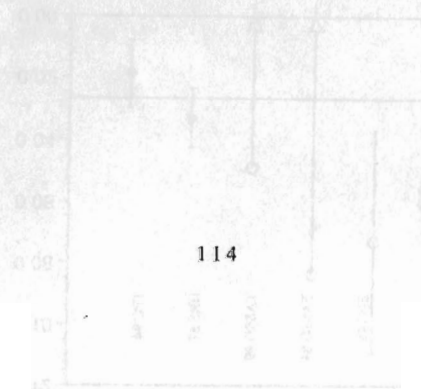
Table 47. This Experiment's 29GeV Results Compared with 10GeV and 91GeV Results
(Γ_{29GeV}*factor - $\Gamma_{10\ or\ 91GeV}$).

ID	10GeV agreement	probability	91GeV agreement	probability
K°	-1.23σ	23%	$+0.48\sigma$	54%
Λ°	-0.43σ	68%	-1.46σ	14%
$\Xi-$	$+0.36\sigma$	77%	$+0.68\sigma$	51%
$\Sigma^{*\pm}$	-0.71σ	49%	-0.32σ	70%
$\Omega-$	-1.45σ	15%	-2.74σ	0.6%

The deviations can be interpreted as a $\sqrt{\chi^2}$ for one degree of freedom (since the 'χ^2 Adjusted' uncertainties were used) from which probabilities for the deviations being statistical are derived. The K° deviation from the average approximate scaling at low E_{cm} is most likely due to the physics of the production, since there are six measurements for the low average and this measurement agrees with the average of eleven others at 29GeV. This weakly suggests the K° produced rate at 10GeV is unusually high, since the local linear approximation is in good agreement at high E_{cm}. The disagreement at high E_{cm} of the Λ° is most likely an indication that the measurement herein is a low statistical fluctuation, since the 29GeV average is in excellent agreement at both low and high E_{cm} ($+0.09\sigma$ and -0.43σ). This $\Xi-$ measurement is not only in excellent agreement with other 29GeV results but with the two 10GeV and the two 91GeV results as well. This $\Sigma^{*\pm}$ result is in good agreement with the low and the high energy results. The HRS value [5] (the only other one at 29GeV) is likewise in good agreement (low $+0.55\sigma$, high $+1.08\sigma$). The best 29GeV value, which forms consistency among these two measurements and two averages, would lie between the two 29GeV values, and so it's likely to be accurate. The $\Omega-$ comparison suggests that this measurement is low, as do the previous two measurements at 29GeV. The spectral extrapolation has a large influence on these

measurements (see Section B). If on the other hand, this measurement is accurate, then the local linear scaling is violated by the $\Omega-$ rate in a way differing from the other hadrons, possibly due to it's triple strangeness.

The spectra agree qualitatively well with previous measurements in this energy region as seen in Figures 57 through 61. The errors shown are statistical errors only. Some scaling has been applied to results published in terms of different variables, for instance $X_E \Rightarrow X_p$ or $s/\beta \cdot d\sigma/dx \Rightarrow 1/(\sigma\beta) \cdot d\sigma/dx$. However no E_{cm} scaling has been applied. The somewhat higher E_{cm} for Cello (at 35GeV) and Tasso (at 34.8GeV) contributes to their lower peak value for K°, their lower peak value and downward shift of their Λ° curves, and the downward shift of their $\Xi-$ curves. This experiment's measurement of the $\Omega-$ rate (especially the lowest 0-0.14 X_p bin) suggests that the previous Mark II measurement was an upward statistical fluctuation, since that integrated rate is dominated by the lowest bin.
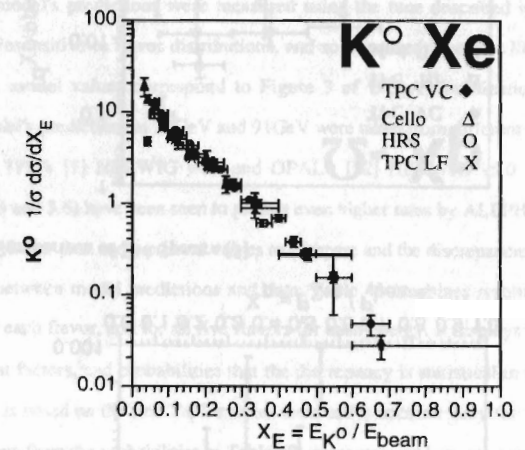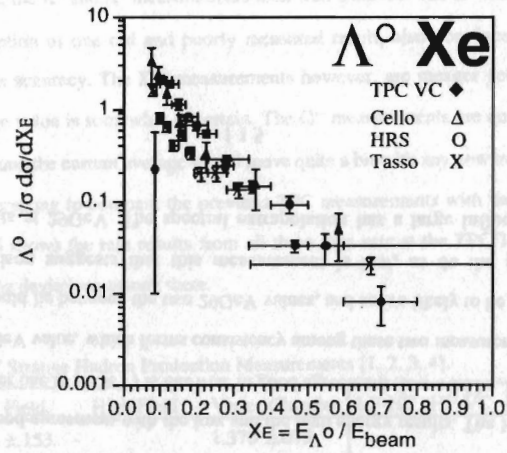

Figure 57. Comparison of K° Spectra [2,6,7].

Figure 58. Comparison of Λ° Spectra [6,8,9].

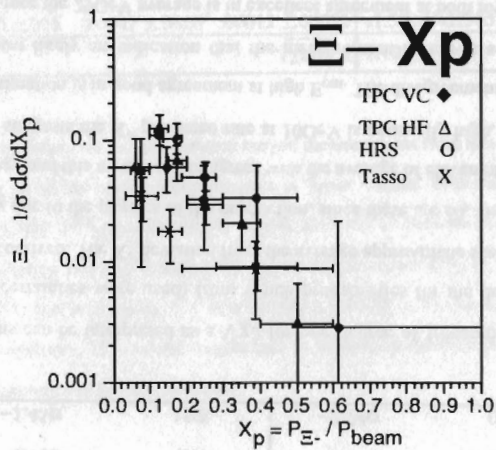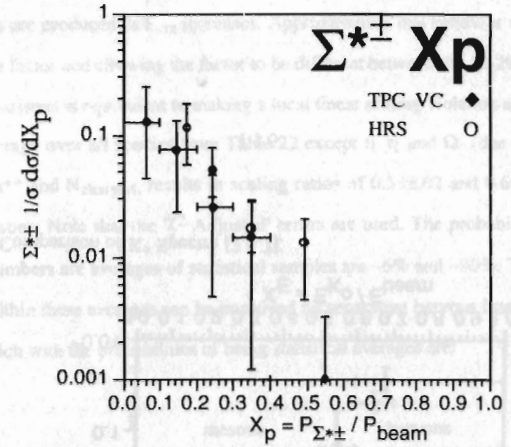
Figure 59. Comparison of $\Xi-$ Spectra [1,5,9].

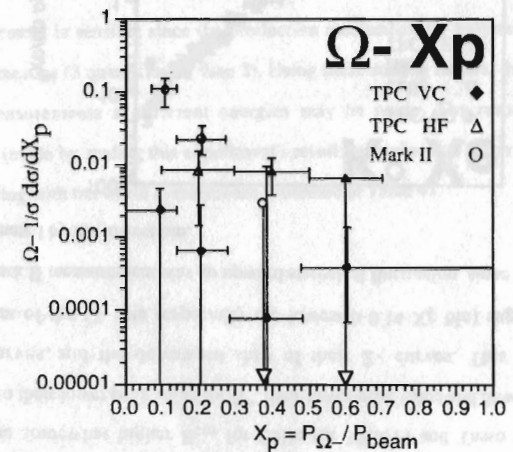Figure 60. Comparison of $\Sigma*^\pm$ Spectra [5].

Figure 61. Comparison of $\Omega-$ Spectra [1,10].

117

118

B.   COMPARISONS WITH MODEL PREDICTIONS

In Tables 48 and 49, the inclusive rate predictions of various models are compared with the world averages from Section A of this chapter (including this experiment's results) and from Table 22.

Table 48. Rate Comparisons with Predictions of Various Models.

Rate:	Data†	Lund	LU-DA	UCLA	UC-DA	Webber	WE-DA
K° 10GeV	0.898 ±.081	0.707 ±.001	-2.36σ	0.865 ±.003	-0.41σ	-	-
K° 29GeV	1.402 ±.085	1.345 ±.002	-0.67σ	1.317 ±.004	-0.99σ	1.60†† ±.03	+2.20σ
K° 91GeV	2.080 ±.096	1.750 ±.002	-3.42σ	2.017 ±.004	-0.65σ	2.07 ±.005‡	-0.10σ
Λ° 10GeV	0.0802 ±.0149	0.0809 ±.0004	+0.05σ	0.0697 ±.0008	-0.70σ	-	-
Λ° 29GeV	0.2051 ±.0149	0.1967 ±.0006	-0.56σ	0.1714 ±.0013	-2.25σ	0.236 ±.0005‡	+2.07σ
Λ° 91GeV	0.3705 ±.0226	0.3033 ±.0008	-2.97σ	0.3298 ±.0018	-1.80σ	0.427 ±.0005‡	+2.50σ
Ξ− 10GeV	0.0058 ±.0010	0.0054 ±.0001	-0.40σ	0.0049 ±.0002	-0.88σ	-	-
Ξ− 29GeV	0.0174 ±.0037	0.0134 ±.0002	-1.08σ	0.0114 ±.0003	-1.62σ	0.036 ±.0005‡	+4.98σ
Ξ− 91GeV	0.0205 ±.0025	0.0214 ±.0002	+0.36σ	0.0229 ±.0005	+0.94σ	0.062 ±.0005‡	+16.28σ
Σ*± 10GeV	0.0107 ±.0021	0.0125 ±.0002	+0.85σ	0.0136 ±.0004	+1.36σ	-	-
Σ*± 29GeV	0.0269 ±.0076	0.0344 ±.0003	+0.99σ	0.0379 ±.0006	+1.44σ	0.071 ±.0005‡	+5.79σ
Σ*± 91GeV	0.0380 ±.0067	0.0574 ±.0003	+2.89σ	0.0756 ±.0009	+5.56σ	0.136 ±.0005‡	+14.59σ
Ω− 10GeV	0.0007 ±.0004	0.00019 ±.00002	-1.27σ	0.0002 ±.00004	-1.24σ	-	-
Ω− 29GeV	0.00042 ±.00168	0.00044 ±.00003	+0.01σ	0.0004 ±.00006	-0.01σ	0.0053 ±.00005‡	+2.90σ
Ω− 91GeV	0.0050 ±.0016	0.00066 ±.00004	-2.71σ	0.0009 ±.00009	-2.56σ	0.0095 ±.00005‡	+2.81σ

† These errors are the 'χ2 Adjusted' errors and include the decay table uncertainty as well.
†† This value is the one that was reported more accurately in HRS [15].
‡ This error was assigned assuming the quoted decimal places were accurate.

119

Table 49. Statistical Agreement of Various Rate Predictions with Data.

$\sqrt{\chi2/dof}$ and probability	Lund		UCLA		Webber†	
K° at all E_{cm}	2.98	0.0%	0.89	45%	2.20	3%
Λ° at all E_{cm}	2.14	1%	2.09	1.5%	3.24	0.1%
Ξ- at all E_{cm}	0.85	45%	1.46	11%	17.02	0.0%
Σ*± at all E_{cm}	2.24	0.7%	4.17	0.0%	15.69	0.0%
Ω− at all E_{cm}	2.12	1%	2.01	2%	4.04	0.0%
10GeV rates	1.42	9%	1.10	32%	-	-
29GeV rates	0.85	55%	1.64	3%	4.36	0.0%
91GeV rates	3.02	0.0%	3.24	0.0%	11.09	0.0%
overall	1.84	0.0%	2.03	0.0%	7.94	0.0%

† These comparisons are between v4.1 at 29GeV and v5.0 at 91GeV and so are not strictly valid.

The Lund model's predictions were measured using the tune described in Chapter II which was insensitive to flavor distributions, and so improved tunes are likely to exist. The UCLA model values correspond to Figure 3 of UCLA's publication [11]. The Webber model's predictions at 29GeV and 91GeV were taken from different versions: the defaults of TPC's [1] HERWIG v4.1 and OPAL's [12] HERWIG v5.0. The newest versions (5.4 and 5.6) have been seen to predict even higher rates by ALEPH [13] and L3 [14]. Table 48 lists data and predicted values to compare and the discrepancies in standard deviations between model predictions and data. Table 49 combines results at all three energies for each flavor, and for all five flavors for each energy. It displays the $\sqrt{\chi2/dof}$ disagreement factors, and probabilities that the discrepancy is statistical in nature. Error propagation is based on the first Taylor series term and is accurate only for small errors. As can be seen from the probabilities in Table 49, the agreement between models and data is good to first or perhaps second order, but disagreements definitely exist. Agreements

120

have less significance, since they may be due to large errors. By studying these probabilities, the places where the models more likely disagree with observations can be identified. By studying the discrepancies in standard deviations, trends in the disagreements can be identified. These observations are made below.

Another way of looking at the production characteristics is with inclusive rate ratios. The following are the interesting flavor-spin ratios that can be constructed from these five rates. The values of these ratios derived from Table 48 at three energies are listed in Tables 50 and 51.

Table 50. Rate Ratio Comparisons with the Predictions of Various Models.

Ratio:	Data	Lund	LU-DA	UCLA	UC-DA	Webber	WE-DA[†]
K°/Λ° 10GeV	11.20 ±2.31	8.74 ±.05	-1.06σ	12.41 ±.15	+0.52σ	-	-
K°/Λ° 29GeV	6.84 ±0.65	6.84 ±.02	-0.00σ	7.69 ±.06	+1.31σ	6.78 ±.13	-0.08σ
K°/Λ° 91GeV	5.61 ±0.43	5.77 ±.02	-0.36σ	6.12 ±.04	+1.17σ	4.85 ±.01	-1.78σ
$K^\circ/\Xi-$ 10GeV	154.90 ±30.14	131.00 ±2.44	-0.79σ	176.55 ±7.23	+0.70σ	-	-
$K^\circ/\Xi-$ 29GeV	80.57 ±17.82	100.37 ±1.50	+1.11σ	115.56 ±3.06	+1.94σ	44.44 ±1.04	-2.02σ
$K^\circ/\Xi-$ 91GeV	101.45 ±13.24	81.76 ±0.77	-1.49σ	88.09 ±1.93	-1.00σ	33.39 ±.28	-5.14σ
$\Lambda^\circ/\Xi-$ 10GeV	13.83 ±3.50	14.98 ±0.29	+0.33σ	14.22 ±0.60	+0.11σ	-	-
$\Lambda^\circ/\Xi-$ 29GeV	11.79 ±2.65	14.68 ±0.22	+1.09σ	15.04 ±0.41	+1.21σ	6.56 ±.09	-1.97σ
$\Lambda^\circ/\Xi-$ 91GeV	18.07 ±2.46	14.17 ±0.14	-1.58σ	14.40 ±0.32	-1.48σ	6.89 ±.06	-4.54σ
$\Xi-/\Sigma^{*\pm}$ 10GeV	0.542 ±.142	0.432 ±.011	-0.78σ	0.360 ±.018	-1.27σ	-	-
$\Xi-/\Sigma^{*\pm}$ 29GeV	0.647 ±.229	0.390 ±.007	-1.12σ	0.301 ±.009	-1.51σ	0.507 ±.008	-0.61σ
$\Xi-/\Sigma^{*\pm}$ 91GeV	0.539 ±.116	0.373 ±.004	-1.44σ	0.303 ±.008	-2.04σ	0.456 ±.004	-0.72σ
$\Sigma^{*\pm}/\Omega-$ 10GeV	15.29 ±9.24	65.79 ±7.00	+4.36σ	68.00 ±13.75	+3.18σ	-	-
$\Sigma^{*\pm}/\Omega-$ 29GeV	64.05 ±256.83	78.18 ±5.37	+0.06σ	94.75 ±14.29	+0.12σ	13.40 ±.16	-0.20σ
$\Sigma^{*\pm}/\Omega-$ 91GeV	7.60 ±2.78	86.97 ±5.29	+13.28σ	84.00 ±8.46	+8.58σ	14.32 ±.09	+2.42σ

† These comparisons are between v4.1 at 29GeV and v5.0 at 91GeV and so are not strictly valid.

Table 51. Statistical Agreement of Various Ratio Predictions with Data.

$\sqrt{\chi^2/dof}$ and probability	Lund		UCLA		Webber[†]	
K°/Λ° at all E_{cm}	0.79	50%	1.29	18%	1.78	7%
$K^\circ/\Xi-$ at all E_{cm}	1.42	12%	1.62	7%	5.52	0.0%
$\Lambda^\circ/\Xi-$ at all E_{cm}	1.38	15%	1.35	16%	4.95	0.0%
$\Xi-/\Sigma^{*\pm}$ at all E_{cm}	1.40	14%	2.01	2%	0.95	37%
$\Sigma^{*\pm}/\Omega-$ at all E_{cm}	9.89	0.0%	6.47	0.0%	2.43	15%
10GeV ratios	2.32	0.0%	1.77	1%	-	-
29GeV ratios	0.96	43%	1.52	5%	1.45	8%
91GeV ratios	6.77	0.0%	4.54	0.0%	3.76	0.0%
overall	3.86	0.0%	2.73	0.0%	2.69	0.0%

† These comparisons are between v4.1 at 29GeV and v5.0 at 91GeV and so are not strictly valid.

These ratios show some E_{cm} dependence. The K°/Λ° ratio, both in data and model predictions, shows a decrease for singly strange hadrons in the (spin 1/2) baryon suppression relative to (spin 0) mesons with increasing energy, presumably because it's easier to produce baryons (in pairs) as E_{cm} increases. The $\Lambda^\circ/\Xi-$ ratio suggests a possible, but statistically inconclusive gradual increase in the doubly strange suppression relative to singly strange spin 1/2 hadrons with increasing energy. The $\Xi-/\Sigma^{*\pm}$ ratio shows no energy dependence of the suppression of spin 3/2 singly strange relative to spin 1/2 doubly strange hadrons. Lastly, the $\Sigma^{*\pm}/\Omega-$ ratio may show a decrease in the suppression of triply strange relative to doubly strange spin 3/2 hadrons with increasing energy, but there is a need for further measurement of these difficult and low rates before any firm conclusion can be reached. In comparing with model predictions, some observables have more influence on modeling than others. The particular observables considered here have less impact for modeling than the parameters used in the models themselves (e.g.: the

Lund model's s/u parameter), but the methodology is appropriate. The various models accurately emulate the above rate and rate ratio observables as follows:

The Lund model most likely agrees with the Ξ- rates, 29GeV rates, K°/Λ° ratios, and the 29GeV ratios. The 29GeV agreements are not too surprising since the parameter values used were determined by tuning to 29GeV data (see Chapter II for specific values). The Lund model most likely disagrees with the K° and Λ° rates (although Delphi's tune to 29GeV accurately predicts both 91GeV rates), $\Sigma^{*\pm}$ rates, Ω- rates, 91GeV rates, $\Sigma^{*\pm}/\Omega$- ratios, 10GeV ratios, and 91GeV ratios. The flavor disagreement might possibly be removed by using a tune more sensitive to hadron flavors. Observed trends in the disagreements can inspire model adjustments. If the model predictions are scaled by an arbitrary factor, the disagreement can be reduced a certain amount, suggesting specific changes in the model. The following independently determined adjustments were found to improve the probability for statistical agreement as follows ($\sqrt{\chi 2/dof}$ are shown in parentheses):

All K°	rates	+14%	$\Rightarrow$ 0.0% to 10% (1.49)
All Λ°	rates	+12%	$\Rightarrow$ 1% to 18% (1.32)
All $\Sigma^{*\pm}$	rates	-27%	$\Rightarrow$ 0.7% to 60% (0.69)
All Ω-	rates	+375%	$\Rightarrow$ 1% to 29% (1.13)
All 91GeV	rates	+11%	$\Rightarrow$ 0.0% to 30% (2.63)
All $\Sigma^{*\pm}/\Omega$-	ratios	-91%	$\Rightarrow$ 0.0% to 58% (0.73)
All 10GeV	ratios	-15%	$\Rightarrow$ 0.0% (2.32 to 2.24)
All 91GeV	ratios	-28%	$\Rightarrow$ 0.0% (6.77 to 6.59)

The adjustments of the K°, Λ°, $\Sigma^{*\pm}$, Ω-, and 91GeV rates as well as the $\Sigma^{*\pm}/\Omega$- ratios significantly improve the agreement. However, the adjustment to the 10GeV and 91GeV ratios have negligible effect.

The UCLA model most likely agrees with the K° rates and 10GeV rates. The parameter values used were determined by tuning to measurements at all three energies. The UCLA model most likely disagrees with the Λ° rates, $\Sigma^{*\pm}$ rates, Ω- rates, 91GeV

rates, Ξ-/$\Sigma^{*\pm}$ ratios, $\Sigma^{*\pm}/\Omega$- ratios, 10GeV ratios, and 91GeV ratios. Scaling the predictions by optimized factors reduces the disagreement in the following ways:

All Λ°	rates	+15%	$\Rightarrow$ 1.5% to 75% (0.47)
All $\Sigma^{*\pm}$	rates	-41%	$\Rightarrow$ 0.0% to 22% (1.21)
All Ω-	rates	+335%	$\Rightarrow$ 2% to 53% (0.77)
All 91GeV	rates	-3%	$\Rightarrow$ 0.0% (3.24 to 3.20)
All Ξ-/$\Sigma^{*\pm}$	ratios	+71%	$\Rightarrow$ 2% to 70% (0.56)
All $\Sigma^{*\pm}/\Omega$-	ratios	-90%	$\Rightarrow$ 0.0% to 60% (0.69)
All 10GeV	ratios	-13%	$\Rightarrow$ 1% to 2% (1.67)
All 91GeV	ratios	-4%	$\Rightarrow$ 0.0% (4.54 to 4.53)

The adjustments of the Λ°, $\Sigma^{*\pm}$ and Ω- rates as well as the Ξ-/$\Sigma^{*\pm}$ and $\Sigma^{*\pm}/\Omega$- ratios significantly improve the agreement. However, the adjustments to the 91GeV rates and 10GeV and 91GeV ratios have little effect.

The Webber model most likely agrees with the Ξ-/$\Sigma^{*\pm}$ ratios. The parameter values used are the defaults. The Webber model most likely disagrees with the Λ° rates, Ξ- rates, $\Sigma^{*\pm}$ rates, Ω- rates, 29GeV rates, 91GeV rates, K°/Ξ-ratios, Λ°/Ξ-ratios, and 91GeV ratios. Scaling the predictions by optimized factors reduces the disagreement in the following ways:

All Λ°	rates	-13%	$\Rightarrow$ 0.1% to 100% (0.05)
All Ξ-	rates	-65%	$\Rightarrow$ 0.0% to 18% (1.38)
All $\Sigma^{*\pm}$	rates	-70%	$\Rightarrow$ 0.0% to 45% (0.85)
All Ω-	rates	-57%	$\Rightarrow$ 0.0% to 22% (1.25)
All 29GeV	rates	-24%	$\Rightarrow$ 0.0% (4.36 to 2.82)
All 91GeV	rates	-40%	$\Rightarrow$ 0.0% (11.09 to 6.84)
All K°/Ξ-	ratios	+144%	$\Rightarrow$ 0.0% to 1% (2.16)
All Λ°/Ξ-	ratios	+126%	$\Rightarrow$ 0.0% to 10% (1.53)
All 91GeV	ratios	+23%	$\Rightarrow$ 0.0% (3.76 to 3.52)

The adjustments of the Λ°, Ξ-, $\Sigma^{*\pm}$, and Ω- rates as well as the Λ°/Ξ-ratios significantly improve the agreement. The adjustments of the 29GeV and 91GeV rates significantly

improve the agreement, but there certainly remains disagreement. The adjustments to the K°/Ξ- and 91GeV ratios have little effect.

The hadron spectra comparisons obtained for this experiment in Chapter IV can be presented in a way which shows model momentum dependent discrepancies more clearly. Figure 62 shows the x_p spectra as the ratio of this experiment's data to the Lund prediction, normalized to the same integrated rates.
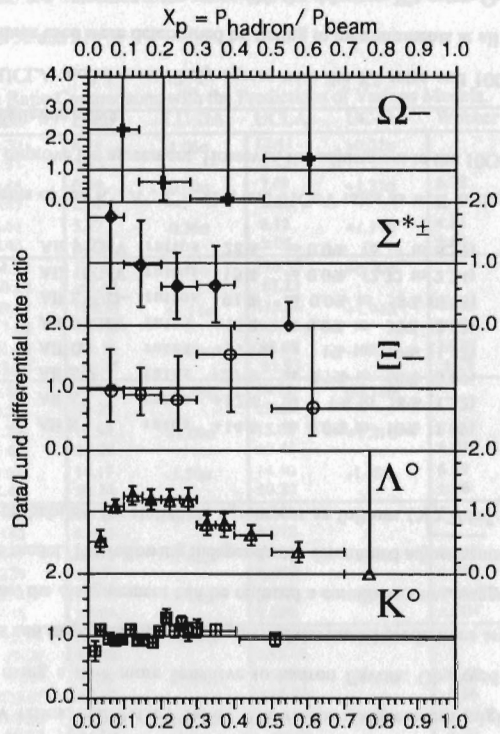

Figure 62. Data/Lund Spectra for K°, Λ°, Ξ-, Σ*±, and Ω-.
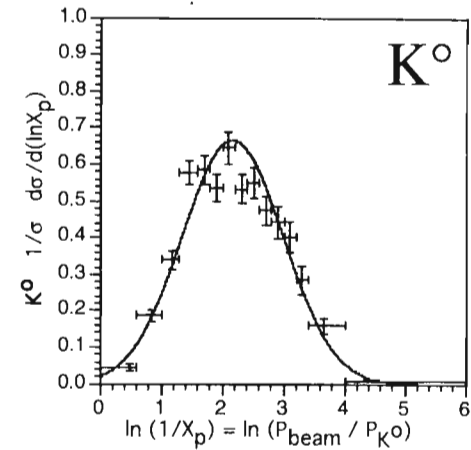
Figure 63. K° MLLA Gaussian Fit.
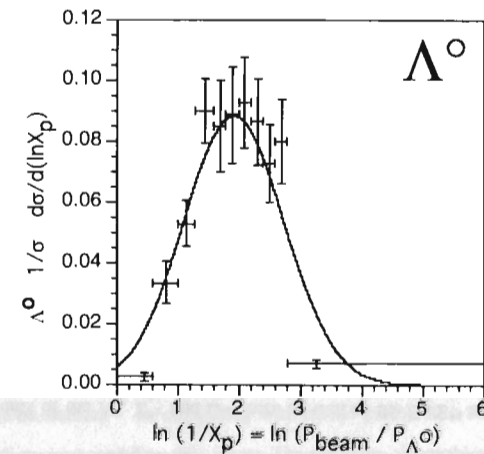
Figure 64. Λ° MLLA Gaussian Fit.

The K° distribution appears to be in agreement with the Lund model. The experimental Λ° spectrum seems definitely softer at high x_p than the Lund model prediction. The $\Sigma^{*\pm}$ spectrum also appears softer than the model. The $\Xi-$ and $\Omega-$ spectra are compatible with either agreement or overly hard model predictions. These results support the previous experimental indication that string models overpredict baryon production at high momentum [1].

The 'hump-backed' spectra of the $-\ln(x_p)$ variable have been studied extensively by phenomenologists [16, 17, 18, 19]. The K° and Λ° $-\ln(x_p)$ spectra are fit here with a reparameterized Gaussian to extract variables for the modified leading log approximation model (see Figures 63 and 64). The Gaussians are reparameterized as in Equation 25 [20] where the overall normalizations, N(Y) have been fixed to the integrated rates.

$$\frac{d\sigma}{\sigma \, d\ln(x)} \approx N(Y) \left(\frac{c_1}{\pi Y^{3/2}}\right)^{1/2} \exp\left(\frac{-c_1[\ln(1/x) - \ln(1/x_o)]^2}{Y^{3/2}}\right)$$

where $\ln(1/x_o) = 0.5Y + c_2\sqrt{Y} + O(1)$ and $Y = \ln(E_{cm}/2\Lambda_{eff})$ (25)

$c_1 = 3.7533$, $c_2 = 0.59272$ at 29GeV (from $N_f = 5$, $N_c = 3$)

The variables, Λ_{eff} and $O(1)$ are fit to the distributions. Λ_{eff} is the scale determining parameter, and $O(1)$ is a constant term which varies with higher order corrections. The resulting values for K° are 0.72±.14 and -0.34±.09 with a $\sqrt{\chi^2/dof} = 1.9$. The values for Λ° are 0.74±.19 and -0.56±.21, where $\sqrt{\chi^2/dof} = 4.6$. This is in good agreement with phenomenological predictions [19], however the actual value is more accurately estimated by fitting the E_{cm} variation as OPAL did resulting in $\Lambda_{eff} = 0.212\pm.020$ and $O(1) = -0.32\pm.60$. The peak values are related to these two parameters, and are expected to increases with E_{cm}. The harder spectra for higher E_{cm} correspond to higher $\ln(1/x_p)$ peak

values. The hadron mass dependence has not been predicted yet. The mean ($\bar{\xi}$), median (ξ^m), and mode (ξ^p) of these spectra have been found to have interesting interrelationships [21]. The K° values of $\bar{\xi}$, ξ^m, ξ^p, and ξ^{p^*} (the ξ^p from the fit to Equation 25) are observed to be 2.21±.44, 2.20±.44, 2.10±.49, and 2.15±.41. The corresponding Λ° values are 1.95±.43, 1.99±.40, 2.10±.52, and 1.91±.87. These lead to values of Pearson's ratio $\left(\frac{\xi^p - \bar{\xi}}{\xi^m - \bar{\xi}}\right)$ of 10±501 and 4±18 for K° and Λ°. Clearly, better statistics are required to compare this measurement with the predicted deviations from the Gaussian value of 3.0. The expected E_{cm} dependence of the maximum value can qualitatively be seen in Figure 65; however the mass dependence is not so apparent. A thorough survey of measurements of these peak values may soon be possible at 10, 29, and 91GeV.
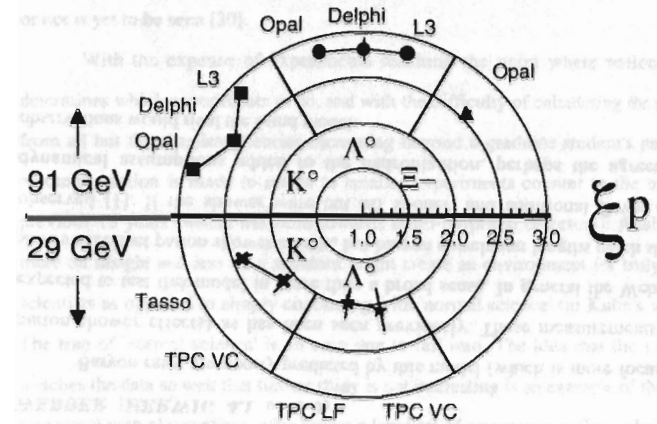

Figure 65. Measurements of ξ^p (or ξ^{p^*}) [14, 16, 19, 22, 23] (the angle coordinate seperates particle type as well as experiment, and the radial coordinate is the value).

C. SUMMARY OF MODEL IMPLICATIONS FROM THIS EXPERIMENT

LUND (JETSET 6.3)

The recent $\Sigma^{*\pm}$ and $\Xi^{*\circ}$ measurements by OPAL at 91GeV disagree with the model's predicted $\Xi^{*\circ}/\Sigma^{*\pm}$ ratio [12]. Attempts to tune the model to both rates were unsuccessful [12]. This experiment's $\Sigma^{*\pm}$ measurement supports this disagreement. The $\Omega-$ rate observed by Mark II at 29GeV was drastically higher than this model's predictions [10]. The value reported by this experiment suggests that the Mark II measurement was not so accurate, and the agreement with the Lund model may be better than previously thought. Baryon spectra observed in this study are softer than the Lund model predicts, as has been seen previously [1]. In general the Symmetric Lund model with MLLA parton shower gives predictions close to observations in most ways, although perhaps this is considerably due to the large set of flavor and spin selection parameters. The JETSET Monte Carlo is very versatile for e+e- annihilation studies because it includes various options for showering as well as hadronization.

UCLA (UCLA 7.31)

OPAL's low $\Sigma^{*\pm}$ rate at 91GeV disagrees with the UCLA model's prediction also. The UCLA model's lack of flexibility (compared with the Lund model) prevents tuning to this rate. The similarity between the previous experimental 29GeV rate (0.033) and the 91GeV rate (0.038) was surprising, and so these data suggested a measurement fluctuation of one of them. The measurement reported here of a low rate at 29GeV is evidence for the fluctuation being at 29GeV and not 91GeV. While improving the apparent energy scaling, this thesis' measurement continues to make the UCLA model's predictions disagree with $\Sigma^{*\pm}$ observations. The UCLA model's $\Omega-$ rate prediction is similar to that of Lund. Thus this experiment's measurement suggests that the UCLA model prediction

likewise is in better agreement with the experimental data than previously thought. Both the Lund and UCLA Monte Carlos predict overly hard baryon x-spectra, and both use the MLLA parton shower and LSFF (for z-selection). Therefore, it is likely that this spectral disagreement is not due to the flavor selection mechanism, which differs between the models. In general the UCLA hadronization technique makes predictions close to most observations. The reduction in parameters relative to the Lund model suggests that the UCLA model's assumptions may be in agreement with the underlying physical mechanisms.

WEBBER (HERWIG 4.1 or 5.0)

Baryon rates are poorly predicted by this model (which is more focused on the parton shower effects) as has been seen previously. These measurements were not expected to test this model in more than a broad sense. In general the Webber model shows excellent parton shower effects, but baryon correlation lengths much shorter than observed [1]. If the shower were cut off sooner, and additional flavor dependent dynamical assumptions added to the hadronization, perhaps the agreement with observations would rival the Lund model.

CONSIDERATIONS FOR FURTHER EXPERIMENTATION

Further observation is warranted if there are few published results, a large uncertainty, or if there is a large disagreement factor among measurements. The following inclusive rates are the ones in the most doubt, where the flavors not in parentheses are more seriously in doubt:

at 10GeV: η', Δ^{++}, $\Xi^{*\circ}$, $\Omega-$, $\pi^{\pm}$, ($K^{\pm}$, $K^{*\pm}$, ϕ, $p^{\pm}$, Λ, $\Sigma^{*\pm}$).

at 29GeV: η', Δ^{++}, $\Xi^{*\circ}$, $\Omega-$, ($\Sigma^{*\pm}$).

at 91GeV: η', Δ^{++}, $\Xi^{*\circ}$, $\Omega-$, ϕ, ($K^{\pm}$, $K^{*\pm}$, ρ°, $p^{\pm}$, $\Sigma^{*\pm}$).

ALEPH may soon publish (presently preliminary) results on $\Xi-$ (a slightly high value) and $\Omega-$ (a smaller value) [24]. OPAL may soon publish results of Δ^{++}, the first such measurement at 91GeV [25]. With the decline of the 15 to 40GeV accelerators, the future of hadronization experimentation is at 10, 58, and 91GeV. At 58GeV measurements of $N_{charged}$, $\pi^{\pm}$, $K^{\pm}$, $p^{\pm}$ and K° have been made (with the TOPAZ detector) [26], and any others may lead to interesting results. Also, deviations from apparent patterns are likely places to find interesting results. K° at 10GeV was vaguely seen to be higher than the E_{cm} scaling suggests, so further comparisons of the differential rates with models is suggested.

Even more interesting would be additional measurements elucidating the discrepancies with current models. Observables which improve the agreement significantly when altered simply in the model are the measurements which more directly reflect those disagreements. The Lund model would be explored further by measuring $\Sigma^{*\pm}$ and $\Omega-$ rates more accurately as well as exploring the overall multiplicity scaling with E_{cm}. The UCLA model would benefit from further measurements of the $\Sigma^{*\pm}$ and $\Omega-$ rates as well as the $\Xi-/\Sigma^{*\pm}$ ratio. The Webber model could use a closer look at the strange baryon rates as well as the $\Lambda^{\circ}/\Xi-$ ratio. The hard baryon spectra predicted by string models could be studied in more detail, perhaps in other variables like $x_{p\perp}$ or in conjunction with baryon correlation studies (e.g.: using rapidity differences). The $\ln(1/x_p)$ distributions have generated much interest, and the need for detailed studies is not going unnoticed. These areas are also places where the modelers would be advised to look closely as well.

Other ideas exist which may contribute to the explanation of hadron production. The idea of rotating color charges [27] (i.e.: the QCD magnetic analog) and transverse quark spin [28] are only a few. The lattice QCD Wilson loop area law from which the Lund symmetric fragmentation function has been derived [11], may be extended to a volume law as in reference [29]. Proponents of lattice QCD recommend other phenomenological approaches because the lattice results are questionable [29]. Strong gravity has been suggested to explain confinement and save the parton model from inconsistency. The field equations work, however whether QCD can be derived from this or not is yet to be seen [30].

With the expense of experiments reaching the point where national opinion determines which experiments to do, and with the difficulty of calculating the predictions from all but the simplest theories increasing beyond a graduate student's patience, the recommendation is made to return to smaller experiments counter to the trend of the previous 15 years (which has been towards multi-purposed detectors). Analyses based more on insight and less on a standard might create an environment for truly insightful scientists as opposed to simply continuing with 'normal science' (in Kuhn's sense [31]). The trap of 'normal science' is an easy one to fall into. The idea that the Lund model matches the data so well that further study is not interesting is an example of this. To be in agreement with observations, after tuning a large set of parameters to those observations is no surprise and does not reflect complete understanding of the system. The idea that QCD explains all strong interactions completely, so we should direct our efforts to learning how to calculate it (at all values of α_s) and not bother with competing theories is another

example. QCD has made many verified predictions and simplifies the observations considerably. Given the quantum field theory formalism, QCD has yet to make a major prediction disagreeing with observation. These characteristics qualify the theory as a good one, and in fact the best one to date. But, until everything we could ever experience is completely and simply explained and deduced from tautologies, we cannot say that any theory is the last one [32,33].

E.   REFERENCES

1.   TPC/Two-Gamma Collaboration, James Yen-Tang Oyang, "Inclusive Production and Flavor Correlations of Strange Baryons in e+e- Annihilation at S**(1/2) = 29-GeV." UMI-92-07711 and UCLA-HEP-91-005, PhD Thesis (1992).

2.   TPC/Two-Gamma Collaboration, (H.Aihara, et al.), "K*0 and K0(S) Meson Production in e+e- Annihilations at 29-GeV." Phys.Rev.Lett. 53: 2378 (1984).

3.   TPC/Two-Gamma Collaboration, (H.Aihara, et al.), "Lambda Production of e+e- Annihilation at 29-GeV." Phys.Rev.Lett. 54: 274 (1985).

4.   TPC/Two-Gamma Collaboration, H.Yamamoto, "QCD Study in e+e- Annihilation at sqrt(s) =29 GeV by PEP4-TPC." 20th Rencontre De Moriond, Gif-Sur-Yvette, 1985.

5.   HRS Collaboration, (S.Abachi, et al.), "Production of Strange Baryons in e+e- Annihilations at 29-GeV." Phys.Rev.Lett. 58: 2627 (1987). error: ibid.59: 2388.

6.   CELLO Collaboration, (H.J.Behrend, et al.), "Inclusive Strange Particle Production in e+e- Annihilation." Z.Phys.C 46: 397 (1990).

7.   HRS Collaboration, (S.Abachi, et al.), "Quark Hadronization Probed by K0 Mesons." Phys.Rev.D 41: 2045 (1990).

8.   HRS Collaboration, (M.Derrick, et al.), "Hadron Production in e+e- Annihilation at S**(1/2) = 29-GeV." Phys.Rev.D 35: 2639 (1987).

9.   TASSO Collaboration, (W.Braunschweig, et al.), "Strange Baryon Production in e+e- Annihilation." Z.Phys.C 45: 209 (1989).

10.   MARK II Collaboration, (S.Klein, et al.), "Observation of Omega- Production in e+e- Annihilation at 29-GeV" Phys.Rev.Lett. 59: 2412 (1987).

11.   S.Chun, C.Buchanan, "A Simple Relativistic-string Description of Meson and Baryon Flavor Formation in e+e- Annihilations." Phys.Lett.B 308: 153 (1993).

12.   OPAL Collaboration, (P.D.Acton, et al.), "A Measurement of Strange Baryon Production in Hadronic Z0 Decays." Phys.Lett.B 291: 503 (1992).

13.   ALEPH Collaboration, (D.Buskulic, et al.), "Production of K* and L in Hadronic Z Decays." CERN-PPE/94-74 (1994), submitted to Z.Phys.C.

14.   L3 Collaboration, (M.Acciarri, et al.), "Measurement of Inclusive Production of Neutral Hadrons from Z Decays." CERN-PPE/94-53 (1994), submitted to Phys.Lett.B.

15.   HRS Collaboration, (S.Abachi, et al.), "Quark Hadronization Probed by K0 Mesons." Phys.Rev.D 41: 2045 (1990).

16.   Y.Azimov, Y.Dokshitzer, V.Khoze, S.Troian, "Hump-Backed QCD Plateau in

Hadron Spectra." Z.Phys.C 31: 213 (1986).

17. Y.Dokshitzer, V.Khoze, S.Troian, "Inclusive Particle Spectra from QCD Cascades." Int.J.Mod.Phys.A 7: 1875 (1992).

18. Y.Dokshitzer, "Improved QCD Treatment of the KNO Phenomenon." LU-TP-93-3, (1993).

19. Y.Dokshitzer, V.Khoze, S.Troian, "Phenomenology of the Particle Spectra in QCD Jets in a Leading Logarithmic Approximation." Z.Phys.C 55: 107 (1992).

20. OPAL Collaboration, (M.Z.Akrawy, et al.), "A Study of Coherence of Soft Gluons in Hadron Jets." Phys.Lett.B 247: 617 (1990).

21. Y.Dokshitzer, V.Khoze, C.Fong, B.Webber, "Mean, Median, and Mode of Hadron Spectrum in QCD Jets." Phys.Lett.B: 273 (1991).

22. OPAL Collaboration, "Measurement of the Production Rates of the Charged Hadrons in e+e- Annihilation at the Z0." CERN-PPE-94-49 (1994), submitted to Z.Phys.C.

23. DELPHI Collaboration, (P.Abreu, et al.), "Production of Strange Particles in the Hadronic Decays of the Z0." Phys.Lett.B 275: 231 (1992).

24. ALEPH Collaboration, private communication. CERN (1993).

25. OPAL Collaboration, private communication. CERN (1993).

26. Ryosuke Itoh, private communication. LBL (1993).

27. Meng Ta-Chung, "Rotating Colour Charges and Polarization Effects in Elastic Proton-Proton Scattering and Inclusive Hyperon Production." 25th Rencontres De Moriond, Les Arcs 1990, 407.

28. X.Artru, M.Mekhfi, "Transverse Spin of the Quarks Inside the Baryon." 25th Rencontres De Moriond, Les Arcs 1990, 415.

29. H.Kouno, F.Takagi, "Hadron-Quark Phase Transition and An Excluded Volume Effect." Workshop on Physics of Quark Gluon Plasma, Tsukuba 1988, proceedings.

30. Abdus Salam, C.Sivaram, "Strong Gravity Approach to QCD and Confinement." Mod.Phys.Lett.A 8: 321 (1993).

31. T.Kuhn, "The Structure of Scientific Revolutions." University of Chicago Press, (1970).

32. S.Hawking, A Brief History of Time. Bantam Books: Chapter 10 (1988).

33. S.Weinberg, Dreams of a Final Theory. Vintage Books, (1992).

A. APPENDIX: KEY TO TABLES

1. ADONE Collaboration, (C.Bacci, et al.), "Experimental Results on Photon-Photon Interactions at ADONE." Phys.Lett.B 86: 234 (1979).

2. ALEPH Collaboration, (D.Decamp, et al.), "Properties of Hadronic Events in e+ e- Annihilation at S**(1/2) = 91-GeV." Phys.Lett.B 234: 209 (1990).

3. ALEPH Collaboration, (D.Decamp, et al.), "Production and Decay of Charmed Mesons at the Z Resonance." Phys.Lett.B 266: 218 (1991).

4. ALEPH Collaboration, (D.Buskulic, et al.), "Measurement of the production rates of eta and eta-prime in Hadronic Z Decays." Phys.Lett.B 292: 210 (1992).

5. ALEPH Collaboration, (D.Buskulic, et al.), 26th Int.Conf.on HEP, Dallas 1992.

6. ALEPH Collaboration, (D.Buskulic, et al.), 28th Rencontres De Moriond, Les Arcs 1993.

7. AMY Collaboration, (H.W.Zheng, et al.), "Charged Hadron Multiplicities in e+e- Annihilation at S**(1/2)=50-GeV-61.4-GeV." Phys.Rev.D 42: 737 (1990).

8. ARGUS Collaboration, (Orr, et al.), "Charm Production and Fragmentation in e+ e- Annihilation at 10-GeV Center-of-mass Energy." 22nd Int.Europhys.Conf.on HEP, Bari 1985: 517.

9. ARGUS Collaboration, (H.Albrecht, et al.), "Production and Decay of the Charged D* Mesons in e+ e- Annihilation at 10-GeV Center-of-mass Energy." Phys.Lett.B 150: 235 (1985).

10. ARGUS Collaboration, (H.Albrecht, et al.), "Production and Decay of the F Meson in e+ e- Annihilation at 10-GeV Center-of-mass Energy." Phys.Lett.B 153: 343 (1985).

11. ARGUS Collaboration, (Orr, et al.), 23rd Int.Conf.on HEP, Berkeley 1986: 1166.

12. ARGUS Collaboration, (H.Albrecht, et al.), "Observation of Octet and Decuplet Hyperons in e+ e- Annihilation at 10-GeV Center-of-mass Energy." Phys.Lett.B 183: 419 (1987).

13. ARGUS Collaboration, (H.Albrecht, et al.), 13th Int.Symp.on Lepton & Photon Interactions at HE, Hamburg 1987: 671.

14. ARGUS Collaboration, (H.Albrecht, et al.), "Hyperon Production in e+ e- Annihilation at 10-GeV Center-of-mass Energy." Z.Phys.C 39: 177 (1988).

15. ARGUS Collaboration, (H.Albrecht, et al.), "Observation of the Charmed Baryon

Lambda(c) in e+ e- Annihilation at 10-GeV." Phys.Lett.B 207: 109 (1988).

16. ARGUS Collaboration, (H.Albrecht, *et al.*), "Observation of Inclusive B Meson Decay Into Lambda(c)+ Baryons." Phys.Lett.B 210: 263 (1988).

17. ARGUS Collaboration, (H.Albrecht, *et al.*), "Inclusive Production of Charged Pions, Charged and Neutral Kaons and Anti-protons in e+ e- Annihilation at 10-GeV and in Direct Upsilon Decays." Z.Phys.C 44: 547 (1989).

18. ARGUS Collaboration, (H.Albrecht, *et al.*), "Observation of Delta++(1232) Production in e+ e- Annihilation Around 10-GeV." Phys.Lett.B 230: 169 (1989).

19. ARGUS Collaboration, (H.Albrecht, *et al.*), "Inclusive Phi Meson Production in Electron-Positron Interactions in the Energy Region of the Upsilon Resonances." Z.Phys.C 41: 557 (1989).

20. ARGUS Collaboration, (H.Albrecht, *et al.*), "Inclusive Pi0 and Eta Meson Production in Electron Positron Interactions at $S^{**}2(1/2) = 10$GeV." Z.Phys.C 46: 15 (1990).

21. ARGUS Collaboration, (H.Albrecht, *et al.*), "Observations of Lambda(Charm) + Semileptonic Decay." Phys.Lett.B 269: 234 (1991).

22. ARGUS Collaboration, (H.Albrecht, *et al.*), "A Search for D0 ---> K+ Pi-." DESY-92-056 (1992).

23. ARGUS Collaboration, (H.Albrecht, *et al.*), "A Measurement of the Inclusive Semileptonic Decay Fraction of Charmed Hadrons." Phys.Lett.B 278: 202 (1992).

24. ARGUS Collaboration, Zimmerman, PhD Thesis (1992).

25. ARGUS Collaboration, (H.Albrecht, *et al.*), "The Measurement of D+(S) and D+ Meson Decays Into Anti-K*+ Anti-K*0." Z.Phys.C 53: 361 (1992).

26. ARGUS Collaboration, (H.Albrecht, *et al.*), "Measurement of R and Determination of the Charge D particle Multiplicity in e+e- Annihilation at $S^{**}(1/2)$ Around 10-GeV." Z.Phys.C 54: 13 (1992).

27. ARGUS Collaboration, (H.Albrecht, *et al.*), "New Results on D0 Decays." Z.Phys.C 56: 7 (1992).

28. ARGUS Collaboration, (H.Albrecht, *et al.*), "Observation of the Decay D(S1) (2536) ---> D*0 K+." DESY-92-124 (1992).

29. ARGUS Collaboration, (H.Albrecht, *et al.*), "Inclusive Production of K* (892), Rho0 (770), and Omega (783) Mesons in the Upsilon Energy Region." DESY-93-084 (1993).

30. ARGUS Collaboration, (H.Albrecht, *et al.*), "Inclusive Production of Eta-prime(958) and F0 (975) Mesons in the Upsilon Energy Region." Z.Phys.C 58: 199 (1993).

31. ARGUS Collaboration, Matthiesen, PhD Thesis, Dortmund University.

32. CELLO Collaboration, (H.J.Behrend, *et al.*), "Measurement of the Inclusive Gamma and Pi0 Spectra and a comparison of the Neutral and Charged Components in Hadronic Events in e+e- Annihilation at 34-GeV." Z.Phys.C 14: 189 (1982).

33. CELLO Collaboration, (H.J.Behrend, *et al.*), "Inclusive Gamma and Pi0 Production in e+e- Annihilation at 14-GeV, 22-GeV, and 34-GeV CM Energy." Z.Phys.C 20: 207 (1983).

34. CELLO Collaboration, (H.J.Behrend, *et al.*), "Measurement of Inclusive Gamma, Pi0 and Eta Production in e+e- Annihilation at $S^{**}(1/2) = 35$-GeV." Z.Phys.C 47: 1 (1990).

35. CELLO Collaboration, (H.J.Behrend, *et al.*), "Inclusive Strange Particle Production in e+e- Annihilation." Z.Phys.C 46: 397 (1990).

36. CLEO Collaboration, (G.Crawford, *et al.*), Phys.Rev.Lett. 39: 1471 (1977).

37. CLEO Collaboration, (A.Brody, *et al.*), "Charged and Neutral Kaon Production at the Upsilon(4S)." CLEO-81-03 (1981).

38. CLEO Collaboration, (M.S.Alam, *et al.*), "Charged Particle Multiplicities in B Meson Decay." Phys.Rev.Lett. 49: 357 (1982).

39. CLEO Collaboration, (C.Bebek, *et al.*), "Inclusive Charged D* Production in e+e- Annihilations at W=10.4-GeV." Phys.Rev.Lett. 49: 610 (1982).

40. CLEO Collaboration, (G.Crawford, *et al.*), 15th Int.Symp.on Multiparticle Dynamics, Lund 1984: 782.

41. CLEO Collaboration, (A.Chen, *et al.*), "Evidence for the F Meson at 1970-MeV." Phys.Rev.Lett. 51: 634 (1984).

42. CLEO Collaboration, (P.Avery, *et al.*), "Production of Charmed Mesons in e+e- Annihilation at 10.5-GeV." Phys.Rev.Lett. 51: 1139 (1984).

43. CLEO Collaboration, (M.S.Alam, *et al.*), "Hyperon Production in e+e- Interactions in the Upsilon Region." Phys.Rev.Lett. 53: 24 (1984).

44. CLEO Collaboration, (S.Behrends, *et al.*), "Inclusive Hadron Production in Upsilon Decays and in Nonresonant Electron-positron Annihilation at 10.49-GeV." Phys.Rev.D 31: 2161 (1985).

45. CLEO Collaboration, (G.Crawford, *et al.*), CLNS-85/645 (1985).

46. CLEO Collaboration, (T.Bowcock, *et al.*), "Lambda(C) Production from e+e- Annihilation in the Upsilon Energy Region." Phys.Rev.Lett. 55: 923 (1985).

47. CLEO Collaboration, (R.S.Galik, *et al.*), "Charm Production and Fragmentation at

CLEO." 22nd Int.Europhys.Conf.on HEP, Bari 1985: 513.

48. CLEO Collaboration, (G.Moneti, et al.), "Measurement of Charm Production at S**(1/2) = 10.55-GeV." 23rd Int.Conf.on HEP, Berkeley 1986: 1162.

49. CLEO Collaboration, (M.S.Alam, et al.), "Evidence for Charmed Baryons in B Meson Decay." Phys.Rev.Lett. 59: 22 (1987).

50. CLEO Collaboration, (D.Bortoletto, et al.), "Charm Production in Nonresonant e+e- Annihilations at S**(1/2) =10.55-GeV." Phys.Rev.D 37: 1719 (1988).

51. CLEO Collaboration, (G.Crawford, et al.), CLNS-90-5 (1990).

52. CLEO Collaboration, (P.Avery, et al.), "Inclusive Production of the Charmed Baryon Lambda(C) from e+e- Annihilations at S**(1/2) = 10.55-GeV." Phys.Rev.D 43: 3599 (1991).

53. CLEO Collaboration, (R.Ammar, et al.), "Unusual Decay Modes of D0 and D+ Mesons." Phys.Rev.D 44: 3383 (1991).

54. CLEO Collaboration, (M.Procario, et al.), "Study of D0 Decays into Anti-K0 and Anti-K*0." CLNS-92-1167 (1992).

55. CLEO Collaboration, (M.Daoudi, et al.), "Two Body D(S)+ Decays to Eta Pi+, Eta-prime Pi+, Eta Rho+, Eta-prime Rho+, Phi Rho+." Phys.Rev.D 45: 3965 (1992).

56. CLEO Collaboration, (J.Alexander, et al.), "D / S+ Decays to Eta Pi+ and Eta-prime Pi+." Phys.Rev.Lett. 68: 1275 (1992).

57. CLEO Collaboration, (P.Avery, et al.), "D / S+ Decays to Eta Rho+, Eta-prime Rho+, and Phi Rho+" Phys.Rev.Lett. 68: 1279 (1992).

58. CLEO Collaboration, (F.Butler, et al.), "Measurement of the D* (2010) Branching Fractions." Phys.Rev.Lett. 69: 2041 (1992).

59. CLEO Collaboration, (M.Procario, et al.), "Study of D0 Decays into Anti-K0 and Anti-K*0." CLNS-92-1167 (1992).

60. CLEO Collaboration, (M.S.Alam, et al.), "Measurement of the Ratio B (D+ ---> Pi0 Lepton+Neutrino) / B (D+ ---> Anti-K0 Lepton+ Neutrino)." Phys.Rev.Lett. 71: 1311 (1993).

61. CLEO Collaboration, (M.Selen, et al.), "The D ---> Pi Pi Branching Fractions." CLNS-93-1225 (1993).

62. CLEO Collaboration, (D.Acosta, et al.), "First Measurement of Gamma (D(S)+ ---> Mu+ Neutrino) / Gamma (D(S)+ ---> Phi Pi+)." CLNS-93-1238 (1993).

63. CLEO Collaboration, (D.S.Akerib, et al.), "Measurement of the Absolute Branching Fraction for D0 ---> K- Pi+." CLNS-93-1242 (1993).

64. CLEO Collaboration, (A.Bean, et al.), "Measurement of Exclusive Semileptonic Decays of D Mesons." CLNS-93-1249 (1993).

65. CRYSTAL BALL Collaboration, (R.Partridge, et al.), "Measurement of Inclusive Eta Production in e+ e- Interactions Near Charm Threshold." Phys.Rev.Lett. 47: 760 (1981).

66. CRYSTAL BALL Collaboration, (J.Irion, et al.), "A Search for Eta(b) and Eta(b)-prime." 23rd Int.Conf.on HEP, Berkeley 1986: 1166.

68. CRYSTAL BALL Collaboration, (C.Bieler, et al.), "Measurement of Pi0 and Eta Meson Production in e+e- Annihilation at S**(1/2) Near 10-GeV." Z.Phys.C 49: 225 (1991).

69. CUSB Collaboration, (G.Giannini, et al.), "Inclusive K0 Production in e+e- Annihilation at the Upsilon Resonances." Nucl.Phys.B 206: 1 (1982).

70. DASP Collaboration, (R.Brandelik, et al.), "Inclusive Hadron Production by e+ e- Annihilation for S Between 13-GeV**2 and 25-GeV**2." Phys.Lett.B 67: 358 (1977).

71. DASP Collaboration, (R.Brandelik, et al.), "Production of Charged Kaons by e+ e- Collisions Between S**(1/2) = 3.6-GeV and 5-GeV." Phys.Lett.B 67: 363 (1977).

72. DASP Collaboration, (R.Brandelik, et al.), "Evidence for the F Meson." Phys.Lett.B 70: 132 (1977).

74. DASP Collaboration, (R.Brandelik, et al.), "Production Characteristics of the F Meson." Phys.Lett.B 80: 412 (1979).

75. DASP Collaboration, (R.Brandelik, et al.), "Results From DASP on e+ e- Annihilation Between 3.1-GeV and 5.2-GeV." Z.Phys.C 1: 233 (1979).

76. DASP Collaboration, (R.Brandelik, et al.), "Charged Pion, Kaon and Nucleon Production by e+ e- Annihilation for C.M. Energies Between 3.6-GeV and 5.2-GeV." Nucl.Phys.B 148: 189 (1979).

77. DASP Collaboration, (H.Albrecht, et al.), "Inclusive Hadron Production in the Upsilon Region." Phys.Lett.B 102: 291 (1981).

78. DELCO Collaboration, H.Yamamoto, "A Study of Charged D* Mesons Produced in e+e- Annihilation at E(cm) = 29-GeV." PhD Thesis, CALT-68-1318 (1968).

79. DELCO Collaboration, M.Duro, "Charged Hadronic Particle Fractions in e+e- Annihilations at 29-GeV." PhD Thesis, RX-1134 (1985).

80. DELCO Collaboration, (H.Yamamoto, et al.), "Charged D* Production in e+e- Annihilation at 29-GeV and a Limit on D0 - Anti-D0 Mixing." Phys.Rev.Lett. 54: 522 (1985).

81. DELPHI Collaboration, (P.Abreu, et al.), "Charged Particle Multiplicity

Distributions in Z0 Hadronic Decays." CERN-PPE-90-173 (1990).

82. DELPHI Collaboration, (P.Aarnio, *et al.*), "Study of Hadronic Decays of the Z0 Boson." Phys.Lett.B 240: 271 (1990).

83. DELPHI Collaboration, (P.Abreu, *et al.*), "Charged Particle Multiplicity Distributions in Z0 Hadronic Decays." Z.Phys.C 50: 185 (1991).

84. DELPHI Collaboration, (P.Abreu, *et al.*), "Charged Particle Multiplicity Distributions in Restricted Rapidity Intervals in Z0 Hadronic Decays." Z.Phys.C 52: 271 (1991).

85. DELPHI Collaboration, (P.Abreu, *et al.*), "Production of Strange Particles in the Hadronic Decays of the Z0." Phys.Lett.B 275: 231 (1992).

86. DELPHI Collaboration, (P.Abreu, *et al.*), "Charged Particle Multiplicity Distributions for Fixed Number of Jets in Z0 Hadronic Decays." Z.Phys.C 56: 63 (1992).

87. DELPHI Collaboration, (P.Abreu, *et al.*), "Measurement of Inclusive Production of Light Meson Resonances in Hadronic Decays of the Z0." Phys.Lett.B 298: 236 (1993).

88. DELPHI Collaboration, (P.Abreu, *et al.*), "A Measurement of D Meson Production in Z0 Hadronic Decays." CERN-PPE-93-70 (1993).

89. HRS Collaboration, (S.Ahlen, *et al.*), "Hadron Production in e+ e- Annihilations at S**(1/2) = 29-GeV." 11th Int.Symp.on Lepton & Photon Interactions at HE, Ithaca 1983.

90. HRS Collaboration, (S.Ahlen, *et al.*), "Inclusive D and D* Production in e+e- Annihilation at 29-GeV." Phys.Rev.Lett. 51: 1147 (1984).

91. HRS Collaboration, (M.Derrick, *et al.*), "Inclusive D0 and D+ Production in e+e- Annihilation at 29-GeV." Phys.Rev.Lett. 53: 1971 (1984).

92. HRS Collaboration, (M.Derrick, *et al.*), "Charm Quark Production and Fragmentation in e+e- Annihilation at 29-GeV." Phys.Lett.B 146: 261 (1984).

93. HRS Collaboration, (S.Abachi, *et al.*), Phys.Lett.B 146: 265 (1984).

94. HRS Collaboration, (M.Derrick, *et al.*), "Hadron Production in e+e- Annihilation at S**(1/2) = 29-GeV." ANL-HEP-PR-85-69 (1985).

95. HRS Collaboration, (D.Bender, *et al.*), "Study of Quark Fragmentation at 29-GeV: Global Jet Parameters and Single Particle Distributions." Phys.Rev.D 31: 1 (1985).

96. HRS Collaboration, (M.Derrick, *et al.*), "Production of Phi and F (1970) ---> Phi Phi Pi in e+e- Annihilation at 29-GeV." Phys.Rev.Lett. 54: 2568 (1985).

97. HRS Collaboration, (M.Derrick, *et al.*), "Neutral K* (890) and Rho0 Meson Production in e+e- Annihilation at the S**(1/2) = 29-GeV." Phys.Lett.B 158: 519 (1985).

98. HRS Collaboration, (M.Derrick, *et al.*), "Inclusive Charged Particle Production Near the Kinematic Limit in e+e- Annihilation at 29-GeV." Phys.Lett.B 164: 199 (1985).

99. HRS Collaboration, (P.Baringer, *et al.*), "Lambda Production in e+e- Annihilations at 29-GeV: a Comparison with Lund Model Predictions." Phys.Rev.Lett. 56: 1346 (1986).

100. HRS Collaboration, (M.Derrick, *et al.*), "Study of Quark Fragmentation in e+e- Annihilation at 29-GeV: Charged Particle Multiplicity and Single Particle Rapidity Distributions." Phys.Lett.D 34: 3304 (1986).

101. HRS Collaboration, (S.Abachi, *et al.*), "Charm D Production in e+e- Annihilation at 29-GeV." ANL-HEP-CP-86-75, 23rd Int.Conf.on HEP, Berkeley 1986: 1173.

102. HRS Collaboration, (M.Derrick, *et al.*), "Comparison of Charged Particle Multiplicities in Quark and Gluon Jets Produced in e+e- Annihilation at 29-GeV." Phys.Lett.B 165:4 49 (1986).

103. HRS Collaboration, (M.Derrick, *et al.*), "Hadron Production in e+e- Annihilation at S**(1/2) = 29-GeV." Phys.Rev.D 35: 2639 (1987).

104. HRS Collaboration, (E.H.Low, *et al.*), "Production and Fragmentation of the D*0 Meson in e+e- Annihilations." Phys.Lett.B 183: 232 (1987).

105. HRS Collaboration, (S.Abachi, *et al.*), "Charged K* Production in e+e- Annihilations at 29-GeV." Phys.Lett.B 199: 151 (1987).

106. HRS Collaboration, (S.Abachi, *et al.*), "Production of Strange Baryons in e+e- Annihilations at 29-GeV." Phys.Rev.Lett. 58: 2627 (1987). error: *ibid.*59: 2388.

107. HRS Collaboration, (S.Abachi, *et al.*), "Search for D*0 ---> D+ Pi-." 13th Int.Symp.on Lepton & Photon Interactions at HE, Hamburg 1987: 671.

108. HRS Collaboration, (S.Abachi, *et al.*), "Production of Eta Mesons in e+e- Annihilations at S**(1/2) = 29-GeV." Phys.Lett.B 205: 111 (1988).

109. HRS Collaboration, (P.Baringer, *et al.*), "Production Cross-section and ElectroWeak Asymmetry of D* and D Mesons Produced in e+e- Annihilations at 29-GeV." Phys.Lett.B 206: 551 (1988).

110. HRS Collaboration, (S.Abachi, *et al.*), "Study of Vector Meson Production in e+e- Annihilation at S**(1/2) = 29-GeV." Phys.Rev.D 40: 706 (1989).

111. HRS Collaboration, (S.Abachi, *et al.*), "Quark Hadronization Probed by K0 Mesons." Phys.Rev.D 41: 2045 (1990).

112. JADE Collaboration, (W.Bartel, *et al.*), "Total Cross-section for Hadron

Production by e+e- Annihilation at PETRA Energies." Phys.Lett.B 88: 171 (1979).

113. JADE Collaboration, (W.Bartel, *et al.*), "Charged Particle and Neutral Kaon Production in e+e- Annihilation at PETRA." Z.Phys.C 20: 187 (1983).

114. JADE Collaboration, (W.Bartel, *et al.*), "Baryon Production in e+e- Annihilation at PETRA." Phys.Lett.B 104: 325 (1983).

115. JADE Collaboration, (W.Bartel, *et al.*), "Observation of Inclusive Eta Production in e+e- Annihilation at CM Energies of 34-GeV." Phys.Lett.B 130: 454 (1983).

116. JADE Collaboration, (W.Bartel, *et al.*), "Inclusive Production of Vector Mesons Rho0 and K*+- in e+e- Annihilation at <S**(1/2)> = 35-GeV." Phys.Lett.B 145: 441 (1984).

117. JADE Collaboration, (W.Bartel, *et al.*), "Charged D* Production in e+e- Annihilation." Phys.Lett.B 146: 121 (1984).

118. JADE Collaboration, (W.Bartel, *et al.*), "A Search for the Supersymmetric Partner of the Z0 in e+e- Annihilation at PETRA." Phys.Lett.B 146: 126 (1984).

119. JADE Collaboration, (W.Bartel, *et al.*), "A Study of Photon Production in Hadronic e+e- Annihilation." Z.Phys.C 28: 343 (1985).

120. JADE Collaboration, (W.Bartel, *et al.*), "Inclusive Neutral D* Production and Limits on F* Production in e+e- Annihilation at PETRA." Phys.Lett.B 161: 197 (1985).

121. D.H.Saxon, "Jet Fragmentation." 22nd Int.Europhys.Conf.on HEP, Bari 1985: 899. private communication: Saxon with Dietrick of JADE Collaboration.

122. JADE Collaboration, (W.Bartel, *et al.*), Phys.Rep. 148: 67 (1987).

123. JADE Collaboration, (D.Pitzl, *et al.*), "A Study of Photon Production in Hadronic Events from e+e- Annihilation." Z.Phys.C 46: 1 (1990).

124. L3 Collaboration, (B.Adeva, *et al.*), "Measurement of the Inclusive Production of Neutral Pions and Charged Particles on the Z0 Resonance." .Phys.Lett.B 259: 199 (1991).

125. L3 Collaboration, (O.Adriani, *et al.*), "Measurement of Inclusive Eta Production in Hadronic Decays of the Z0." Phys.Lett.B 286: 403 (1992).

126. L3 Collaboration, (B.Adeva, et al.), "Studies of Hadronic Event Structure and Comparisons with QCD Models at the Z0 Resonance." Z.Phys.C 55: 39 (1992).

127. LENA Collaboration, (B.Niczyporuk, *et al.*), "Charged Hadron Production in e+e- Annihilation in the Upsilon and Upsilon' Region." Z.Phys.C 9: 1 (1981).

128. LGW Collaboration, (D.L.Scharre, *et al.*), "Inclusive Gamma and Pi0 Production in e+ e- Annihilation." Phys.Rev.Lett. 41: 1005 (1978).

129. MAC Collaboration, (E.Fernandez, *et al.*), "Precision Measurement of the Total Cross-section for e+e- ---> Hadrons at a Center-of-mass Energy of 29-GeV." Phys.Rev.D 31: 1537 (1985).

130. MARK I Collaboration, (J.L.Siegrist, *et al.*), Phys.Rev.D 26: 969 (1982).

131. MARK II Collaboration, (G.S.Abrams, *et al.*), Phys.Rev.Lett. 44: 10 (1980).

132. MARK II Collaboration, (G.S.Abrams, *et al.*), Phys.Rev.D 26: 3298 (1982).

133. MARK II Collaboration, (Hollebeek, *et al.*), "Recent Results from PEP." 10th Int.Symp.on Lepton & Photon Interactions at HE, Bonn 1981: 1.

134. MARK II Collaboration, (E.Vella, *et al.*), "Observation of Semileptonic Decays of Charmed Baryons." Phys.Rev.Lett. 48: 1515 (1982).

135. MARK II Collaboration, (J.M.Yelton, *et al.*), "D*+ Production in e+e- Annihilation at 29-GeV." Phys.Rev.Lett. 49: 430 (1982).

136. MARK II Collaboration, (J.F.Patrick, *et al.*), "Measurement of S d Sigma / dx for Hadron Production by e+e- Annihilation at S**(1/2) = 5.2-GeV, 6.5-GeV and 29.0-GeV." Phys.Rev.Lett. 49: 1232 (1982).

137. MARK II Collaboration, (H.Schellman, *et al.*), "Inclusive Production of Vector Mesons in e+e- Annihilation at 29-GeV." SLAC-PUB-3448 (1984). same as LBL-18391 (1984).

138. MARK II Collaboration, (H.M.Schellman, *et al.*), "Inclusive Production of Strange and Vector Mesons in e+e- Annihilation at 29-GeV." LBL-18699: 46 (1984).

139. MARK II Collaboration, (G.S.Abrams, *et al.*), Phys.Rev.D 29: 804 (1984).

140. MARK II Collaboration, (G.S.Abrams, *et al.*), Phys.Rev.D 31: 1537 (1985).

141. MARK II Collaboration, (H.Schellman, *et al.*), "Measurement of K+- and K0 Inclusive Rates in e+e- Annihilation at 29-GeV." Phys.Rev.D 31: 3013 (1985).

142. MARK II Collaboration, (C.delaVaissiere, *et al.*), "Lambda Production in e+e- Annihilation at 29-GeV." Phys.Rev.Lett. 54: 2071 (1985).

143. MARK II Collaboration, (P.C.Rowson, *et al.*), "Charged Multiplicity of Hadronic Events Containing Heavy Quark Jets." Phys.Rev.Lett. 54: 2580 (1985).

144. MARK II Collaboration, (A.R.Baden, *et al.*), "Lambda Production in Electron-Positron Annihilation at 29-GeV." LBL-22046 (1986).

145. MARK II Collaboration, (G.S.Abrams, *et al.*), "Observation of Xi- Production in e+e- Annihilation at 29GeV." Phys.Rev.Lett. 58: 644 (1987).

146. MARK II Collaboration, (S.Klein, *et al.*), "Observation of Omega- Production in e+e- Annihilation at 29-GeV" Phys.Rev.Lett. 59: 2412 (1987).

147. MARK II Collaboration, (G.Wormser, *et al.*), "Eta and Eta-prime Production in e+e- Annihilation at 29-GeV: Indications for the D(S)+- Decays into Eta Pi+- and Eta-prime Pi+-." Phys.Rev.Lett. 61: 1057 (1988).

148. MARK II Collaboration, Spencer Klein, "Charmed and Strange Baryon Production in 29-GeV Electron-Positron Annihilation." PhD Thesis, SLAC-0330 (1988).

149. MARK II Collaboration, (S.Klein, *et al.*), "Lambda(C)+ Production and Semileptonic Decay in 29-GeV e+e- Annihilation." Phys.Rev.Lett. 62: 2444 (1989).

150. MARK II Collaboration, S.R.Klein, "Charmed Baryons: a New Laboratory for Charm Studies." Int.J.Mod.Phys.A 5: 1457 (1990).

151. MARK II Collaboration, (K.F.O'Shaughnessy, *et al.*), "Charged Particle Inclusive Distributions from Hadronic Z0 Decays." SLAC-PUB-5216, (1990). same as 15th APS Div.of Part. and Fields 1990: 314.

152. MARK II Collaboration, C.Fordham, "Neutral Kaon and Lambda Production in Electron-Positron Annihilation at 29-GeV and the Z Boson Resonance." PhD Thesis, (1990).

153. MARK II Collaboration, (G.S.Abrams, *et al.*), "Measurements of Charged-Particle Inclusive Distributions in Hadronic Decays of the Z Boson." Phys.Rev.Lett. 64: 1334 (1990).

154. MARK J Collaboration, (D.Barber, *et al.*), "Measurement of the Relative Total Hadronic Cross-section R at PETRA." Phys.Rev.Lett. 42: 1113 (1979).

155. OPAL Collaboration, (M.Z.Akrawy, et al.), "A Study of Coherence of Soft Gluons in Hadron Jets." Phys.Lett.B 247: 617 (1990).

156. OPAL Collaboration, (M.Z.Akrawy, *et al.*), "A Measurement of Global Event Shape Distributions in the Hadronic Decays of the Z0." Z.Phys.C 47: 505 (1990).

157. OPAL Collaboration, (G.Alexander, *et al.*), "A Study of K0(S) Production in Z0 Decays." Phys.Lett.B 264: 467 (1991).

158. OPAL Collaboration, "Measurement of the Production Rates of the Charged Hadrons in e+e- Annihilation at the Z0." CERN-PPE-94-49 (1994), submitted to Z.Phys.C.

159. OPAL Collaboration, (P.D.Acton, *et al.*), "A Study of Charged Particle Multiplicities in Hadronic Decays of the Z0." Z.Phys.C 53: 539(1992).

160. OPAL Collaboration, (P.D.Acton, *et al.*), "Inclusive Neutral Vector Meson Production in Hadronic Z0 Decays." Z.Phys.C 56: 521 (1992).

161. OPAL Collaboration, (P.D.Acton, *et al.*), "A Measurement of Strange Baryon Production in Hadronic Z0 Decays." Phys.Lett.B 291: 503 (1992).

162. OPAL Collaboration, (P.D.Acton, *et al.*), "A Study of K0(S) K0(S) Bose-Einstein Correlations in Hadronic Z0 Decays." Phys.Lett.B 298: 456 (1993).

163. OPAL Collaboration, (P.D.Acton, *et al.*), "A Measurement of K*+- (892) Production in Hadronic Z0 Decays." Phys.Lett.B 305: 407 (1993).

164. PLUTO Collaboration, (J.Burmester, *et al.*), "Observation of Associated K0(S) Electron Production in e+e- Annihilation." Phys.Lett.B 64: 369 (1976).

165. PLUTO Collaboration, (C.Berger, *et al.*), DESY-F33-77-03 (1977).

166. PLUTO Collaboration, (J.Burmester, *et al.*), "Inclusive K0(S) Production in e+e- Annihilation at Energies of 3.6-GeV to 5.0-GeV." Phys.Lett.B 67: 367 (1977).

167. PLUTO Collaboration, (C.Berger, *et al.*), "A Study of Jets in Electron-Positron Annihilation into Hadrons in the Energy Range 3.1-GeV to 9.5-GeV." Phys.Lett.B 78: 176 (1978).

169. PLUTO Collaboration, (C.Berger, *et al.*), "Cross-sections and Event Topologies in e+e- Annihilation at 13-GeV and 17-GeV Observed with the PLUTO Detector." Phys.Lett.B 81: 410 (1979).

170. PLUTO Collaboration, (C.Berger, *et al.*), "Multiplicity Distributions in e+e- Annihilation at PETRA Energies." Phys.Lett.B 95: 313 (1980).

171. PLUTO Collaboration, (C.Berger, *et al.*), "Inclusive K0 Production in e+e- Annihilation for 9.3-GeV < S**(1/2) < 31.6-GeV." Phys.Lett.B 104: 79 (1981).

172. SPEAR Collaboration, (M.A.Allen, *et al.*), Phys.Rev.Lett. 35: 704 (1975).

173. SPEAR Collaboration, (V.Luth, *et al.*), "K0 Production in e+ e- Annihilation." Phys.Lett.B 70: 120 (1977).

174. SPEAR Collaboration, (M.Piccolo, *et al.*), "Inclusive Baryon Production in e+ e- Annihilation." Phys.Rev.Lett. 39: 1503 (1977).

175. SPEAR Collaboration, (M.A.Allen, *et al.*), Phys.Lett.D 17: 2901 (1978).

176. SPEAR Collaboration, (D.Aschman, *et al.*), "Inclusive Hadron Production in e+ e- Annihilation at <S> = 53-GeV**2." Phys.Rev.Lett. 41: 445 (1978).

177. SPEAR Collaboration, (M.W.Coles, *et al.*), "D Meson Production in e+ e- Annihilation at Ecm Between 3.8-GeV and 6.7-GeV." Phys.Rev.D 26: 2190 (1982).

178. TASSO Collaboration, (R.Brandelik, *et al.*), "Properties of Hadronic Final States in e+e- Annihilation at 13-GeV and 17-GeV Center-of-mass Energies." Phys.Lett.B 83: 261 (1979).

179. TASSO Collaboration, (R.Brandelik, *et al.*), "Rapid Growth of Charged Particle Multiplicity in High Energy e+e- Annihilations." Phys.Lett.B 89: 418 (1980).

180. TASSO Collaboration, (R.Brandelik, et al.), "K0 Production in e+e- Annihilations at 30-GeV Center-of-mass Energy." Phys.Lett.B 94: 91 (1980).

181. TASSO Collaboration, (R.Brandelik, et al.), "Charged Pion, Kaon, Proton and Anti-proton Production in High Energy e+e- Annihilation." Phys.Lett.B 94: 444 (1980).

182. TASSO Collaboration, (R.Brandelik, et al.), "Lambda, Anti-lambda Production in e+e- Annihilation at 33-GeV Center-of-mass Energy." Phys.Lett.B 105: 75 (1981).

184. TASSO Collaboration, (W.Braunschweig, et al.), DESY-F1-82-03 (1982).

185. TASSO Collaboration, (R.Brandelik, et al.), "Pi0 Production by e+e- Annihilation at 14-GeV C.M. Energy." Phys.Lett.B 108: 71 (1982).

186. TASSO Collaboration, (R.Brandelik, et al.), "Charged Pion Production in e+e- Annihilation at 14-GeV, 22-GeV and 34-GeV CM Energy." Phys.Lett.B 113: 98 (1982).

187. TASSO Collaboration, (R.Brandelik, et al.), "A Measurement of Sigma-T (e+e- ---> Hadrons) for CM Energies Between 12.0-GeV and 36.7-GeV." Phys.Lett.B 113: 499 (1982).

188. TASSO Collaboration, (R.Brandelik, et al.), "Scale Breaking in Inclusive Charged Particle Production by e+e- Annihilation." Phys.Lett.B 114: 65 (1982).

189. TASSO Collaboration, (R.Brandelik, et al.), "Inclusive Rho0 Production in e+e- Annihilation at High Energy." Phys.Lett.B 117: 135 (1982).

190. TASSO Collaboration, (M.Althoff, et al.), "Charged Hadron Composition of the Final State in e+e- Annihilation at High Energies." Z.Phys.C 17: 5 (1983).

191. TASSO Collaboration, (R.M.Althoff, et al.), "D*+- Production by e+e- Annihilation Near 34.4-GeV CM Energy." Phys.Lett.B 126: 493 (1983).

192. TASSO Collaboration, (M.Althoff, et al.), "Observation of Xi-, Anti-Xi- Production in e+e- Annihilation." Phys.Lett.B 130: 340 (1983).

193. TASSO Collaboration, (M.Althoff, et al.), "Observation of F Meson Production in High-energy e+e- Annihilation." Phys.Lett.B 136: 130 (1983).

194. TASSO Collaboration, (M.Althoff, et al.), "Observation of F Meson Production in High Energy e+ e- Annihilation." Phys.Lett.B 136: 139 (1983).

195. TASSO Collaboration, (M.Althoff, et al.), "Experimental Test of the Flavor Independence of the Quark-gluon Coupling Constant." Phys.Lett.B 138: 317 (1984)

196. TASSO Collaboration, (W.Braunschweig, et al.), Phys.Rep. 107: 59 (1984).

197. TASSO Collaboration, (M.Althoff, et al.), "Jet Production and Fragmentation in

e+e- Annihilation at 12-GeV to 43-GeV." Z.Phys.C 22: 307 (1984).

198. TASSO Collaboration, (M.Althoff, et al.), "Upper Limits on the Production Rate of the decuplet Baryons Delta and Sigma* in e+e- Annihilation at 34.4-GeV." Z.Phys.C 26: 181 (1984).

199. TASSO Collaboration, (W.Braunschweig, et al.), 15th Int.Symp.on Multiparticle Dynamics Lund 1984: 678 (1984).

200. TASSO Collaboration, (M.Althoff, et al.), "A Detailed Study of Strange Particle Production in e+e- Annihilation at High Energy." DESY-84-093 (1984).

201. TASSO Collaboration, (Saxon, et al.), 22nd Int.Europhys.Conf.on HEP, Bari 1985: 901.

202. TASSO Collaboration, (W.Braunschweig, et al.), 22nd Int.Europhys.Conf.on HEP, Bari 1985: 509.

203. TASSO Collaboration, (M.Althoff, et al.), "A Detailed Study of Strange Particle Production in e+e- Annihilation at High-energy." Z.Phys.C 27: 27 (1985).

204. TASSO Collaboration, Michael Dittmar, "Investigation of Baryon Production in e+ e- Annihilation With the TASSO Detector." PhD Thesis (In German), (1985).

205. TASSO Collaboration, (W.Braunschweig, et al.), "Inclusive Pi0 Production by e+e- Annihilation at 34.6-GeV Center-of-mass Energy." Z.Phys.C 33: 13 (1986).

206. TASSO Collaboration, (W.Braunschweig, et al.), "Strange Baryon Production in e+e- Annihilation." DESY-88-173 (1988).

207. TASSO Collaboration, I.R.Tomalin , "Strange Baryon Production in e+e- Annihilation." PhD Thesis, RALT-069 (1988).

208. TASSO Collaboration, (W.Braunschweig, et al.), "Pion, Kaon, and Proton Cross-sections in e+e- Annihilation at 34-GeV and 44-GeV CM Energy." Z.Phys.C 42: 189 (1989).

209. TASSO Collaboration, (W.Braunschweig, et al.), "Charged Multiplicity Distributions and Correlations in e+e- Annihilation at PETRA Energies." Z.Phys.C 45: 193 (1989).

210. TASSO Collaboration, (W.Braunschweig, et al.), "Strange Baryon Production in e+e- Annihilation." Z.Phys.C 45: 209 (1989).

211. TASSO Collaboration, (W.Braunschweig, et al.), "Strange Meson Production in e+e- Annihilation." Z.Phys.C 47: 167 (1990).

212. TASSO Collaboration, (W.Braunschweig, et al.), "Global Jet Properties at 14-GeV to 44-GeV Center of Mass Energy in e+e- Annihilation." Z.Phys.C 47: 187 (1990).

213. TOPAZ Collaboration, (R.Enomoto, et al.), "Measurement of the D*+- Cross-

section in Two-Photon Processes." KEK-PREPRINT-93-107 (1993).

214. TPC/Two-Gamma Collaboration, N.Hadley, "Charged Hadron Production in e+e- Collisions at PEP with the TPC." PhD Thesis, LBL-16116 (1983).

215. TPC/Two-Gamma Collaboration, (H.Aihara, *et al.*), "Charged Hadron Production in e+e- Annihilation at 29-GeV." Phys.Rev.Lett. 52: 577 (1984).

216. TPC/Two-Gamma Collaboration, (H.Aihara, *et al.*), "Phi Meson Production in e+e- Annihilations at 29-GeV." Phys.Rev.Lett. 52: 2201 (1984).

217. TPC/Two-Gamma Collaboration, (H.Aihara, *et al.*), "Characteristics of Proton Production in Jets from e+e- Annihilation at 29-GeV." Phys.Rev.Lett. 53: 130 (1984).

218. TPC/Two-Gamma Collaboration, (H.Aihara, *et al.*), "K*0 and K0(S) Meson Production in e+e- Annihilations at 29-GeV." Phys.Rev.Lett. 53: 2378 (1984).

219. TPC/Two-Gamma Collaboration, (H.Aihara, *et al.*), "Baryon Production in e+e- Annihilation at 29-GeV." 19th Rencontre De Moriond, La Plagne 1984.

220. TPC/Two-Gamma Collaboration, (H.Aihara, *et al.*), 15th Int.Symp.on Multiparticle Dynamics, Lund 1984: 678.

223. TPC/Two-Gamma Collaboration, (H.Aihara, *et al.*), "Lambda Production of e+e- Annihilation at 29-GeV." Phys.Rev.Lett. 54: 274 (1985).

224. TPC/Two-Gamma Collaboration, (H.Aihara, *et al.*), "Baryon Production in e+e- Annihilation at S**(1/2) = 29-GeV: Clusters, Diquarks, Popcorn?." Phys.Rev.Lett. 55: 1047 (1985).

225. TPC/Two-Gamma Collaboration, (H.Aihara, *et al.*), "Inclusive Gamma and Pi0 Production Cross-sections and Energy Fractions in e+e- Annihilation at 29-GeV." Z.Phys.C 27: 187 (1985).

226. TPC/Two-Gamma Collaboration, H.Yamamoto, "QCD Study in e+e- Annihilation at sqrt(s) =29 GeV by PEP4-TPC." 20th Rencontre De Moriond, Gif-Sur-Yvette, 1985.

227. TPC/Two-Gamma Collaboration, (H.Aihara, *et al.*), 22nd Int.Europhys.Conf.on on HEP, Bari 1985

228. TPC/Two-Gamma Collaboration, (H.Aihara, *et al.*), "Charged D* Meson Production in e+e- Annihilation at S**(1/2) = 29-GeV." Phys.Rev.D 34: 1945 (1986).

229. TPC/Two-Gamma Collaboration, (H.Aihara, *et al.*), "Comparison of Pi+-, K+- and P, anti-P Production in the Central Rapidity Region in Hadron-Hadron Collisions and in e+e- Annihilation." Phys.Lett.B 184: 114 (1987).

230. TPC/Two-Gamma Collaboration, (H.Aihara, *et al.*), "Pion and Kaon Multiplicities

in Heavy Quark Jets from e+e- Annihilation at 29-GeV." Phys.Lett.B 184: 299 (1987).

231. TPC/Two-Gamma Collaboration, Z.Wolf, "Charged Hadron Production in e+e- Annihilation at S**(1/2) = 29-GeV." PhD Thesis, LBL-23738 (1987).

232. TPC/Two-Gamma Collaboration, (H.Aihara, *et al.*), "Charged Hadron Inclusive Cross-sections and Fractions in e+e- Annihilation at S**(1/2) = 29-GeV." Phys.Rev.Lett. 61: 1263 (1988).

233. TPC/Two-Gamma Collaboration, (H.Aihara, *et al.*), "Charged Hadron Production in e+e- Annihilation at S**(1/2) = 29-GeV." LBL-23737 (1988).

234. TPC/Two-Gamma Collaboration, (T.K.Edberg, *et al.*), "Inclusive Production of Vector Mesons in e+e- Annihilation at S**(1/2) = 29-GeV." LBL-25652 (1988).

235. TPC/Two-Gamma Collaboration, (H.Aihara, *et al.*), 25th Int.Conf.on HEP, Singapore 1990.

236. TPC/Two-Gamma Collaboration, (H.Aihara, *et al.*), " Inclusive Production of Λ, Ξ−, Ω−, and Ξ°* and Strange Baryon Correlations in e+e- Annihilation at sqrt(s) = 29GeV." paper to be submitted.

237. TPC/Two-Gamma Collaboration, James Yen-Tang Oyang, "Inclusive Production and Flavor Correlations of Strange Baryons in e+e- Annihilation at S**(1/2) = 29-GeV." UMI-92-07711 and UCLA-HEP-91-005, PhD Thesis (1992).

238. TPC/Two-Gamma Collaboration, S.Khacheryan, "Lambda(c) and Sigma(c) Baryons Production in e+ e- Annihilation at S**(1/2) = 29-GeV." UCLA-HEP-92-007, PhD Thesis (1992).

239. VENUS Collaboration, (F.Hinode, *et al.*), "A Study of Charged D* Production in e+e- Annihilation at an Average Center-of-mass Energy of 58-GeV." Phys.Lett.B 313: 245 (1993).

240. VENUS Collaboration, (H.Takaki, *et al.*), "Particle Spectrum in Gluon Jets Produced in e+e- Annihilations at S**(1/2) Around 58-GeV." Phys.Rev.Lett. 71: 38 (1993).

242. SPEAR Collaboration, (M.A.Allen, et al.), Phys.Rev.Lett. 34: 764 (1975).

243. Triangle Conference on HE Particle Interactions, Smolenice 1975.

246. SPEAR Collaboration, (G. Hanson, *et al.*), "e+ e- Hadron Production and Jet Structure at SPEAR." SLAC-PUB-1814, 7th Int.Colloq.on Multiparticle Reactions, Tutzing 1976. also 18th Int.Conf.on HEP, Tbilisi 1976.

247. MARK I Collaboration, (G.Goldhaber, *et al.*), "Observation in e+ e- Annihilation of a Narrow State at 1865-MeV/C**2 Decaying to K Pi and K Pi Pi Pi." Phys.Rev.Lett. 37: 255 (1976).

248. Phys.Rev.Lett. 37: 569 (1976).

249. Phys.Rev.Lett. 38: 1313 (1977)

250. 13th Rencontre De Moriond, Dreux 1978.

252. Gunter Wolf, "High-energy Trends in e+ e- Physics." DESY-79-41, Int.Europhys.Conf.on HEP, Geneva 1979.

255. Phys.Lett.B 86: 108 (1979).

256. PLUTO Collaboration, (C.Berger, *et al.*), "Jet Analysis of the Upsilon (9.46) Decay into Charged Hadrons." Phys.Lett.B 82: 449 (1980).

259. Schindler *et al.*, Phys.Rev.D 24: 78 (1980).

260. Phys.Rev.Lett. 46: 701 (1981).

262. Phys.Rev.Lett. 49: 439 (1982).

263. Phys.Lett.B 139: 320 (1983).

264. SPEAR Collaboration, J.Siegrist, "Hadron Production by e+ e- Annihilation at Center-of-mass Energies Between 2.6-GeV and 7.8-GeV." SLAC-0225, PhD Thesis, (1979).

265. HRS Collaboration, (M.Derrick, *et al.*), "Neutral K* (890) and Rho0 Meson Production in e+e- Annihilation at S**(1/2) = 29-GeV." Phys.Lett.B 158: 519 (1985).

266. Int.Symp.on the Production & Decay of Heavy Flavors, Stanford 1987.

267. Ali, High Energy e-e+ Physics: 273. article by Gittelman and Stone (1987).

268. Phys.Rep. 177: 141 (1989).

300. ALEPH Collaboration, (D.Buskulic, *et al.*), "Production of K° and Λ in Hadronic Z Decays." CERN-PPE/94-74 (1994), submitted to Z.Phys.C.

301. L3 Collaboration, (M.Acciarri, *et al.*), "Measurement of Inclusive Production of Neutral Hadrons from Z Decays." CERN-PPE/94-53 (1994), submitted to Phys.Lett.B.

302. DELPHI Collaboration, (P.Abreu, *et al.*), Phys.Lett.B 316: 253 (1993).

As the Uni-verse breathes---

our little supercluster drifts, anywhere to go

one cluster of many, moving to join Virgo

local group scattered, in such local disarray

lovely Andromeda, opposed with Milky Way

disk spinning, a bright Frisbee of dots

density, bending, and some waves - lots

star cluster, surfing until mellow

Sol - around we go, young and yellow

rising, falling we spin to sleep

I AM HERE!

lungs fill, my heart shocks to wake me

some brain - waves for me inside, B-side

sent pattern to nexus, at least tried

with epinephrine the synapse fires

where O-16 drifts until it tires

electrons shielded by polarized nothingness

every raindrop's protons, a fused nucleus

not quite quantized, and only up, down, up but no flight

nothing but glue between the red, green, blue but no white

---my spirit finds its next